A Szilikátipari Tudományos Egyesület lapja

építőanyag

Journal of Silicate Based and Composite Materials

A TARTALOMBÓL:

2017/2

NANOMAT2017

INTERNATIONAL CONFERENCE ON FUNCTIONAL NANOMATERIALS AND NANODEVICES

» 24-27 September 2017, Budapest, Hungary

Symposia

- **Energy Conversion and storage Materials**
- **Synthesis and Characterization of Nanomaterials**
- **Catalysis for Clean Energy and Chemical Production**
- **Nanobiotechnologies**

Plenary Speakers

» **Prof. M. Hoffmann**
Caltech, USA

» **Prof. R. Popovtzer**
Bar-Ilan University, Israel

» **Dr. S. Cabrini**
Lawrence Berkeley Lab, USA

International Functional Nanomaterials and Nanodevice Conference 2017 aims to bring together leading scientists, researchers, engineers, and technology developers in nanotechnology to exchange information on their latest research progress and innovation.
This Conference will include a series of symposia focused on four main areas which are: Functional Nanomaterials Synthesis and Characterization; Devices for Energy Storage and Energy Conversion; Nanobiotechnologies and Nanodevices; and Nanotechnology for Environmental Studies & Safety Issues.

European Nanoscience and Nanotechnology Association

ORGANIZED BY
EUROPEAN NANOSCIENCE AND NANOTECHNOLOGY ASSOCIATION

WWW.NANOMAT2017.COM

építőanyag

Journal of Silicate Based and Composite Materials

2017/2

TARTALOM

CONTENT

A finomkerámia-, üveg-, cement-, mész-, beton-, tégla- és cserép-, kő- és kavics-, tűzállóanyag-, szigetelőanyag-iparágak szakmai lapja
Scientific journal of ceramics, glass, cement, concrete, clay products, stone and gravel, insulating and fireproof materials and composites

A folyóiratot referálja · The journal is referred by:
Cambridge Scientific Abstracts
ProQuest

A folyóiratban lektorált cikkek jelennek meg.
All published papers are peer-reviewed.
Kiadó · Publisher: Szilikátipari Tudományos Egyesület (SZTE)
Elnök · President: ASZTALOS István
1034 Budapest, Bécsi út 122–124.
Tel.: +36-1/201-9360 ▪ E-mail: epitoanyag@szte.org.hu
Tördelő szerkesztő · Layout editor: NÉMETH Hajnalka

Címlapfotó · Cover photo: KÓSA Luca Kornélia

WWW.EPITOANYAG.ORG.HU
EN.EPITOANYAG.ORG.HU

Online ISSN: 2064-4477
Print ISSN: 0013-970x
INDEX: 2 52 50 ▪ 69 (2017) 33–72

Vol. 69, No. 2

Compaction characteristics of lateritic soils stabilised with cement-calcined clay blends

G. Matthew AYININUOLA ▪ Civil Engineering Department, University of Ibadan, Nigeria
O. Ayoola ADEKITAN ▪ Civil Engineering Department, Moshood Abiola Polytechnic, Abeokuta Nigeria ▪ adekitan.olasunkanmi@mapoly.edu.ng

Érkezett: 2017. 01. 06. ▪ Received: 06. 01. 2017. ▪ https://doi.org/10.14382/epitoanyag-jsbcm.2017.7

Abstract

Investigations on the potentials of pozzolans - silicate and aluminate materials - in civil engineering works is on the rise. Calcined kaolinite clay (CKC) is one of such pozzolans that has been regarded as an option for mitigating the release of greenhouse gases from cement. While investigations on its use with cement in concrete works is widespread, there is a gap in literature about its impact as a soil stabiliser for flexible road pavements. This work studies the compaction behaviour of two lateritic soils stabilised with a blend of Portland cement (PC) and CKC combined in CKC:PC ratios of 0:1, 1:3, 1:1, 3:1 and 1:0 with total binder percentages of 0 (control), 2.5, 5, 7.5 and 10 of the weight of soils. CKC was obtained by calcining clay samples sourced from south-west Nigeria at 700 °C for 1 hour. Two lateritic soils samples were adopted and classified as A-1-a and A-2-6 based on AASHTO system. Corresponding fineness modulus were 2.18 and 4.33 with cation exchange capacities (CECs) of 1.678 meq/100 gms and 1.738 meq/100 gms respectively. The results show that, as the CKC:PC mixes varies, compaction behaviour of the stabilised A-2-6 soil was widely varied whereas it was minimally varied for the stabilised A-1-a soil. The differences in the particle sizes (fineness modulus) and CEC are adduced as factors responsible for these differences in compaction behaviour. However, the CECs of the soils is about the same. Thus, the differences in compaction performance could only be attributed to differences in the particles sizes of the soils. Statistical evaluation of differences in the results using ANOVA confirms that the differences for the A-2-6 soil are significant whereas that of the A-1-a soil are not.

Keywords: calcined kaolinite clay, ordinary Portland cement, stabilisation, compaction, cation exchange capacity, particle size

G. Matthew AYININUOLA
holds a PhD in Geotechnical Engineering. He is currently an Associate Professor with the Department of Civil Engineering, University of Ibadan, Ibadan, Nigeria.

O. Ayoola ADEKITAN
is currently with the Department of Civil Engineering, Moshood Abiola Polytechnic, Abeokuta, Nigeria and a PhD student with the Department of Civil Engineering, University of Ibadan, Ibadan, Nigeria

1. Introduction

The increasing emission of environmentally detrimental CO_2, a Green House Gas (GHG) in the cement manufacturing and consumption processes has been considered as one of the contributors to environmental pollution and global warming [1, 2, 3]. In this regards, attempts have been made to find suitable replacements for cement. The emergence of substances such as fly ash, silica fume, various biomass ash and geopolymers among others have been a response to this drive [1, 2, 3, 4]. These supplementary cementitious materials (SCMs) or pozzolans are compounds of silicates or aluminosilicates, which reacts with calcium hydroxide ($Ca(OH)_2$) from the cement to form cementitious compound [2, 3, 4]. They could be adopted in replacing cement (partially and sometimes wholly) in civil engineering works.

Calcined kaolinite clay (CKC) is a pozzolan that has produced excellent results in cement concrete works [1, 2, 5). It is produced by calcining or heat-treating kaolinite rocks/clay (hydrated aluminium silicate, $Al_2Si_2O_5(OH)_4$) under controlled temperature ranging between 650°C and 900°C, depending on the source [1, 2, 6, 7]. The calcining alters the structure of the kaolinite rocks, removing the attached hydroxyl ions (OH^-) in the process [2, 7].

Though CKC have been used to replace cement partially with commendable results in concrete works, there is a gap in the literature as to its consideration in soil stabilisation. Thus, the pattern of its effect on soils is not yet clear. This calls for investigations to ascertain if the reported upper edge in cement concrete works could be corresponded in soil stabilisation. This work investigated the compaction characteristics of lateritic soils stabilised with CKC-PC blends. The intention is to explore possible attributes of soils that can be used to explain the compaction behaviour of CKC-PC stabilised soils.

2. Methodology

Two sources of lateritic soils were identified and used for this work. Samples were obtained from two locations (both in South-west Nigeria) having soils that are characteristically different from one another. An area that had not been previously disturbed was identified at the two locations and excavated to depths not less than 1.0 m below the surface. Disturbed samples were collected into an airtight container, labelled and transported to the laboratory. The soils were labelled as samples A and B respectively.

The samples were subjected to soil classification tests at the soil laboratory based on the British Standard procedures [8], for classification using the American Association of State Highway and Transportation Officials (AASHTO) classification system. The system classifies soils using group indices, which are determined, as [9]:

$$GI = 0.2a + 0.005ac + 0.01bd \quad (1)$$

where,

a = that portion of the percentage passing 200 sieve greater than 35% and not exceeding 75% (0 – 40)
b = that portion of the percentage passing 200 sieve greater than 15% and not exceeding 55% (0 – 40)
c = that portion of the liquid limit greater than 40 and not exceeding 60 (0 – 20)
d = that portion of the PI greater than 10 and not exceeding 30 (0 – 20).

From the particle size analysis, the levels of fineness of the two soils were also determined and compared. The fineness modulus is determined by adding the cumulative percentages retained on each of sieves size 150 μm, 300 μm, 600 μm, 1.18 mm, 2.36 mm and 4.75 mm respectively and dividing by 100.

In addition, the soil samples were also subjected to chemical analysis test using X-ray Fluorescence (XRF). Their respective cation exchange capacities (CECs) were also determined in the laboratory.

CKC was obtained by calcining kaolinite clay samples sourced from its natural deposit in South-west Nigeria. The kaolinite was located at a level ranging from about 10 meters depth from the ground level, underlying a layer of lateritic soil. The samples were milled into powder and calcined at 700°C for 1hour; the calcining specification based on earlier works on the same clay sample [10]. The calcining was done using an electric muffle furnace fitted with a temperature control device to adjust temperature to the target calcining temperature. The calcined clay samples were then sieved using a 90 μm sieve and the portion passing through was used. This is based on the premise that particle sizes of cement ranged from the maximum of between 75-100 μm [11, 12]. The particle size of the pozzolan to be combined with it in stabilisation should therefore be within similar range. The CKC was also subjected to chemical analysis test using XRF for comparison with the standard for classification of materials as natural pozzolans [13]. The CEC was also determined as well.

The standard proctor compaction tests (British Light) were carried out in line with the procedures of [8] for compaction on soils for civil engineering purpose and of [14] for tests on stabilised soils. The portion of the lateritic soils passing the 20 mm test sieve was used. The stabilisers (CKC and PC) were applied in a definite format. They were combined in total percentages of 2.5, 5.0, 7.5 and 10 (of the weight of the soils) respectively with CKC:PC combining ratios of 0:1, 1:3, 1:1, 3:1 and 1:0 respectively. With the inclusion of the control (0% total binder), 21 different compositions of soil-binders were adopted for each of the two soils.

For each CKC-PC-lateritic soil mix, four or five samples were compacted, each sample at increasing water content over the previous. The same was done for the control sample (0% binder). The maximum dry densities (mdds) and optimum moisture contents (omcs) of the mixes were obtained from these tests. The tests were repeated two more times per CKC-PC-lateritic soil mix and averages were determined.

The compaction results were then compared and explanations were found for possible differences, if any. In addition, comparison is drawn by running a statistical analysis to determine if any significant differences exist across the combining ratios as the total binder percentages increase. This analysis was executed using *ANOVA* tool on *Microsoft® Excel* software package.

3. Results

3. 1. Properties of soils

Lateritic soil sample A was dark-reddish brown silty sandy clay material. Sample B lateritic soil was light-reddish brown gravelly sandy clay; less reddish compared to sample A. There are specks with creamy/white colorations within the soil mass. The soil has fragments of stones identified by physical inspection. These soil samples are generally adopted for road works and especially suitable for stabilisation works.

The results of the particle size analysis of the two soils are detailed in *Figs. 1a* and *1b*. Sample A is a fine-grained (silty sandy clay) soil whereas sample B is gravelly (about 50% retained on 4.75 mm benchmark and almost no fines). These particle size results were consistent with the plasticity indices of the soils presented in *Table 1*. Typical of fine soils, sample A has higher plasticity with plasticity index of 20.5%, whereas sample B has low value of 6.3%. The table also presents the result of AASHTO group classification for the two soils. The soils were classified as A-2-6 (sample A) and A-1-a (sample B). These classifications indicate that the soils are amenable to stabilisation [15, 16]. The fineness modulus obtained from the particle size result is also presented in *Table 1*. The fineness modulus for the A-2-6 soil was 2.18 whereas it was 4.33 for the A-1-a soil, indicating that the A-2-6 soil is twice as fine as the A-1-a soil.

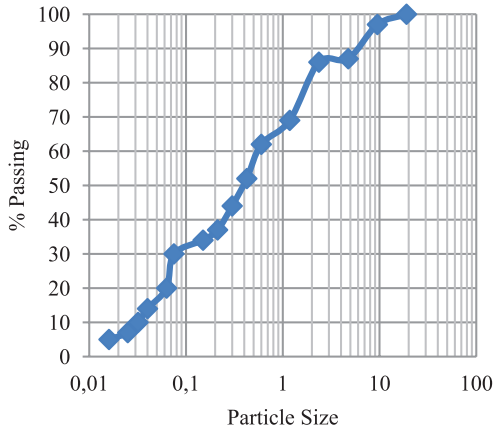

Fig. 1a. Particle size analysis for soil sample A
1a. ábra A jelű talaj minta szemcseméret eloszlása

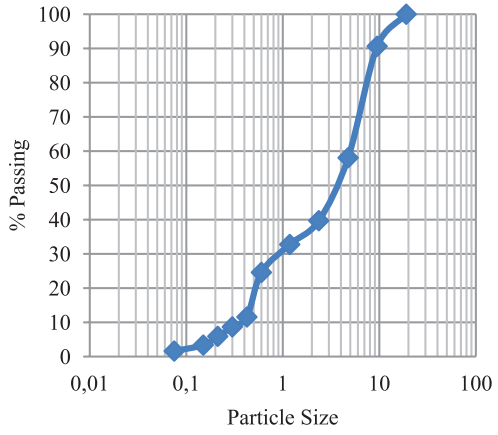

Fig. 1b. Particle size analysis for soil sample B
1b. ábra B jelű talaj minta szemcseméret eloszlása

Soil sample	% Passing sieve No 10 (2 mm)	% Passing sieve No 40 (425 μm)	% Passing sieve No 200 (75 μm)	Liquid limit	Plastic limit	Plasticity index	Group index, GI*	AASHTO classification*	Fineness modulus
A	84%	52%	30%	39.8%	19.3%	20.5%	2	A-2-6	2.18
B	36%	12%	2%	47.9%	41.6%	6.3%	0	A-1-a	4.33

*Classification and group indices are based on the AASHTO soil classification

Table 1. Physical properties of the lateritic soil samples
1. táblázat Laterit talaj minták fizikai jellemzői

Chemical constituents	CKC (%)		ASTM C618-12 requirement for pozzolans	Soil sample A	Soil sample B
SiO_2	41.08	95. 22	$SiO_2+Al_2O_3+Fe_2O_3$;≥70%	53.85	41.26
Al_2O_3	52.86			29.01	40.02
FeO_3	1.28			6.03	4.32
CaO	3.00			4.15	1.55
MgO	0.10			0.04	0.00
K_2O	0.12		1. 5% max	0.04	0.00
Na_2O	0.06		1. 5% max	0.10	0.08
P_2O_5	0.03			0.07	1.06
SO_3	0.12		4% max	0.10	1.58
LOI	1.16		10% max	6.66	10.25
Total	99.81			100.05	100.12
CEC (meq/100gm)	2.455			1.738	1.678

Table 2. Chemical analysis of the materials used
2. táblázat Vizsgált anyagok kémiai összetétele

The chemical analysis results are presented in *Table 2*. Typical of lateritic soils, the soils predominantly consists of silicates and aluminates. For the two soils, the oxides add up to about the same amount – 82.86% for the A-2-6 soil and 81.28% for the A-1-a soil respectively. However, the A-2-6 soil has more silicates. The A-2-6 soil has silicates constituents of 53.85% (more than half the total chemical constituents) and aluminate only about half of this (29.01%). However, the silicate-aluminate ratio is almost equal for the A-1-a soil (41.26%-40.02%). Moreover, the CEC results as presented in *Table 2* shows that the two soils have CEC of 1.678 meq/100gm (A-1-a soil) and 1.738 meq/100gm (A-2-6 soil).

3. 2. Properties of CKC

The CKC came out as creamy-white material after calcining. The result of chemical analysis, also presented in *Table 2*, shows that the material passed the ASTM requirements with the constituents of SiO_2, Al_2O_3 and Fe_2O_3 totalling 95.22%; more than the required 70% minimum. Other conditions were satisfied as well signifying the suitability of the calcined clay as a pozzolan. The CEC of the pozzolan is also determined as 2.455 meq/100gms.

3. 3. Compaction results

The compaction results are presented in *Figs. 2a* and *2b* for maximum dry densities and *Figs. 3a* and *3b* for optimum moisture contents respectively. The unstabilised A-2-6 soil (0% binder) has the mean maximum dry density (mdd) of 1.77 kg/m³ (*Fig. 2a*) while the corresponding optimum moisture content (omc) is 15.4% (*Fig. 3a*). For A-1-a soil, corresponding values are 1.87 kg/m³ (*Fig. 2b*) and 9.1% (*Fig. 3b*). The mdd is higher for the A-1-a soil possibly due to the presence of coarser particles, which are likely to be of higher mass than the particles of the A-2-6 soil. As such, the densification brought about by compaction will lead to higher mdd for the A-1-a soil. However, the corresponding omc is lower. This agrees with [17] that this is typical of soils with low plasticity index. Moreover, *Figs. 2a* and *2b* show a general downward trend in the mdd as total binder increases for the two stabilised soils. For each of the five binder mix ratios, the mdd initially increased from control (0%); rising to the peak at 2.5% total binder content in all the cases of the binder mix ratios considered. Thereafter, the mdd reduced gradually as the total binder percentages increased from 2.5% up to 10% total binder content. Expectedly, the omc graph took a reverse trend for the two soils.

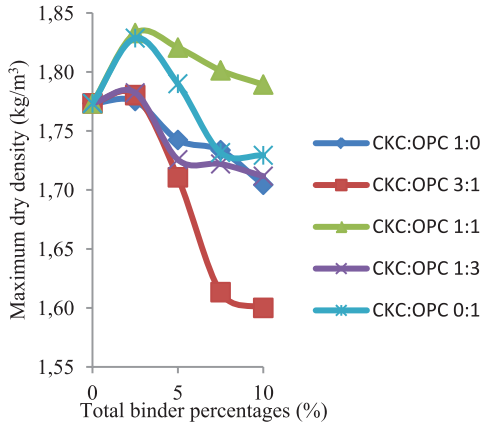

Fig. 2a. Graph of mdd – stabilised A-2-6 soil (sample A)
2a. ábra Stabilizált A-2-6 talaj (A jelű minta): mdd eredmények

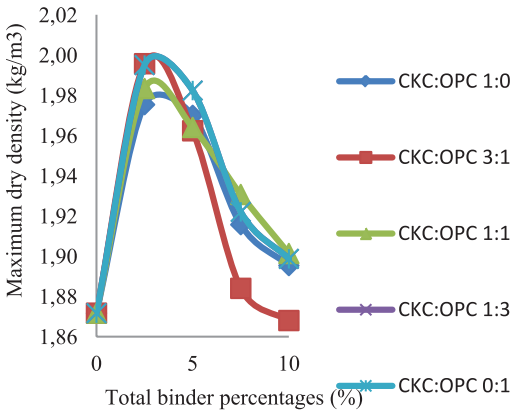

Fig. 2b. Graph of mdd – stabilised A-1-a soil (sample B)
2b. ábra Stabilizált A-1-a talaj (B jelű minta): mdd eredmények

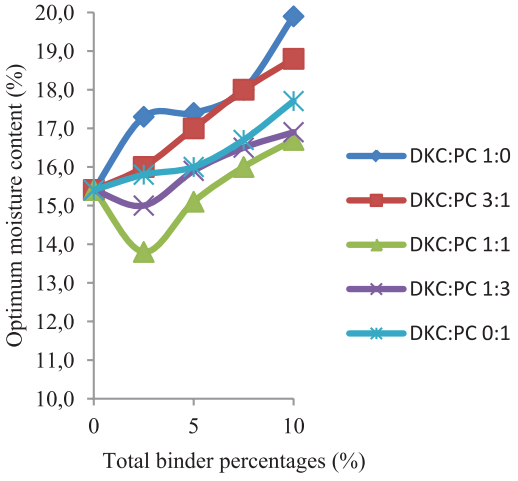

Fig. 3a. Graph of omc – stabilised A-2-6 soil (sample A)
3a. ábra Stabilizált A-2-6 talaj (A jelű minta): omc eredmények

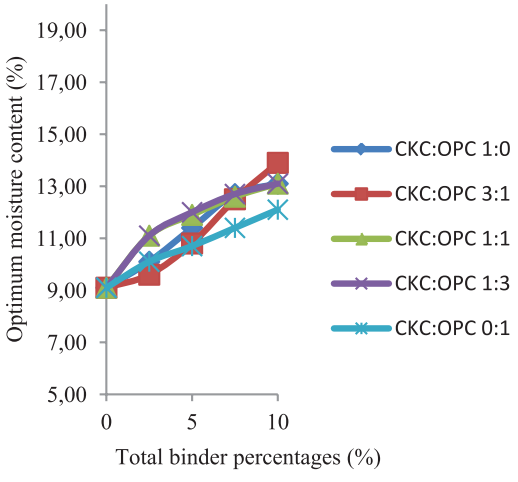

Fig. 3b. Graph of omc – stabilised A-1-a soil (sample B)
3b. ábra Stabilizált A-1-a talaj (B jelű minta): omc eredmények

The general trend in the mdd is attributed to the formation of cementitous products from the added binders, which aids the cementation and agglomeration of the particles of the stabilised soils. This results to formation of coarse particles, which occupy larger spaces, implying an increased volume. Once volume increases, the density reduces for the same weight of soil. It is premised that the degree of flocculation/agglomeration increases with increasing content of binders (increasing percentages), leading to further formation of large particles and increasing volumes for the same soil weight. As such, the mdds will further reduce as more binders are added. In another vein, the observed trends can also be explained using the concept of the replacement of lateritic soils by less dense binder materials such as CKC and PC. The replacement causes a reduction in the overall weight, and by extension, the dry density. The more the replacement, the more the density reduces [15, 18]. However, the initial increase in mdd at 2.5% could be due to the filler effect of the binder which increases the density.

The increasing trend in moisture content is also typical. With the increasing addition of cementitious binders, more moisture is needed to facilitate movement of ions in the hydration/pozzolanic processes [4, 18, 19]. As a result, more water is added, increasing the moisture content. Thus, typical of the effect of stabilisers on the compaction characteristics of soils, the mdd generally decreased at increasing total binder content while the omc generally took a reverse trend. These identified trends are typical of compaction behaviour of lateritic soil stabilisation with binders such as cement, lime, rice husk ash, bamboo leaf ash etc [18, 19, 20, 21].

Though the trend as binder percentage increase was similar for the two soils, the results show that, across the binder mix ratios, the mdds are not the same in values for A-2-6 soil (*Fig. 2a*). The mdds at the 2.5% total binder level for CKC:PC ratio 1:1 and 0:1 were 1.833 kg/m^3 and 1.829 kg/m^3 respectively. The mix ratios of 3:1, 1:3 and 1:0 had mdd values of 1.780 kg/m^3, 1.782 kg/m^3 and 1.775 kg/m^3 respectively. Also, corresponding values at 5.0% were 1.821 kg/m^3 and 1.790 kg/m^3 for CKC:PC ratio 1:1 and 0:1 while mix ratios of 3:1, 1:3 and 1:0 had mdds of 1.711 kg/m^3, 1.726 kg/m^3 and 1.742 kg/m^3 respectively. These differences were also reported at the other binder levels (7.5% and 10.0%). However, for A-1-a soil, the graphs show that performances are close across the mix ratios that it becomes difficult to distinguish between them (*Fig. 2b*). In other words, at each binder percentage, the differences in mdds across the five binder mix ratios were not very clear-cut. At 2.5%, the soil stabilised using CKC:PC mix ratios of 3:1 and 0:1 had about the same mdds; 1.996 kg/m^3 and 1.995 kg/m^3 respectively. The mdds for mix ratios 1:0 and 1:3 also had almost the same value of 1.975 kg/m^3 and 1.974 kg/m^3 respectively. The soil stabilised with binder mix ratio 1:1 had mdd of 1.983 kg/m^3. The mdds at 5%, and 7.5% also showed similar tendencies. It was only at 10% total that there seem to be marked differences in the mdds across the binder mixes. In a similar manner, the variations of the corresponding omcs across the binder mixes show the same trend as the mdds. This is as shown in *Figs. 3a* and *3b* for the two stabilised soil samples.

The variations of the compaction characteristics of the stabilised soils across the different binder mixes can be attributed to the differences in particle size and CEC of the soils. Soils with fine particles possesses high specific surface but the total volume of voids or pore spaces is low. The cementitous products could easily fill up the pore spaces and cause agglomeration of the particles. Thus, the variations in the volume of cementitous products formed

due to the variations in binder mixes could easily be reflected in the compaction attributes of the A-2-6 soil being a fine-particle soil. However, the A-1-a soil with larger particles possesses larger pore spaces. This requires more volumes of cementitous products to fill. Thus, the effect of varying the binder mixes only will be felt at high binder contents. This explains why differences in compaction behaviour across the binder mixes became only visible at about 10% binder content. The CEC can also influence pozzolanic reactions as well. However, the CECs of the two soils are almost the same (1.738 meq/100gm and 1.678 meq/100gm respectively). Thus, the differences noticed in the compaction behaviour of the two stabilised soils cannot be significantly attributed to their CECs. Moreover, the pozzolan CKC with a higher CEC of 2.455 meq/100gm is likely to prefentially participate in cation exchange reaction (pozzolanic reaction) between the excess lime from cement hydration and available aluminosilicate material. Thus, rather than the soils, the pozzolan with a higher CEC goes into the pozzolanic reaction as the preferred source of aluminosilicates.

3. 4. Statistical analysis

The observed differences in the mdds and in the omcs across the five binder mixes at each level of binder content (the percentages) were tested for significance using ANOVA statistical tool. The result shows that, for mdd, ANOVA's F (4.17) is greater than the critical F value of 3.06 for the A-2-6 soil (*Table 3*). The corresponding ANOVA analysis on omc gives the ANOVA's F being 4.03 versus the critical value of 3.06 ($p \leq 0.05$ in both cases). These results show that the variations in the binder mix ratios have given rise to signifcant differences in the compaction charateristics of the stabilised soils.

	mdd for sample A	mdd for sample B	omc for sample A	omc for sample B
F	4.18	0.19	4.03	0.56
Fcritical	3.06	3.06	3.06	3.06
P-value	0.02	0.94	0.02	0.70

Table 3. Summary of ANOVA (single factor)
3. táblázat Egy faktoros ANOVA eredményei

Moreover, for the A-1-a soil, *Table 3* shows that there are no statistically significant differences in the mdd values across the binder mix ratios at each total binder level. The F value of 0.19 was less than the critical F's value of 3.06 ($p = 0.94$). For omc, the critical value of F (3.06) was more than the F's value of 0.56 ($p = 0.70$). Thus, it implies that, irrespective of any binder combination, about the same results are observed.

4. Conclusions

From the results, it can be concluded that compaction characteristics of CKC-stabilised soil depends on the attributes of the soil; the particle size in particular. Considering this, it can be concluded that CKC as a pozzolan could not solely alter behavior through pozzolanic stabilisation. Rather, the soils' properties also have a significant role to play in the compaction outcome. Thus, in the use of CKC-cement blends for stabilisation for flexible road pavement, the property of the soil is a major factor to consider. The pozzolanic potential of CKC does not override this factor.

References

[1] Aboubakar, M. A. – Ganjian, E. – Pouya, H. – Akashi, A. (2013): A study on the effect the addition of thermally treated Libyan natural pozzolan has on the mechanical properties of ordinary Portland cement mortar, *International Journal of Science and Technology*, Vol. 3, No. 1, pp. 79-84.

[2] Justice, J. M. (2005): Evaluation of metakaolins for use as supplementary cementitious materials. An *Unpublished MSc thesis*, School of Material Science and Engineering, Georgia Institute of Technology.

[3] Kolovos, K. G. – Asteris, P. G. – Cotsovos, D. M. – Badogiannis, E. – Tsivilis, S. (2013): Mechanical properties of soilcrete mixtures modified with metakaolin. *Construction and Building Materials*, Vol. 47, pp. 1026–1036. https://doi.org/10.1016/j.conbuildmat.2013.06.008

[4] Amu, O. O. – Adetuberu, A. A. (2010): Characteristics of bamboo leaf ash stabilisation on lateritic soil in highway construction. *International Journal of Engineering and Technology*, Vol. 2, No. 4, pp. 212-219.

[5] Olonade, K. A – Jaji, M. B – Adekitan, O. A. (2016): Experimental Comparison of Selected Pozzolanic Materials. *Proceedings of the 2nd International Conference on Advances in Cement and Concrete Technology in Africa*, Dares Salaam, Tanzania, January 27 -29, pp. 309-314.

[6] Ilić, B. R. – Mitrović, A. A. – Miličić, L. R. (2010): Thermal treatment of kaolin clay to obtain metakaolin, *Hemijska industrija*, Vol. 64, No. 4, pp. 351–356. https://doi.org/10.2298/HEMIND100322014I

[7] Justice, J. M. – Kennison, L. H. – Mohr, B. J. – Beckwith, S. L. – McCormick, L. E. – Wiggins, B. – Zhang, Z. Z. – Kurtis, K. E. (2005): Comparison of two metakaolins and silica fume used as supplementary cementitious material. *Proceeding of the Seventh International Symposium on Utilization of High-Strength/High Performance Concrete,* Washington DC, 20-24 June, 2005.

[8] BS 1377 (2000) British standard methods for testing soils in civil engineering, parts 1 – 9. *British Standards Institute*, London.

[9] Das, B. – Sobhan, K. (2013): Principles of Geotechnical Engineering, 8th ed. *Cengage Learning*, US.

[10] Adekitan, O. – Ayininuola, G. M. – Jaji M. B. (2016): Optimizing the Thermal Treatment of Abeokuta Kaolin (South-West Nigeria) for Production of Natural Pozzolan. *Proceedings of the 2nd International Conference on Advances in Cement and Concrete Technology in Africa*, Dar es Salaam, Tanzania, 27-29, January 2016. BAM Federal Institute for Materials Research and Testing, Berlin, pp. 99-105.

[11] Fernandez, R. – Martirena, F. – Scrivener, K. L. (2011): The origin of the pozzolanic activity of clay minerals: A comparison between kaolinite, illite and montmorillonite, *Cement and Concrete Research,* Vol. 41, pp. 113-122. https://doi.org/10.1016/j.cemconres.2010.09.013

[12] Ferraris, C. F. – Hackley, V. A. – Avil´es, A. I. (2004): Measurement of particle size distribution in Portland cement powder: analysis of ASTM round robin studies. *Cement, Concrete, and Aggregates*, Vol. 26, No. 2, pp. 1 – 11. https://doi.org/10.1520/CCA11920

[13] ASTM C618-12. (1994): Standard specification for coal fly ash and raw or calcined natural pozzolan for use in concrete. *ASTM International*, US.

[14] BS 1924 (2000): British standard methods of testing for stabilised soils. *British Standards Institute*, London.

[15] Jimoh, Y. A. – Apampa, O. A. – Adekitan, O. (2014): Enhancing the agricultural value chain through the use of corn cob ash in pavement construction. *Technical Transactions of the Nigerian Society of Engineers*, Vol. 48, No. 1, pp. 13 – 22.

[16] Indiana Department of Transportation (INDOT), (2008). Design procedures for soil modification or stabilisation. Report of Production

Division, Office of Geotechnical Engineering, *Indiana Department of Transportation*, US.

[17] Laskar, A. – Pal, S. K. (2012): Geotechnical characteristics of two different soils and their mixture and relationships between parameters. *EJGE 17*, pp. 2821 – 2832.

[18] Grytan, S. – Rafiqul, I. – Muhammed, A. – Rokonuzzaman (2012): Study on the geotechnical properties of cement based composite fine-grained soil. *International Journal of Advanced Structures and Geotechnical Engineering*, Vol. 1, No. 2, pp. 42 – 49.

[19] Otoko, G. R. (2014): On the economic use of cement in soil stabilisation. *International Journal of Engineering and Technology Research*, Vol. 2, No. 1, pp. 1-7.

[20] Ola, S.A. (1983): Tropical soils in engineering practice. *Balkema Publishers*, Rotterdam, Netherlands.

[21] Amu, O. O. – Bamisaye, O. F. – ad Komolafe, I. A. (2011): The suitability and lime stabilisation requirement of some lateritic soil samples as pavement material. *International Journal of Pure and Applied Sciences and Technology*, Vol. 2, No. 1, pp. 29-46.

Ref.:
Ayininuola G. M. – **Adekitan,** O. A.: *Compaction characteristics of lateritic soils stabilised with cement-calcined clay blends*
Építőanyag – Journal of Silicate Based and Composite Materials, Vol. 69, No. 2 (2017), 33–39. p.
https://doi.org/10.14382/epitoanyag-jsbcm.2017.7

Cementtel és kalcinált agyaggal stabilizált laterit talajok tömöríthetőségi jellemzői

A kalcinált kaolin egyike azoknak a cement kiegészítő anyagoknak, amelyekkel csökkenthető a cement felhasználásából eredő üvegházhatású gázok kibocsátásának mértéke. A betonban történő felhasználás szakirodalma gazdag, azonban a rugalmas útpálya szerkezetek alatti talaj stabilizáció terén kevés vizsgálat történt. Jelen cikk ezt mutatja be. Két laterit talaj stabilizálását tanulmányozták a kutatás során. A vizsgált portlandcement (PC) : kalcinált kaolin (CKC) arányok a következők voltak; CKC:PC = 0:1, 1:3, 1:1, 3:1 és 1:0. A talajok tömegére vonatkoztatott kötőanyag arán 0 (kontroll), és 2.5, 5, 7.5, 10% volt. A kalcinált kaolint laboratóriumban állították elő, dél-nyugat Nigériából származó kaolin 700°C-on történő, 1 órás hőkezelésével. A vizsgált laterit talajok AASHTO szerinti osztályozása A-1-a és A-2-6 volt, 2,18 és 4,33 finomsági modulussal, illetve 1,678 meq/100 gms és 1,738 meq/100gms kation cserekapacitással. A vizsgálati eredmények szerint aa A-2-6 osztályú laterit talaj minta tömöríthetősége nagymértékben változott a kötőanyag CKC:PC arányának változtatásával, míg az A-1-a osztályú talajnál ez a hatás minimális volt. Ennek oka elsősorban a szemeloszlásban kereshető, mert a két vizsgált talaj kation cserekapacitása csaknem teljesen azonos.
Kulcsszavak: kalcinált kaolinit agyag, normál Portland cement, stabilizálás, tömörítés, kation cserekapacitás, szemcseméret

Synthesis and characterization of MK/Slag geopolymer composites enhanced by various ratios of nano kaolin

Hisham Mustafa Mohamed KHATER ▪ Housing and Building National Research Centre (HBNRC), Cairo ▪ Hkhater4@yahoo.com
Hamdy A. ABDEL GAWWAD ▪ Housing and Building National Research Centre (HBNRC), Cairo
Érkezett: 2017. 03. 13. ▪ Received: 03. 13. 2017. ▪ https://doi.org/10.14382/epitoanyag-jsbcm.2017.8

Abstract
Alkaline activation of slag – metakaolin (AAS) binder enhanced with nano-kaolin for preparation of eco-friendly geopolymer materials (40:60 wt. %), of geopolymer binder results in formation of C-A-S-H as well as N-A-S-H gel. Activators used are 10% NaOH solution in addition to 5% liquid sodium silicate both used from the total binder weight), while nano-kaolin was added in the ratio from 0 up to 9% from the total dry weight and replaced the used metakaolin. The properties of the produced geopolymer bricks have been studied through measurement of compressive strength, FTIR, XRD and SEM imaging. Results demonstrate enhancement in both mechanical and microstructural characteristics with nano-kaolin up to 5%, while further increase resulted in agglomeration and strength decrease, also uses of additional activators as sodium aluminate in the ratio of 5% results in strength decline as a results of zeolite increase.
Keywords: Nano-kaolin, Geopolymer, activation, eco-friendly.

Hisham Mustafa Mohamed KHATER
Ph.D. in Physical Chemistry, 2009. Associated Professor in Cement chemistry and Raw Building Materials Technology and Processing since 2015. Researcher in Raw Building Materials Technology and Processing Research Institute, Housing and Building National Research Center (HBRC). Supervisor of XRF laboratory for the chemical analysis of all type of raw building materials, accredited from International American Service IAS 17025 since 2005. Research interest: X-ray fluorescence spectroscopy, X-ray diffraction, Fourier Tranformer-IR spectroscopy, differential thermal analysis, chemical analysis of cements, recycling of waste materials, assessment of clay minerals, low cost and environmentally green building materials, nanotechnology in building materials. Author of more than 20 papers.

Hamdy A. ABDEL GAWWAD
Researcher in Raw Building Materials Technology and Processing Research Institute, Housing and Building National Research Center (HBRC). Research interest: alkali activated geopolymers, carbon nano-tubes, supplementary cementing materials

1. Introduction

Alkali activated cements refer to any system uses an alkali activator to initiate a reaction or a series of reactions which will produce a material with cementitious property. Alkali activated cement, alkali activated slag and fly ash, and geopolymers are all considered to be alkali activated cementitious systems, however, it is expected that the structures of these materials are vastly different and result from different chemical mechanistic paths. It is commonly acknowledged that calcium silicate hydrate (CSH) is the major binding phase in Portland cement [1, 2] and alkali activated slags [3]. However, the binding property of geopolymers is generally assumed to be as the result of the formation of a three-dimensional amorphous aluminosilicate network [4–6]. Davidovits stated that geopolymers formed by polymerization of individual aluminate and silicate species, dissolved from their original sources at high pH in the presence of alkali metals [6-7]. The resultant products are reported to have the general formula $Mn–[[–Si–O_2]z–Al–O]_n$- wH_2O where M is the alkali element, –indicates the presence of a bond, z is 1, 2 or 3 and n is the degree of polymerization. Theoretically, any cations in the medium can be used in balancing the three dimensional network, however sodium (Na^+) and potassium (K^+) ions are the most common univalent cations [7, 8].

Major difference between geopolymers and Portland cement in terms of chemical composition is calcium, where calcium is not essential in any part of a basic geopolymeric structure, but can form CSH which form nucleation sites for geopolymer accumulation. On the other hand, CSH which is the most important binder in cement formed as a results of hydration of tri-calcium silicate and di-calcium silicate.

Recently, many studies conducted on various metakaolin (MK)/ lime (calcium hydroxide) and MK-blended cement systems [9, 10]. Cabrera and coworkers [10, 12, 13] found that activation of metakaolin in the presence of calcium hydroxide caused rapid formation of CSH, C_2ASH_8 (stratlingite) and C_4AH_{13} (tetracalcium aluminate hydrate). Alonso and Palomo [9, 11] found alkaline activation of metakaolin in the presence of calcium hydroxide in a highly alkaline environment, led to formation of an amorphous sodium aluminosilicate, with the same characteristics as a geopolymeric gel. This geopolymeric gel formed was found to be similar to that obtained when metakaolin was activated in the absence of calcium hydroxide, in addition to a secondary product which is CSH gel. There are many factors affecting the nature of the end alkaline product [9, 10] such as: elemental composition, mineralogy, physical properties (e.g. surface properties, particle size distribution) of both aluminosilicate and calcium sources, alkalinity, nature of soluble alkaline metal present, as well as curing conditions and use of any pre-treatment. The chemical reactions that take place in the MK/GGBFS system are expected to be more complex than in the MK/lime system, as GGBFS consists of a mixture of glassy phases reacting at different rates depending on the ratio of water cooled slag to metakaolin and molar ratio of Na_2O/SiO_2 molar ratio.

Uses of nano-particles in cement and concrete can lead to improvements in the nanostructure of building materials [14]. Nano-materials show unique physical and chemical properties that can lead to the development of more effective materials than ones which are currently available [15]. The extremely fine size of nano-particles yields favorable characteristics. Ginebara et al. [16] reported that the particle size can greatly affect the hydration kinetics of cement. Ultra small magnetic ferrite

Oxide content (%)	SiO_2	Al_2O_3	Fe_2O_3	CaO	MgO	SO_3	K_2O	Na_2O	TiO_2	MnO	P_2O_5	Cl^-	L.O.I.	BaO	SrO	Total
Water-cooled slag (GGBFS)	36.67	10.31	0.50	38.82	1.70	2.17	1.03	0.48	0.57	4.04	0.04	0.050	0.12	3.28	0.18	99.96
Kaolin	56.33	27.61	1.32	0.18	0.06	0.06	0.04	0.08	3.73	-	0.13	0.05	10.17	-	-	99.97
MK (fired kaolin at 800°C for 2 hrs)	57.50	35.10	1.59	0.64	0.17	0.25	0.15	0.12	2.85	0.00	0.13	0.06	1.14	-	-	99.70
Nano-kaolin	57.53	38.63	0.35	0.11	0.30	0.56	0.03	0.01	1.02	0.01	0.41	-	0.93	-	-	99.88

Table 1. Chemical composition of starting materials (Mass, %)
1. táblázat Alapanyagok kémiai összetétele (m%)

nano particles (diameter smaller than 15 nm) when dispersed in liquid carrier possess both fluid and magnetic properties, and may lead to numerous industrial applications [17]. Several studies were performed concerning with applications of nanotechnology and nano materials in Construction [18-20], whereas nano-kaolin considered to be high reactive and low price nano-material which can be used as alternative to the high price nano-materials. Where, nano-silica and nano-alumina are mainly constituents present in nano-metakaolin (NMK) chemical structure. Various improvements obtained when NMK used as cementitious materials due to its high pozzlolanic activity [21].

Several author used NMK to improve the physico-mechanical properties and durability of cement mortar. Morsy et al. [22] reported an increase in compressive strength by 18% when adding 6% NMK compared to control cement mortar. Also, a significant increase in the compressive and flexural strength was observed when different amount of NMK added to cement mortar containing fly ash [23]. The fire resistant of cement mortar with or without NMK was studied by Morsy et al. [24]; they showed that cement mortar containing 10 and 15 wt.% NMK exhibited slow decrease in compressive strength compared to control sample as the exposure temperature increased up to 800°C. On the other hand, Baueregerm and co-authors [25] found an enhancement of 50 and 60% in the 16 hr early compressive and flexural strength, respectively, by the addition of 5% NMK to Portland cement.

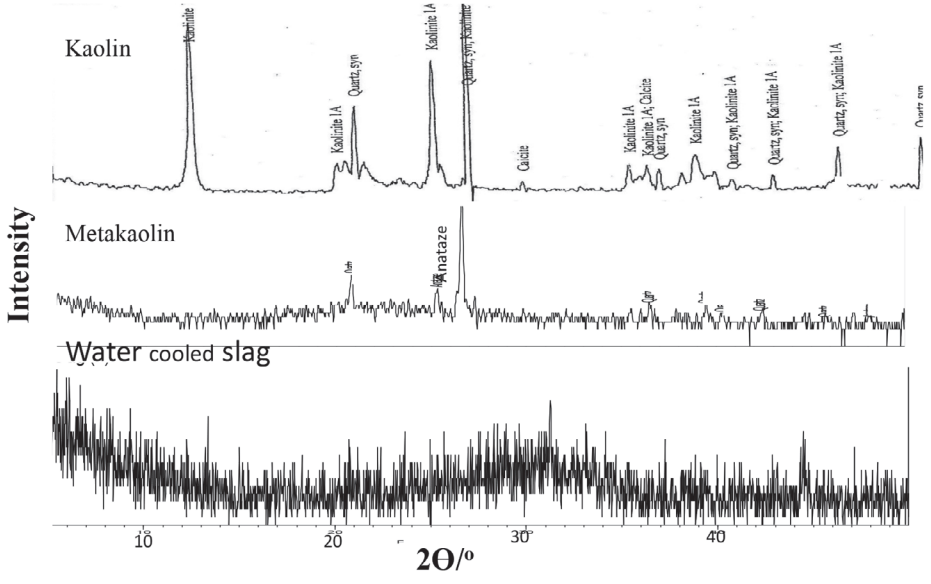

Fig. 1. X-Ray diffraction pattern of the starting raw materials
1. ábra Alapanyagok röntgendiffraktogramjai

There are few researches studied the impact of nano-kaolin on the properties of geopolymer based binder. Khater and co-authors studied the effect of NMK on the physico-mechanical properties of alkali activated slag geopolymer [26]. They found better enhancing in the mechanical properties of geopolymer by addition of 1% NMK compared with control mix up to 90 days, while higher ratio leads to matrix dilution and so negatively affect mechanical characteristics of the resulting products.

The main purpose of this work is to demonstrate the activation and enhancement effect of nano-kaolin materials on the performance of the produced geopolymer materials by alkaline activation of amorphous water cooled slag/Mk materials, where this target can be fulfilled by tracing of the hardened geopolymeric products by X-ray diffraction, FTIR and SEM are used for scanning and analysis of the composite structure of nano geopolymer. While, the compressive strength measurement was used to evaluate the mechanical performance of the geopolymer mixes.

2. Experimental procedures

2.1. Materials

Studied materials are water cooled slag sourced from Iron and Steel Factory-Helwan, Egypt, and Kaolinite material collected from El-Dehesa, South Sinai, Egypt, both chemical composition illustrated in Table 1. Sodium hydroxide (NaOH) with purity 99% in the form of pellets used as alkali activators, obtained from SHIDO Co., Egypt, while liquid sodium silicate (LSS, Na_2SiO_3. $9H_2O$) from Fisher company consists of 32% SiO_2 and 17% Na_2O with Silica modulus SiO_2/Na_2O equal 1.88 and its density is 1.46 g/cm^3, also laboratory prepared sodium aluminate with 47% Al_2O_3 and 48.10% Na_2O. Kaolinite material used for Nano-kaolin (NK) preparation brought from Middle East for Mining Investment Co., Egypt.

Composition of the starting raw materials is illustrated in *Table 1*, while mineralogical characterization of the raw materials is represented in *Fig. 1*. Water cooled slag is a rich aluminosilicate material and composed from the dominant content

of SiO_2, CaO, Al_2O_3 Fe_2O_3,and MnO as illustrated from *Table 1*, while its mineralogical composed of amorphous materials.

Whereas, the chemical composition of kaolin showed that it contains high percentage of alumina of about 56% with about 27% of silica, in addition to little amount of calcium and magnesium as presented in *Table 1*, however the mineralogical composition indicated that kaolinite composed of minor amount of quartz minerals 30% and 70% kaolin, whilst NK composed of about 95% pure kaolin and 5% quartz. This kaolinite material was thermally treated at 800°C for 2 hrs with a heating rate of 5°C /min., to form MK. This temperature was chosen on the basis of an earlier research works, where calcinations below 700°C results in a less reactive metakaolinite with more residual kaolinite, above 850°C crystallization occurs and reactivity declines [27-30].

2.2 Synthesis of NK

Kaolin nanoparticles are synthesized by firing ultra-pure kaolin at 800°C for 2 hrs with a heating rate of 5°C/min to form an amorphous nano precursors, where firing results in the formation of NK particles with the average particle size 35-53 nm, while its raw material before firing has a grain size about 100% < 10 μm as indicated from the TEM (see *Fig. 2*). *Fig. 3* illustrates XRD pattern of fired treated and untreated kaolin materials, the pattern reflects that mostly all the kaolin residues are distorted and dehydrated forming amorphous NK material.

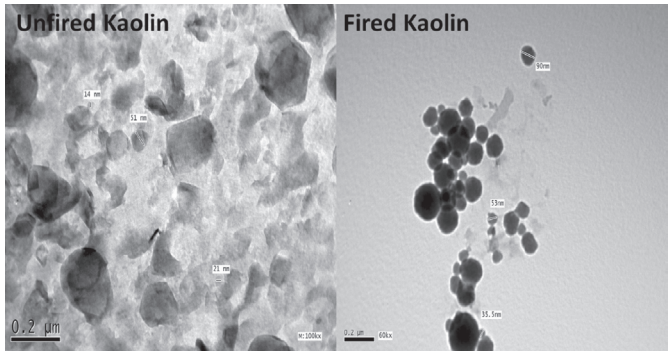

Fig. 2. Transmission electron micrograph of fired and unfired Kaolinite material provided from Middle East for mining investment
2. ábra Kiégetett és eredeti kaolin elektronmikroszkópos felvételei (forrás: Közel-Keleti bányafeltárás)

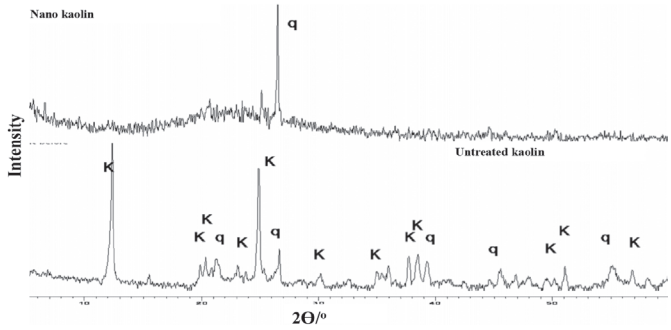

Fig. 3. X-Ray diffraction pattern of kaolin material before and after firing (provided from Middle East for mining investment) (K: kaolin, Q: quartz)
3. ábra Kiégetett és eredeti kaolin röntgendiffraktogramjai (forrás: Közel-Keleti bányafeltárás) [K: kaolin, Q: kvarc]

2.3. Geopolymerization and curing

Geopolymer made by hand-mixing raw materials of each mixture passing a sieve of 90 μm with the alkaline solution for 10 min and a further 5 min with a mixer. All investigations involved using 15 % NaOH and 5 % Na_2SiO_3 of dry mixes, while uses an additional 5% sodium aluminate as a method for comparative activation. The water-binder material ratio (w/b) was in the range of 0.22:0.24 by mass. NK was added to the binding material (Blast furnace slag and metakaolin in the ratio of 40: 60, wt.%) in small quantities 0 up to 9% from the total weight and as a replacement of metakaolin as illustrated in Table 2, mixed well with part of the total water using a magnetic stirrer, the other part of water is mixed with the activators, then added to the binding material in the mixer followed by the deflocculated NK, and finally superplasticizer (Glenium Ace) in the range of 1.50 : 2.30 %. Paste mixture were cast into 25×25×25 mm cubic-shaped moulds, vibrated for compaction and sealed with a lid to minimize any loss of evaporable water.

All mixes were left to cure undisturbed under ambient temperature for 24 hrs, followed by curing temperature at 40°C with a 100 % relative humidity. At the end of the curing regime, the specimens were subjected to the compressive strength measurements and then the resulted crushed specimens were subjected to stopping of hydration process using solution of alcohol/acetone (1:1), followed by washing with acetone as recommended by [31, 32] in order to prevent further hydration

Mix no.	Water-cooled slag (WCS), %	Metakaolin (MK), %	Nano-kaolin (NK), %	NaOH, %	Sodium silicate, %	Sodium aluminate, %	Superplasticizer, %	Water/binder, %	T.M_2O/Al_2O_3	SiO_2/Al_2O_3	T.M_2O/SiO_2
Y0	40	60	0	15	5	-	1.50	0.22	1.063	2.04	0.31
Y1	40	59	1	15	5	-	1.50	0.22	1.048	2.01	0.31
Y3	40	57	3	15	5	-	1.70	0.22	1.060	2.03	0.31
Y5	40	55	5	15	5	-	1.90	0.24	1.060	2.03	0.31
Y7	40	53	7	15	5	-	2.12	0.24	1.056	2.02	0.31
Y9	40	51	9	15	5	-	2.30	0.24	1.054	2.01	0.31
X	40	60	0	15	5	5	1.50	0.24	1.163	1.88	0.36

Table 2. Composition of the geopolymer mixes (m%)
2. táblázat Alapanyagok kémiai összetétele (m%)

and for further analysis and followed by drying of the crushed specimens for 24 hrs at 80°C and then preserved in a well tight container until the time of testing.

2.4. Methods of investigation

Chemical analysis was carried out using Axios, WD-XRF Sequential Spectrometer (Panalytical, Netherland, 2009). Compressive strength tests were carried out using five tones German Brüf pressing machine with a loading rate of 100kg/min determined according to ASTM-C109 [33]. The XRD analysis was carried out using a Philips PW3050/60 Diffractometer. The data were identified according to the XRD software. The microstructure of the hardened alkali activated water cooled slag was studied using SEM Inspect S (FEI Company, Netherland) equipped with an energy dispersive X-ray analyzer (EDX). The removal of free water was accomplished by using alcohol/acetone method as recommended as recommended by [31, 32]. Transmission Electronic Microscopic (TEM) (type JEOL – JEM – 1230) of magnification up to 60000 was to measure the particle size of the nanoparticles. Bonding characteristics of the alkali activated specimens were analyzed using a Jasco-6100 Fourier transformed infrared spectrometer FTIR. Test sample was ground and uniformly mixed with KBr at a weight ratio KBr: specimen=200:1. The mixture, 0.20 g was pressed to a disk of 13 mm in diameter for analysis at 8 t/cm^2. The wave number was ranging from 400 to 4000 cm^{-1} [34, 35].

3. Results and discussion

3.1. Mineralogical investigation

Fig. 4, shows XRD pattern of 90 days alkali activated slag / MK (40: 60, wt.%) geopolymer mixes incorporated various NK content from 0 up to 9% as a partial replacement of MK. Pattern illustrate a band in the region of 6° to 10° 2θ for aluminosilicate gel and band in the region of 25° to 35° 2θ characterizing glassy phase of geopolymer constituents, the formation of intense peak of Faujasite of zeolite, zeolite A as well as sodalite in the control mix along with a sharp intense peaks for metastable phases of hydroxysodalite favours the lower geopolymer characteristic as known by their lower branching ability, the previous notice comes in accordance with Zuhua et al. [36], where the crystalline zeolite phases are destructive to the consistent distribution of geopolymers.

Addition of 1% NK results in decreasing crystalline zeolites as the nanomaterials offers a nucleation sites [29, 30] or geopolymer accumulation and so increases in the formed amorphous constituents in addition to shifting of the geopolymer region into lower 2θ, reflecting the increased amorphous constituents on the expense of the crystalline geopolymer. Increasing NK to 5% results in an extra enhancement in the geopolymerization reactions as the possibility for extra nucleation sites facilitate the accumulation and activation of the formed geopolymer as well as formation of CSH phases as allocated at 29.4° as well as Reversedite at 5.5 and 7.2°, where the formed CSH results from the interaction of freely dissolved silica with Ca species in the matrix forming CSH, in spite this binder can positively affect the structure by acting as nucleation sites for geopolymer formation and crystallization [37] as reflected on the mineralogical and structural composition of the formed geopolymer which can be in coherent with the increased Si/Al ratio (2.03) with NK forming poly-sialate siloxy chains, as well as T.M_2O/A_2O_3 which favours the amorphous geopolymer formation than crystalline one.

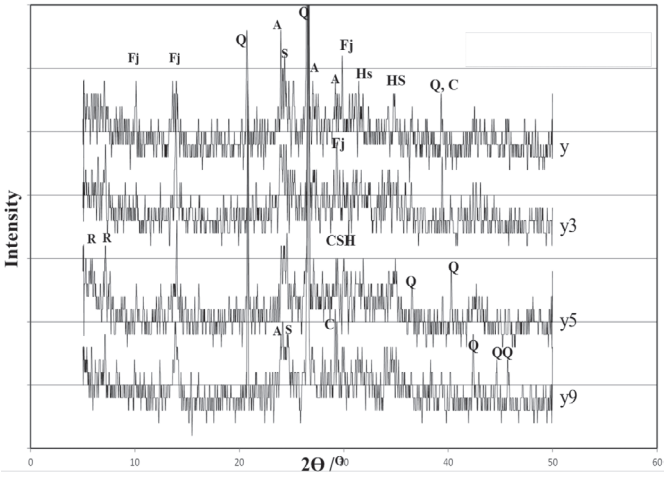

Fig. 4. XRD pattern of 90 days alkali activated MK-slag Geopolymer specimens having various NK rations as a partial replacement of metakaoline (Q: Quartz, A: ZeoliteA, FJ: Faujastine, R: Reversedite, CSH: Calcium silicate hydrate, S: Sodalite, HS: Hydroxysodalite, C: Calcite)

4. ábra 90 napos korú alkáli aktivált MK-kohósalak geopolimer keverékek röntgendiffraktogramjai különböző NK adagolás mellett [Q: kvarc, A: zeolit A, Fj: Faujasit, R: Reversedit, CSH: kalcium-szilikát-hidrát, S: szodalit, HS: hidroxoszodalit, C: kalcit]

However, further increase in NK content up to 9%, results again in an increase in the zeolitic phases as reflected on an increased broadness and intensity of Faujasite, sodalite and zeolite-A peaks, related mainly to the increased agglomeration of the added nanomaterial that will negatively affect the contact between the interacting geopolymer particles and so hinder the propagation of the geopolymerization reaction, so that the formed chains will be more prone to crystallization than propagation as well as formation of three dimensional network. Also, the agglomerated NK results in an increased porosity as well as increased carbonation within the matrix as indicated in calcite peak at 29.35°.

On investigating the effect of curing time up to 180 days on the control geopolymer specimen without NK, XRD pattern *Fig. 5*, illustrate the increase in CSH phases (reversedite, CSH) emphasizing an increased dissolution of binding slag's calcium and interacting with available free silica forming additional CASH binder phases in addition to CSH as a result of increased dissolution with time, also a noticeable increase in transformation of amorphous geopolymer structure into crystalline zeolite (Faujasite, sodalite, zeolite-A) with time is predominant which confirmed by the increased intensity of the previous phases with time up to 90 days, however further time increase results in the decrease in the broadness of the zeolite phases as a results of nucleation effect by CSH which facilitate and offer nucleation sites for geopolymer condensation and so hinder crystallization of geopolymer, then strengthen the formed matrix with time. There is small peak for calcite at 23.05° which may be resulted from the carbonation of CSH as well as any free alkalis within the matrix.

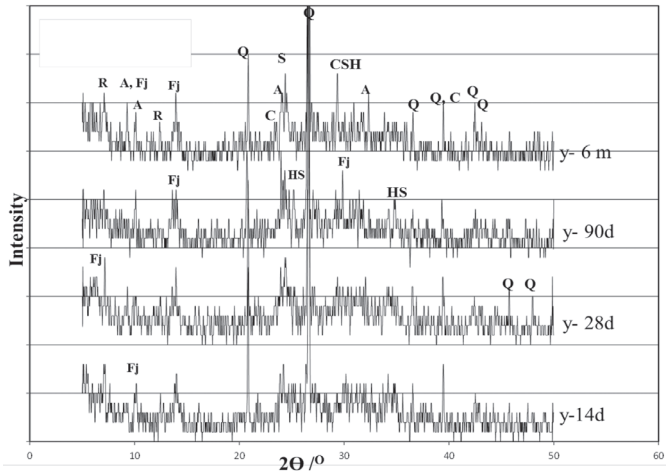

Fig. 5. XRD pattern of alkali activated control Geoplymer specimens MK-salg cured up to 180 days (Q: Quartz, A: ZeoliteA, FJ: Faujastine, R: Reversedite, CSH: Calcium silicate hydrate, S: Sodalite, HS: Hydroxysodalite, C: Calcite)

5. ábra 180 napos korú alkáli aktivált kontroll MK-kohósalak geopolimer keverékek röntgendiffraktogramjai [Q: kvarc, A: zeolit A, Fj: Faujasit, R: Reversedit, CSH: kalcium-szilikát-hidrát, S: szodalit, HS: hidroxoszodalit, C: kalcit]

Increasing in the activator by adding 5% sodium aluminate, results in an increase in the available sodium within the matrix which undergoes carbonation as depicted from increased calcite content in *Fig. 6*, also the increased sodium cations suppressed the propagation of geopolymer network and favours the oligomer formation as well as short chains geopolymer which will be susceptible to crystallization into zeolite as come in accordance with increased Faujasite and hydroxysodalite peaks [34] as compared with the control mix without aluminate source.

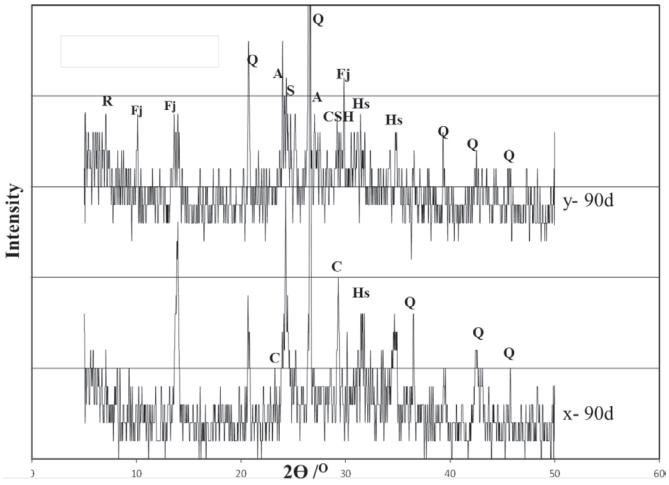

Fig. 6. XRD pattern of 90 days alkali activated slag/MK Geoploymer specimens activated by various activators (Q: Quartz, A: ZeoliteA, FJ: Faujastine, R: Reversedite, CSH: Calcium silicate hydrate, S: Sodalite, HS: Hydroxysodalite, C: Calcite)

6. ábra 90 napos korú alkáli aktivált MK-kohósalak geopolimer keverékek röntgendiffraktogramjai különböző aktivátorok alkalmazása esetén [Q: kvarc, A: zeolit A, Fj: Faujasit, R: Reversedit, CSH: kalcium-szilikát-hidrát, S: szodalit, HS: hidroxoszodalit, C: kalcit]

3.2. FTIR investigations

FTIR spectra of 90 days cured MK/slag geopolymer specimens having various NK content as a partial replacement of metakaolin are shown in *Fig. 7*. The characteristics bands for the present geopolymer structure are: hydration groups and combined water allocated for stretching vibration of O-H bond at about 3450 cm^{-1} and bending vibration for H-O-H at about 1640 cm^{-1}, stretching vibration of CO_2 located at about1430-1450 cm^{-1}, asymmetric stretching vibration (Si–O–Si) at about 1060 cm^{-1} for non-solubilized silica where T=Si or Al, asymmetric stretching vibration (Ti–O–Si) at about 975 cm^{-1} where T=Si or Al, out of plane bending vibration of CO_2 at about 870 cm^{-1}, symmetric stretching vibration (Si–O–Si)in the region 650-680 cm^{-1} and bending vibration (Si–O–Si and O–Si–O) in the region 420-440 cm^{-1}.

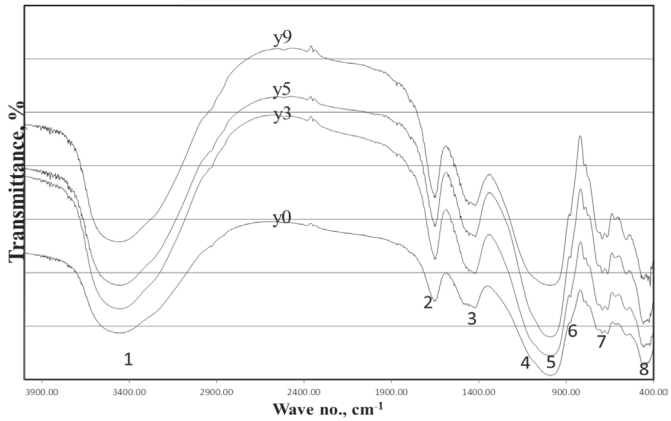

Fig. 7. FTIR spectra of 90 days cured (40 °C and 100% R.H.) MK-slag geopolymer specimens having various NK content [1: Stretching vibration of O-H bond; 2: Bending vibrations of (HOH); 3: Stretching vibration of CO_2; 4: Asymmetric stretching vibration (Si-O-Si); 5: Asymmetric stertching vibration (T-O-Si); 6: Symmetric stretching vibration of CO_2; 7: Symmetric stretching vibrations (Si-O-Si); 8: Bending vibration (Si-O-Si and O-Si-O)]

7. ábra 90 napos korú (40 °C, 100% RH) MK-kohósalak geopolimer keverékek FTIR spektrumai különböző NK adagolás mellett [1: Vegyértékrezgés O-H kötés, 2: Deformációs rezgés (HOH), 3: Vegyértékrezgés CO_2, 4: Aszimmetrikus vegyértékrezgés (Si-O-Si), 5: Aszimmetrikus vegyértékrezgés (T-O-Si), 6: Szimmetrikus vegyértékrezgés CO_2, 7: Szimmetrikus vegyértékrezgés (Si-O-Si), 8: Deformációs rezgés (Si-O-Si és O-Si-O)]

The pattern indicates an increased growth in the hydration bands and combined water at about 3400 and 1600 cm^{-1} with increasing NK increase up to 5% (Y5), then subjected to decrease with further NK increase up to 9%, this can be linked to the enhancement of NK [29, 30] in facilitating the interaction of free dissolved Ca and Si species forming nucleation sites for geopolymer accumulation [37] in addition to the their strengthen effect forming hydration materials (CSH, CASH) that acquire more water content in addition to the chemically combined water within the matrix structure.

It can be seen a gradual increase in the main asymmetric band for T-O-Si which related to the amorphous geopolymer structure with NK as a results of increasing the enhancement effect with NK addition up to 5% NK in addition to the shifting of the asymmetric band into lower wave number (958 cm^{-1}) as a results of increasing of the vitreous enhancement effect of NK by the formation of agglomerated bundles that segregate the reacting geopolymer chains which then underwent crystallization and inhibited the formation of more branched geopolymer structure with NK, however further increase of NK results in an increased broadness of the previous band and shifting a higher wave number with the presence of shoulder at about 1100 cm^{-1} for non-solublized silica, which linked directly to the negative effect of increased NK.

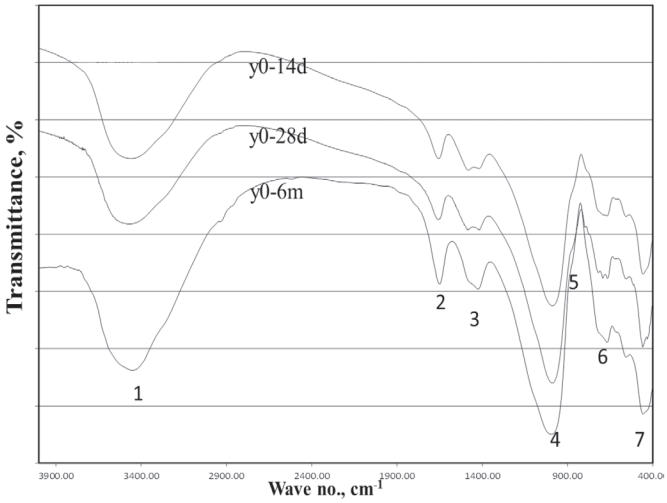

Fig. 8. FTIR spectra of control MK-geopolymer specimens cured up to 180 days [1: Stretching vibration of O-H bond; 2: Bending vibrations of (HOH); 3: Stretching vibration of CO_2; 4: Asymmetric stretching vibration (T-O-Si); 5: Symmetric stretching vibration of CO_2; 6: Symmetric stretching vibrations (Si-O-Si); 7: Bending vibration (Si-O-Si and O-Si-O)]

8. ábra 180 napos korú kontroll MK-kohósalak geopolimer keverékek FTIR spektrumai különböző NK adagolás mellett [1: Vegyértékrezgés O-H kötés, 2: Deformációs rezgés (HOH), 3: Vegyértékrezgés CO_2, 4: Aszimmetrikus vegyértékrezgés (T-O-Si), 5: Szimmetrikus vegyértékrezgés CO_2, 6: Szimmetrikus vegyértékrezgés (Si-O-Si), 7: Deformációs rezgés (Si-O-Si és O-Si-O)]

The appearance of bands in the regions of 1430-1450 cm^{-1} (ν C–O), and 867 cm^{-1} (δ C–O) are typical of $CO3^{2-}$ vibrational groups, present in inorganic carbonates [38], the increased contents of GBFS also lead to the growth of the carbonate band as discussed above, showing that the carbonates identified in this raw material do not react significantly under alkaline activation conditions [39]. These notices are in alignment with the XRD data where the amorphous vitreous structure increases up to 5% as well as increase in binding CSH phases that has an important role in binding the reacting materials however it may interfere with the required silica needed for geopolymer formation and accumulation [40].

Investigating the effect of increasing the curing time on the control geopolymer mix without NK (see *Fig. 8*), results in gradual increase in the main asymmetric band at about 950 cm^{-1} up to sharp increase at 6 months, as a results of increasing the rate of geopolymer formation and accumulation in the open pores resulting in the formation of well compacted structure, this is in consistent with the increased hydration band at about 3450 cm^{-1}, reflecting the increased combined water content in the geopolymer network as well as the formed CSH and CASH phases. It can be noticed also the splitting of the carbonation bands at about 1450 cm^{-1}, indicating the distorted nature of the formed carbonate as well as exposure of CSH binding phases into air carbonation [41, 42], this splitting turned to be diminished with time indicating the stability of the formed CSH against air carbonation.

3.3. SEM Observation

Microstructure of the control MK-slag geopolymer specimens without NK and cured at 90 and 180 days are shown in *Fig. 9*. It can be noticed that morphology of geopolymer specimens cured up to 90 days (*Fig. 9.a*), the coexistence of the aluminosilicate gel and the amorphous geopolymer in addition to CSH which fill mostly all the voids within the matrix, however increasing curing time to 180 days (*Fig. 9.b*) results in an increased transformation of the aluminosilicate gel into geopolymer plates that spread and forming a homogeneous structure; this is in coincide with the XRD and FTIR explanations.

Replacing MK by NK from 0 to 9% cured at 90 days *Fig. 10*, where the transformation of aluminosilicate gel in the control mix (*Fig. 10.a*) into geopolymer plates for mix containing 1% NK (*Fig. 10.b*) is a major feature as a result of the enhancement effect of NK in forming a nucleation sites for gel growth and precipitation. The previous nucleation illustration emphasized by increased formation of dense geopolymer plates that spread and fill most of the matrix forming a dense and well compact structure, where the added NK offers an extra nucleation sites for geopolymer growth in addition to the formed CSH by enhanced interaction of dissolved Ca and Si species (*Fig. 10.c*). On the other hand, further increase in NK to 9% results in the formation of agglomerates as a results of incomplete dispersion of high nano dose, these agglomerates results in the formation of weak zones and so result in formation of heterogeneous structure with many pores that spread within the structure,

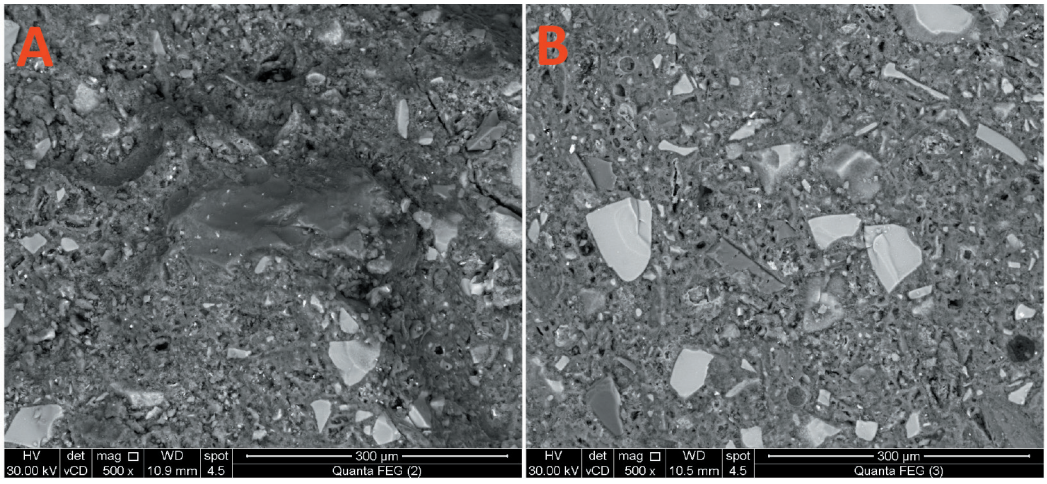

Fig. 9. SEM micrographs of alkali activated control Geopolymer specimens composed af 40% slag and 60% metakaoline cured at: A) 90 days B) 180 days

9. ábra Geopolimer keverékek (40% kohósalak, 60% metakaolin) elektronmikroszkópos felvételei különböző utókezelés mellett, a) 90 napig, b) 180 napig tartó utókezelés

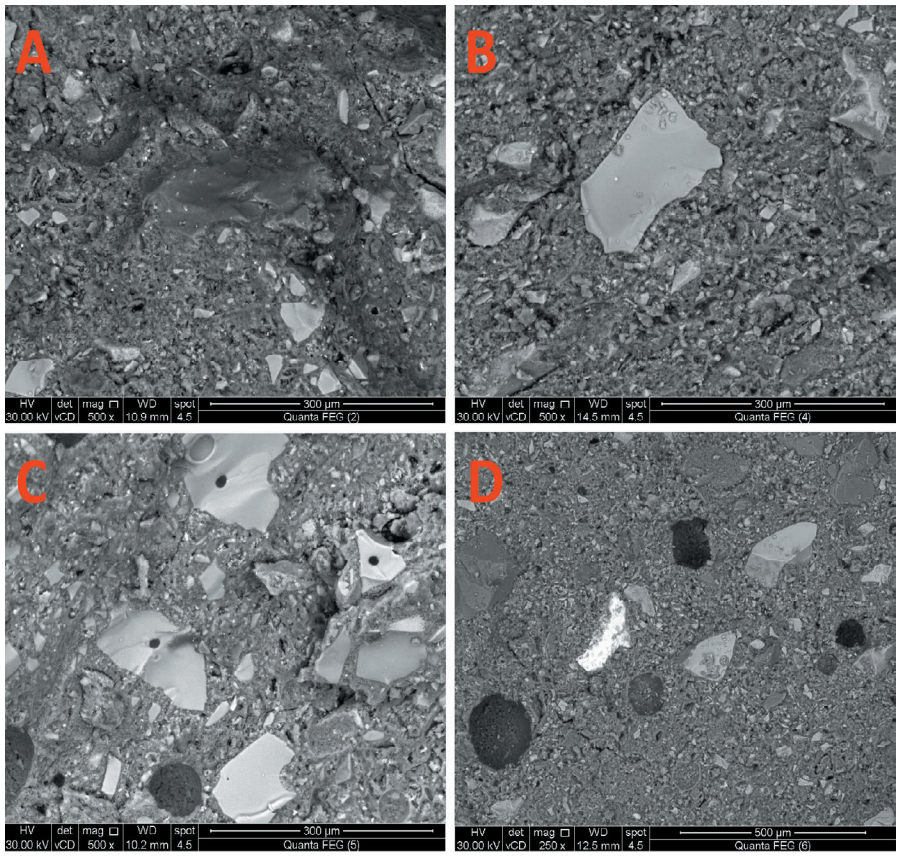

Fig. 10. SEM micrographs of 90 days alkali activated Geopolymer specimens having various Nanokaolin content. A) 0% NK, B) 3% NK, C) 5% NK, and D) 9% NK

10. ábra 90 napos korú alkáli aktivált geopolimer keverékek elektronmikroszkópos felvételei különböző nano-kaolin adagolás mellett, a) 0% NK, b) 3% NK, c) 5% NK, d) 9% NK

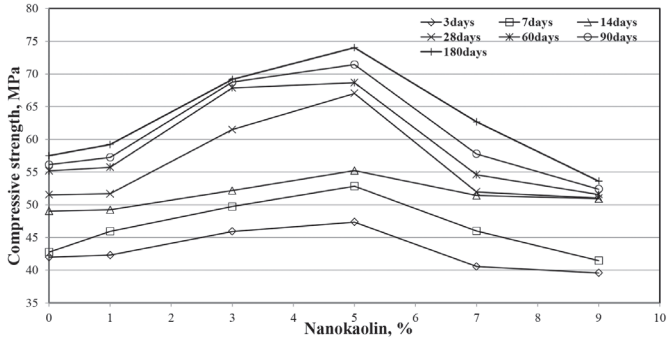

Fig. 11. Compressive strength of alkali activated MK-slag geopolymer specimens with various NK contents ratios as partial replacement of metakaoline cured up to 180 days

11. ábra Alkáli aktivált MK-kohósalak geopolimer keverékek nyomószilárdsága különböző NK adagolás és utókezelési időtartam mellett, 180 napos korig

these agglomerates inhibit the intact between geopolymer chains and so results in the formation less dense geopolymer structure (*Fig. 10.d*).

3.4. Compressive strength properties

The results of compressive strength for hardened MK/slag geopolymer mixes incorporated various NK content and cured in 100% relative humidity at 40°C up to 180 days are shown in *Fig. 11*. Results showed an increase of strength for all mixes along with hydration age as attributed to the continuing pozzolanic reaction as well as continuous growth of the geopolymer chains forming tightly bound structure, also the strength increase with NK up to 5%, and then subjected to gradual decrease with further NK addition. This increase with NK can be explained by increased geopolymer chain networks as results of increased nucleation sites for gel growth, in addition to the enhancement of NK to the interaction of dissolved Ca supplied by the GBFS with some of the excess dissolved silicate present, forming additional strengthen binding materials in addition to their role in providing nucleating agent for geopolymer formation and accumulation [43, 44], as illustrated clearly from XRD, FTIR, and SEM micrographs.

The decreased compressive strength up on increasing NK ratio more than 5% aroused primarily from incomplete dispersion of added nanomaterial forming agglomerates and result in formation of weak zones within the matrix providing more pores with susceptible for carbonation, as well as inhibiting the interaction and growth of the geopolymer networks. These previous findings confirmed with the XRD and FTIR which illustrated the growth of the amorphous geopolymer as well as CSH with NK up to 5%, while suffering of amorphous constituents as well as shifting of the main asymmetric geopolymer band to higher wave number favouring the zeolite formation than amorphous geopolymer increase, emphasizing the segregation effect of NK and so zeolite structure with lower chains formed on the expense of three dimensional networks, also the increased carbonate with NK increase (9%) confirms the presence of more pores as well as the presence of available cations exposed for carbonations. This increased porosity coincide with SEM micrographs illustrations where an increased pores in high NK content is the predominant feature.

However, on comparing mechanical compressive strength of control geopolymer mix specimens activated by sodium hydroxide, silicate and aluminate and cured up to 180 days (*Fig. 12*), where adding aluminate source in spite benefits the geopolymerization by adding extra sodium cations and alumina source, it lowered the SiO_2/Al_2O_3 (1.88 as compared with 2.04 for non-aluminate activator source) and so transferred from the category of polysialate-siloxo into polysilate species which known by its lowering branching ability than the previous one, in addition exceeding of the sodium cation over the required balancing ions necessary for charge balancing as resulted from Table 2 which gives the values of 1.163 and 0.36 for $T.M_2O/Al_2O_3$ and $T.M_2O/SiO_2$ and resulting in:

1. Sodium cations, which are normally presented at high concentrations in the geopolymeric systems, are specifically adsorbed ions on the surface of geopolymer particles changing

the surface speciation according to the following chemical Equation:

> T–OH + Na^+ <=> T–ONa + H^+

The stability area of >T–O-Na surface species is pH dependent and is located at extremely high pH values [45].

2. The sodium cations adsorption in highly alkaline conditions consumes the surface species (>T–OH and >T–O–), on which the chemical bonding between the insoluble solid particles and the geopolymeric framework takes place in the final stage of the geopolymerization process. Thus, the resulted geopolymeric materials have low mechanical strength [34].

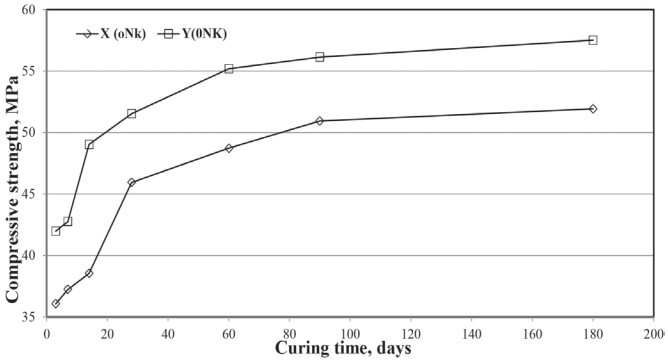

Fig. 12. Compressive strength of alkali activated MK-slag geopolymer specimens activated by different activators cured up to 180 days

12. ábra Alkáli aktivált MK-kohósalak geopolimer keverékek nyomószilárdsága különböző aktivátor és utókezelési időtartam mellett, 180 napos korig

The compressive strength confirmed and emphasized by XRD and FTIR where an increased amorphous geopolymer structure in the control mix without aluminate source as compared with one aluminate activator mix, where an increased Faujasite content in XRD as well as shifting to higher wave number in FTIR as a results of increased zeolite. The compressive strength results give a values of 45.93, 50.93 and 51.90 MPa after 28, 60 and 90 days, respectively, for aluminate activated mix, while gives 51.53, 56.13 and 57.51 MPa for non-aluminate mix geopolymer specimen which can be applied in various building application purposes.

4. Conclusions

The most important findings of the present paper are summarized below:

1. Addition of NK results in better enhancement in mechanical and morphological by using NK up to 5%, however further increase results in an agglomeration and decrease in efficiency of added nanomaterials.
2. SEM micrographs have proved an increased enhancement in microstructural properties of the NK-mixes up to formation of dense and homogenous morphological shape when using 5% NK, whilst an increase in the matrix porosity is a common feature of higher NK-mixes.
3. XRD and FTIR spectra confirm an intense amorphous geopolymer structure up on using 5% NK, while an increased crystalline phase with an increased carbonate bearing compounds are predominant with further NK.
4. Geopolymer mixes possess high mechanical properties that exceed 50 MPa after 28 days for control mix and increased with further NK up to 5%, giving a value of 67 MPa at 28 days and 71 MPa at 6 months, which can be used in various building applications as infrastructure as well as fire resistant building materials.
5. Using sodium aluminate activating source results in lowering in mechanical and physical characteristics of the produced specimens whilst their strength values reaches 45 MPa and 52 MPa after 28 and 90 days of curing.

Conflict of Interest: The authors declare that they have no conflict of interest.

References

[1] Taylor, H.F.W. (1964): The Chemistry of Cements, Vol. 1, 1st Ed., Academic Press, London.

[2] Gani, M.S.J. (1997): Cement and Concrete, 1st Ed., Chapman and Hall, London.

[3] Richardson, I.G. – Cabrera, J.G. (2000): The nature of C–S–H in model slag cements, *Cement and Concrete Composites*, Vol. 22, No. 4, pp. 259-266. https://doi.org/10.1016/S0958-9465(00)00022-6

[4] Van Jaarsveld, J.G.S. – van Deventer, J.S.J. – Lorenzen, L. (1997): The potential use of geopolymeric materials to immobilise toxic metals: Part I. *Theory and applications, Minerals Engineering*, Vol. 10, No. 7, pp. 659-669. https://doi.org/10.1016/S0892-6875(97)00046-0

[5] Van Jaarsveld, J.G.S. – van Deventer, J.S.J. (1999): The effect of metal contaminants on the formation and properties of waste-based geopolymers, *Cement and Concrete Research*, Vol. 29, No. 8, pp. 1189-1200. https://doi.org/10.1016/S0008-8846(99)00032-0

[6] Xu, H. – van Deventer, J.S.J. (2000): The geopolymerization of alumino-silicate minerals, *International Journal of Mineral Processing*, Vol. 59, No. 3, pp. 247-266. https://doi.org/10.1016/S0301-7516(99)00074-5

[7] Phair, J.W. – van Deventer, J.S.J. (2002): Characterization of fly-ash based geopolymeric binders activated with sodium aluminate, *Industrial and Engineering Chemistry Research*, Vol. 41, pp. 4242– 4251. https://doi.org/10.1021/ie010937o

[8] Alonso, S. – Palomo, A. (2001): Alkaline activation of metakaolin and calcium hydroxide mixtures: influence of temperature, activator concentration and solids ratio, *Materials Letters*, Vol. 47, No. 1–2, pp. 55-62. https://doi.org/10.1016/S0167-577X(00)00212-3

[9] Alonso, S. – Palomo, A. (2001): Calorimetric study of alkaline activation of calcium hydroxide–metakaolin solid mixtures, *Cement and Concrete Research*, Vol. 31, No. 1, pp. 25-30. https://doi.org/10.1016/S0008-8846(00)00435-X

[10] Frias, M. – Cabrera, J. (2001): Influence of MK on the reaction kinetics in MK/lime and MK-blended cement systems at 20°C, *Cement and Concrete Research*, Vol. 31, No. 4, pp. 519-527. https://doi.org/10.1016/S0008-8846(00)00465-8

[11] Frias, M. – Sanchez de Rojas, M.I. – Cabrera, J. (2000): The effect that the pozzolanic reaction of metakaolin has on the heat evolution in metakaolin-cement mortars, *Cement and Concrete Research*, Vol. 30, No. 2, pp. 209-216. https://doi.org/10.1016/S0008-8846(99)00231-8

[12] Cabrera, J. – Rojas, M.F. (2001): Mechanism of hydration of the metakaolin–lime–water system, *Cement and Concrete Research*, Vol. 31, No. 2, pp. 177-182. https://doi.org/10.1016/S0008-8846(00)00456-7

[13] Coleman, N.J. – McWhinnie, W.R. (2000): The solid state chemistry of metakaolin-blended ordinary Portland cement, *Journal of Materials Science*, Vol. 35, No. 11, pp. 2701–2710. https://doi.org/10.1023/A:1004753926277

[14] Aiu, M.(2006): The Chemistry and Physics of Nano-Cement, *Loyola Mary Mount University*, Advisor: Dr. C.P. Huang Submitted to: NSF-REU University of Delaware August 11, 2006.

[15] Li, H. – Xiao, H. – Ou., Jinping (2004): Microstructure of cement mortar with nano particles, *Composites Part B: Engineering*, Vol. 35, No. 2, pp. 185-189. https://doi.org/10.1016/S1359-8368(03)00052-0

[16] Ginebra, M.P. – Driessens, F.C.M. – Planell, J.A. (2004): Effect of the particle size on the micro and nano structural features calcium phosphate cement: a kinetic analysis, *Biomaterials*, Vol. 25, No. 17, pp. 3453-3462. https://doi.org/10.1016/j.biomaterials.2003.10.049

[17] Zins, D. – Cabuil, V. – Massart, R. (1999): New aqueous magnetic fluids, *Journal of Molecular Liquids*, Vol. 83, No. 1–3, pp. 217-232. https://doi.org/10.1016/S0167-7322(99)00087-2

[18] Ge, Z. – Gao, Z. (2008): Applications of Nanotechnology and Nano materials in Construction, *First International Conference on Construction In Developing Countries (ICCIDC-I)* "Advancing and Integrating Construction Education, Research & Practice" August 4-5, 2008, Karachi, Pakistan

[19] Hanehara, S. – Ichikawa., M. (2001): Nanotechnology of cement and concrete, *Journal of the Taiheiyo Cement Corporation*, Vol. 141, pp. 47-58.

[20] Scrivener, K. L. (2009): Nanotechnology and cementitious materials. In: Bittnar Z, Bartos PJM, Nemecek J, Smilauer V and Zeman J, editors. *Nanotechnology in construction: proceedings of the NICOM3* (3rd international symposium on nanotechnology in construction). Prague, Czech Republic. pp. 37–42.

[21] Abo-El-Enein, S.A. – Amin, M.S. – El-Hosiny, F.I. – Hanafi, S. – ElSokkary, T.M. – Hazem, M.M. (2014): Pozzolanic and hydraulic activity of nano-metakaolin, *HBRC Journal*, Vol. 10, No. 1, pp. 64-72. https://doi.org/10.1016/j.hbrcj.2013.09.006

[22] Morsy, M.S., Alsayed, S.H., Aqel, M. (2011) Hybrid effect of carbon nanotube and nano-clay on physico-mechanical properties of cement mortar, *Construction and Building Materials*, Vol. 25, No. 1, pp. 145-149. https://doi.org/10.1016/j.conbuildmat.2010.06.046

[23] Morsy, M.S. – Al-Salloum, Y.A. – Almusallam, T. – Abbas, H. (2014): Effect of nano-metakaolin addition on the hydration characteristics of fly ash blended cement mortar, *Journal of Thermal Analysis and Calorimetry*, Vol. 116, No. 2, pp. 845–852. https://doi.org/10.1007/s10973-013-3512-6

[24] Morsy, M.S. – Al-Salloum, Y.A. – Abbas, H. – Alsayed, S.H. (2012): Behavior of blended cement mortars containing nano- metakaolin at elevated temperatures, *Construction and Building Materials*, Vol. 35, pp. 900–905. https://doi.org/10.1016/j.conbuildmat.2012.04.099

[25] Baueregger m, S. – Lei, L. – Plank, J. – Perello, M. (2015): Use of Nano-MK for early strength enhancement of Portland cement, *Nano-technology in construction: Proceeding of NICOM5*, 199 Springer international publishing, 199-206, Switzerland, 2015.

[26] Khater, H.M. – El-Sabbagh, B.A. – Fanny, M. – Ezzat, M. – Lottfy, M. (2013): Effect of Nano-Clay on Alkali Activated Water-Cooled Slag Geopolymer, *British Journal of Applied Science and Technology*, Vol. 3, No. 4, pp. 764-776. https://doi.org/10.9734/BJAST/2013/2690

[27] Kakali, G. – Perraki, T. – Tsivilis, S. – Badogiannis, E. (2001): Thermal treatment of kaolin: the effect of mineralogy on the pozzolanic activity, *Applied Clay Science*, Vol. 20, No. 1-2, pp. 73–80. https://doi.org/10.1016/S0169-1317(01)00040-0

[28] Wenying, G. – Guolin, W. – Jianda, W. – Ziyun, W. – Suhong, Y. (2008): Preparation and Performance of Geopolymers, *Journal of Wuhan University of Technology – Materials Science Edition*, Vol. 23, No. 3, pp. 326–330. https://doi.org/10.1007/s11595-007-3326-0

[29] Khater, H.M. (2012): Effect of Calcium on Geopolymerization of Aluminosilicate Wastes, *Journal of Materials in Civil Engineering*, Vol. 24, No. 1, https://doi.org/10.1061/(ASCE)MT.1943-5533.0000352

[30] Khater, H.M. (2013): Effect of Silica Fume on the Characterization of the Geopolymer Materials, *International Journal of Advanced Structural Engineering*, Vol. 5, No. 12, https://doi.org/10.1186/2008-6695-5-12

[31] Khater, H.M. (2013): Effect of cement Kiln dust on geopolymer composition and its resistance to sulfate attack, *Green materials Journal,* Vol. 1, No. 1, pp. 36-46. https://doi.org/10.1680/gmat.12.00003

[32] El-Sayed, H.A. – Abo El-Enein, S.A. – Khater, H.M. – Hasanein, S.A. (2011): Resistance of Alkali Activated Water Cooled Slag Geopolymer to Sulfate Attack, *Ceramics – Silikáty*, Vol. 55, No. 2, pp. 153-160.

[33] ASTM C109M (2016) Standard Test Method for Compressive Strength of Hydraulic Cement Mortars.

[34] Panias, D. – Giannopolou, L.P. – Peraki, T. (2007): Effect of synthesis parameters on the mechanical properties of fly ash-based geopolymers, *Colloids and Surfaces A: Physicochemical and Engineering Aspects*, Vol. 301, No. 1–3, pp. 246-254. https://doi.org/10.1016/j.colsurfa.2006.12.064

[35] Bakarev, T. (2006): Thermal behavior of geopolymer prepared using class F fly ash and elected temperature curing, *Cement and Concrete Research*, Vol. 36, No. 6, pp. 1134-1147. https://doi.org/10.1016/j.cemconres.2006.03.022

[36] Zuhua Z. – Xiao, Y. – Huajun, Z. – Yue, C. (2009): Role of water in the synthesis of calcined kaolin-based geopolymer, *Applied Clay Science*, Vol. 43, No. 2, pp. 218-223. https://doi.org/10.1016/j.clay.2008.09.003

[37] Temuujin, J. – Van Riessen, A. – Williams, R. (2009): Influence of calcium compounds on the mechanical properties of fly ash geopolymer pastes, *Journal of Hazardous Materials*, Vol. 167, No. 1–3, 15 pp. 82-88. https://doi.org/10.1016/j.jhazmat.2008.12.121

[38] Garcia-Lodeiro, I. – Fernandez-Jimenez, A. – Palomo, A. – Macphee, D.E. (2010): Effect on fresh CS-H gels of the simultaneous addition of alkali and aluminium, *Cement and Concrete Research*, Vol. 40, No. 1, pp. 27-32. https://doi.org/10.1016/j.cemconres.2009.08.004

[39] Bernal, S.A. – Rodríguez, E.D. – Mejia de Gutiérrez, R. – Provis, J-L. – Delvasto, S. (2012): Activation of Metakaolin/Slag Blends Using Alkaline Solutions Based on Chemically Modified Silica Fume and Rice Husk Ash, *Waste and Biomass Valorization*, Vol. 3, No. 1, pp. 99–108. https://doi.org/10.1007/s12649-011-9093-3

[40] Catalfamo, P. – Di Pasquale, S. – Corigliano, F. – Mavilia, L. (1997): Influence of the calcium content on the coal fly ash features in some innovative applications, *Resources, Conservation and Recycling*, Vol. 20, No. 2, pp. 119-125. https://doi.org/10.1016/S0921-3449(97)00013-X

[41] Kalinkin, A. M. – Politov, A. A. – Boldyrev, V. V. – Kalinkina, E. V. – Makarov, V. N. – Kalinnikov V. T. (2002): Study of Mechanical Activation of Diopside in a CO_2 Atmosphere. *Journal of Materials Synthesis and Processing*, Vol. 10, No. 1, pp. 61–67. https://doi.org/10.1023/A:1021057231463

[42] Kalinkin, A. M. – Kalinkina, E. V. – Politov, A. A. – Makarov, V. N. – Boldyrev, V. V. (2004): Mechanochemical interaction of Ca silicate and aluminosilicate minerals with carbon dioxide. *Journal of Materials Science*, Vol. 39, No. 16–17, pp. 5393–5398. https://doi.org/10.1023/B:JMSC.0000039252.13062.63

[43] Van Deventer, J.S.J. – Provis, J.L. – Duxson, P. – Luckey, G.C. (2007): Reaction mechanisms in the geopolymeric conversion of inorganic waste to useful products, *Journal of Hazardous Materials*, Vol. 139, No. 3, pp. 506-513. https://doi.org/10.1016/j.jhazmat.2006.02.044

[44] Lee, W.K.W. – Van Deventer, J.S.J. (2002): The effect of ionic contaminants on the early age properties of alkali-activated fly ash based cements, *Cement and Concrete Research*, Vol. 32, No. 4, pp. 577-584. https://doi.org/10.1016/S0008-8846(01)00724-4

[45] Skoufadis, C. – Panias, D. – Paspaliaris, I. (2003): Theoretical determination of electrochemical properties of boehmite–water interface, as a tool for understanding the mechanism of boehmite precipitation, in: *European Metallurgical Conference*, vol. 1, Hanover, Germany, 2003; pp. 321–338.

Ref.:
Khater, H. M. – **Abd el Gawwad,** H.: *Synthesis and characterization of MK/ Slag geopolymer composites enhanced by various ratios of nano kaolin*
Építőanyag – Journal of Silicate Based and Composite Materials, Vol. 69, No. 2 (2017), 40–48. p.
https://doi.org/10.14382/epitoanyag-jsbcm.2017.8

Nano-kaolin tartalmú MK/kohósalak geopolimerek szintézise és tulajdonságai

A cikk nano-kaolin tartalmú metakaolin/kohósalak geopolimer keverékek alkáli aktiválási lehetőségét mutatja be és ismerteti a C-A-S-H és N-A-S-H gél képződés részleteit. Aktivátorként 10% NaOH oldatot és 5% nátrium-szilikát oldatot használtak és a nano-kaolin adagolás 0 és 9% között változott. A kialakuló geopolimerek mechanikai tulajdonságait (nyomószilárdság) prizmatikus próbatesteken vizsgálták. A struktúra és fázisösszetétel vizsgálata során pásztázó elektronmikroszkópot, röntgendiffraktométert és infravörös spektroszkópot használtak. Az eredmények rávilágítottak, hogy a nano-kaolin adagolása 5%-os mennyiségig javítja a mikrostruktúrát és szilárdságnövekedést eredményez, de ennél nagyobb mennyiség adagolása agglomerációhoz és szilárdságcsökkenéshez vezet. Nátrium-aluminát aktivátor adagolása szilárdságcsökkenést eredményez a zeolit képződés következtében.

Kulcsszavak: Nano-kaolin, Geopolimer, aktiválás, környezetbarát.

Bentonite-based organoclays using chalcone and azo dye as organophilic reagents

Manar Ghyath ABD-ALMUTALIB AL-MOSAWY ▪ Department of Chemistry, Faculty of Science, University of Kufa ▪ manarghyth@yahoo.com
Emad A. Jaffar AL-MULLA ▪ Department of Chemistry, Faculty of Science, University of Kufa ▪ imad.almulla@uokufa.edu.iq
Majed Jari MOHAMAD ▪ Department of Chemistry, Faculty of Science, University of Kufa
Érkezett: 2017. 03. 20. ▪ Received: 20. 03. 2016. ▪ https://doi.org/10.14382/epitoanyag-jsbcm.2017.9

Abstract
Organoclays (OBNTs) was prepared using two new organic surfactants including 3-(4-aminophenyl)-1-(4-chlorophenyl)prop-2-en-1-on (CH) synthesized from a Claisen–Schmidt condensation reaction between p-aminoacetophenone and p-chloro benzaldehyde; and 4-((4-nitrophenyl) diazenyl)-N-(pyrimidin-2-yl) (AZ) prepared from reaction sulfadiazine and p-nitoaniline. OBNTs were characterized by Fourier Transform infrared spectroscopy (FTIR) to evaluate the incorporation above surfactants in bentonite. The X-ray diffraction (XRD) technique was utilized to indicate the basal spacing of the treated clay as a measure of susceptibility of new organo clays. The FTIR and XRD results show that the OBNTs were successfully incorporated in the bentonite clay. Thermogravimetric analysis (TGA) was also used to determine thermal stability. An enhancement in stability was observed in OBNTs compare to pure bentonite. OBNTs prepared in this study can be used to produce disposable packaging polymer nanocomposite.
Keywords: sodium bentonite, modification, surfactants, organic cations

Manar Ghyath ABD-ALMUTALIB AL-MOSAWY
is a PhD student at Department of Chemistry, Faculty of Science, University of Kufa, Iraq; She has received her MSc from Faculty of Education for Girls, University of Kufa, Iraq in 2010. Main fields of interest: organic synthesis, nano-materials, biopolymer nano-composites. She has published many scientific papers in citation and non-citation indexed journals .

Emad Abbas Jaffar AL-MULLA
is an Asst. Prof., College of Health and Medical Techniques, Al-Furat Al-Awsat Technical University, Iraq; He has received his PhD from University Putra Malaysia, Malaysia in 2010, He was a Post Doctoral researcher at the same University from April 2012 to April 2013; main fields of interest: bioorganic synthesis, nano-materials, biopolymer nano-composites; He has more than 50 papers in Scopus and ISI journals; his H-Index = 14 according to Scopus database.

Majed Jari MOHAMAD
is an Asst. Prof., Department of Chemistry, Faculty of Science, University of Kufa, Iraq; He has received his PhD from University of Baghdad, College of Education for Pure Science, Ibn al-Haytham, Department of Chemistry in 2006. Main fields of interest: organic synthesis, nano-materials, heterocyclic compounds. He has published many scientific papers in citation and non-citation indexed journals.

1. Introduction

Bentonite, which is predominantly amontmorillonitic clay, is characterized by one Al octahedral sheet placed between two Si tetrahedral sheets. The isomorphous substitution of Al^{3+} for Si^{4+} in the tetrahedral layer and Mg^{2+} for Al^{3+} in the octahedral layer results in a netnegative surface charge on the clay. This charge imbalance is offset by exchangeable cations typically Na^{+} and Ca^{2+} at the clay surface. The layered structure of the clay allows expansion after wetting. Na^{+} and Ca^{2+} are strongly hydrate in the presence of water, resulting in ahydrophilic environment at the clay surface [1]. However, cation-exchange reaction have been traditionally exploited as an effective method to replace these inorganic ions with organic cationic surfactant molecules , which intercalate into the clay gallery, resulting in expansion of the interlayer spacing and leading to an increase in the basal spacing. These organic cations render the surface of the clay mineral hydrophobic, leading to the increase of the clay wettability and providing favourable interactions with organic molecules. Both organic-modified and unmodified clays have been used for different industrial applications such as rheological additives, thickeners in coating products glues, plastisols, drilling fluids and cosmetics [2,3]. Recently, clays were used in the field of materials science such as solid phase polymeric nanocomposites. In the 1990's, the use of organically modified clays in the polymer-clay nanocomposites has attracted researchers into this area of materials science and technology [4]. The organic modification of clay minerals leads to a decrease in surface energy making clays compatible with polymers. The surface energy of clay minerals and polymer can be determined from contact angle measurements [5,6] reported that melt processed nylon 6-clay nanocomposites was prepared using organoclay. Based on X-ray diffraction analysis, various arrangement of alkyl chains in organoclays had proposed by Lagaly (1986). Novel organo montmorillonites have been synthesized and characterized using different ammonium compounds [7,8]. In this study, two new different ammonium compounds *3-(4-aminophenyl)-1-(4-chlorophenyl)prop-2-en-1-on (CH)* and *4-((4-nitrophenyl) diazenyl)-N-(pyrimidin-2-yl)* (AZ) were used to modify the compatibility of bentonite clay. These organo-bentonites can be used in various research and industrial application specially polymer nanocomposites.

2. Experimental

2.1. Materials

Hydrochloric acid from J.T. Baker,USA. p-amino acetophenone were obtained from Fluka andp-chlorobenzaldehyde were obtained from Fluka sodium hydroxide were obtain from B.D.H.

2.2. Characterization

Organoclay were characterized using two different techniques including X-Ray Diffraction (XRD) and Fourier Transform Infrared spectroscopy(FTIR).

2.2.1. X-ray diffraction (XRD) analysis

X-ray diffraction (XRD) study was carried out using a Shimadzu XRD 6000 diffractometer with Cu K radiation (k = 0.15406 nm).The diffractogram was scanned in the ranges from 2° to 10° at a scan rate of 1°/min.

2.2.2. Fourier-transform infrared (FT-IR) spectroscopy

The FTIR spectra of the blends samples were recorded by the FTIR spectrophotometer (Perkin Elmer FT-IR-Spectrum BX, USA) using KBr disc technique. Measurements were made at the faculty of Pharmacy, University of Kufa.

2.2.3. Nuclear magnetic resonance (NMR)

The ^{1}H- NMR and ^{13}C-NMR spectra were obtained with Bruker, Ultra Shield 300 MHZ , using DMSO as solvent and TMS as an internal standard.

2.2.4. Thermogravimetric analysis (TGA)

TGA was recorded by thermal gravimetric analyser, STA PT-1000 Iinseis TGA, Germany, Measurements were made at the College of Education for Sciences Ibn Al-Haitham, University of Baghdad.

2.3. Preparation of Chalcone

Amixture of p-aminoacetophenone (1 mmol) 0.5 g, p-chlorobenzaldehyde 1 mmol, was treated a 10% NaOH aqueous solution 0.5 mL, and 99% EtOH 5 mL. The mixture was stirred at room temperature for 4hrs. The solid formed was filtered then washed with ethanol and water 5 mL. Recrystallization from 99% ethanol afforded (97% yield, yellow solid, m.p. 160-165 °C) [9].

2.4. Preparation of AZO

2 gm (0.0145 mole) of 4- nitro anilin was dissolved in 3ml of concentrated hydrochloric acid and 15 ml of distilled water. The mixture was cooled at 0-5 °C in ice-water bath, Then a solution of sodium nitrite (0.0145 mole) 0.9 gm was dissolved in 5 mLof distilled water then it will be cooled at (0-5 °C). This solution was added a drop wise to the mixture with stirring at the same temperature. The diazonum salt solution was added portion wise to solution of (0.0145 mol) 3.62 g sulfadiazine in distilled water with sodium hydroxide 1.5 gmdissolved in 100 mL distilled water. The pH was maintained with 6-7 and temperature at 0-5 °C. The mixture was stirred for 30 minutes. The mixture was left over night. The product was precipitated and filtered, washed well with sodium bicarbonate and distilled water andre-crystallized from ethanol (yield 95% , brown solid, m.p. 193-198 °C) [10].

2.5. Preparation of organoclays (OBNT)

Organoclay was prepared in an aqueous solution. Sodium Bentonite (Na-BNT) 4.00 g was stirred vigorously in 600 mL of hot distilled water for 1 h to form a clay suspension. Subsequently, *3-(4-aminophenyl)-1-(4-chlorophenyl)prop-2-en-1on* (CH) and *4-((4-nitrophenyl)diazenyl)-N-(pyrimidin-2-yl)* (AZ) 4.50 g, which had been dissolved in 400 mL of hot water and concentrated hydrochloric acid 16.00 mL was added into the clay suspension of. After being stirred vigorously for 1 h at 80 °C, the organoclay suspension was filtered and washed with distilled water until no chloride was detected with a 1.0 M silver nitrate solution. It was then dried at 60 °C for 72 h [11]. The dried organoclay was ground until the particle size was 100 μm before the preparation of the nanocomposite [12,13]. *Table 1* shows the structures of two organoclays.

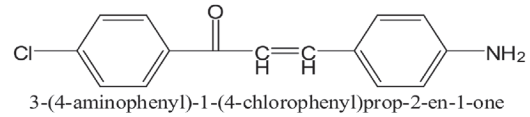

3-(4-aminophenyl)-1-(4-chlorophenyl)prop-2-en-1-one

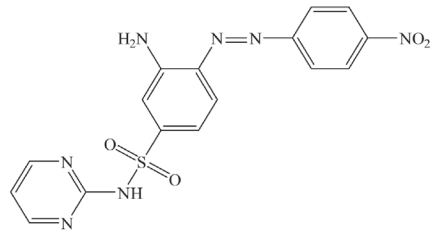

3-amino-4-((4-nitrophenyl)diazenyl)-*N*-(pyrimidin-2-yl)benzenesulfonamide

Table 1. Structure of the two organoclays
1. táblázat A két szerves agyag szerkezete

3. Results and discussion

3.1 X-ray diffraction (XRD) analysis

The alkyl ammonium cation exchange enable the conversion of the hydrophilic interior clay surface into the hydrophobic surface and consequently increase the layer distance as well [14]. In this study, Na-BNT was surface treated with *3-(4-aminophenyl)-1-(4-chlorophenyl)prop-2-en-1on* (CH) and *4-((4-nitrophenyl)diazenyl)-N-(pyrimidin-2-yl)* (AZ) as intercalation agent through cation exchange process. The cationic head groups of the intercalation agent molecule would preferentially reside at the layer surface and the tail of the compound will radiate a ways from the surface. The presence of these chains in the galleries makes the originally hydrophilic silicate to organophilic and thus increase the layer-to-layer spacing of Na-BNT [15]. The obtained *3-(4-aminophenyl)-1-(4-chlorophenyl)prop-2-en-1on*-BNT and *4-((4-nitrophenyl)diazenyl)-N-(pyrimidin-2-yl)*-BNT were studied by using X-ray diffraction measurements in the 2Θ ranges from 2Θ-10Θ. Na-BNT shows diffraction peak at 2Θ = 7.0762 which assigns to the interlayer distance of the natural Bentonite with a basal spacing of 1.25 nm as known in *Fig. 1* [16]. After the ion exchange reaction, the basal spacing (d001value) increase from 1.25-1.77 for *3-(4-aminophenyl)-1-(4-chlorophenyl)prop-2-en-1on*–BNT and *4-((4-nitrophenyl)diazenyl)-N-(pyrimidin-2-yl)*–BNT respectively, suggesting that CH^{+}, AZ^{+} have been intercalated into the Na-BNT galleries. These results are summarized in *Table 2*. Thus, X-ray diffraction results indicate that are successfully intercalated into the silicate layer.

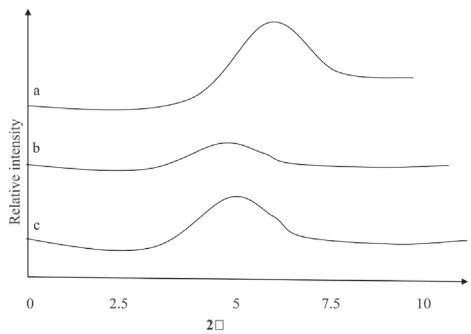

Fig. 1. XRD patterns of (a) Na-BNT; (b) CH-BNT; (c) AZ-BNT
1. ábra Röntgendiffraktogramok (a) Na-BNT; (b) CH-BNT; (c) AZ-BNT

Sample	exchange change	2Θ(°)	d spacing (nm)
Bentonite	Na^+	7.08	1.25
CH-modified	$C_{15}H_9ClO\ NH_3^+$	4.99	1.77
AZ-modified	$C_{16}H_9N_5O_4SNH_3^+$	5.01	1.76

Table 2. Diffraction angle and basal spacing of montmorillonite and modified montmorillonite with different organic cations
2. táblázat Montmorillonit és modifikált montmorillonit diffrakciós szöge és bázistávolsága különböző szerves kationokkal

3.2 Fourier transform infrared (FTIR) spectroscopy

FTIR spectroscopy is a useful technique to verify the presence of CH^+ and AZ^+ in the clay, respectively. *Fig. 2* shows the FTIR spectra of Na-BNT, pure CH and CH-BNT. *Fig. 3* shows the FTIR spectra of Na-BNT, pure AZ and AZ-BNT. The infrared spectrum of the Na-BNT shows two peaks, which correspond to Si-O stretching at 1047 Cm^{-1} and interlayer water deformation vibrational 1645 Cm^{-1} [17]. 3628 Cm^{-1} result from the O-H stretching vibration. The peaks observed in the CH-BNT (2850-2920 Cm^{-1}) and AZ-BNT (2872-2939 Cm^{-1}) infrared spectra correspond to the presence of the C-H asymmetric and symmetric stretching vibration, respectively.

In the spectra of CH-BNT and AZ-BNT, the absorption bands 3626 and 3640 Cm^{-1} indicate the presence of free O-H stretching and at 1091 and 1109 Cm^{-1} correspond to C-N stretching, respectively [18] in addition to the bands of the original Na-BNT. The band at 1490 and 1438 Cm^{-1} suggests the existence of the ammonium ion. Therefore, these indicate that of CH^+ and AZ^+ were intercalated in the silicate layers. This suggests that CH and AZ are absorbed into the silicate layers of Na-BNT.

3.3 Nuclear magnetic resonance

Nuclear magnetic spectroscopy is a useful technique to verify the presence of the ^{1}H-NMR spectra of CH pure and AZ pure (*Fig. 4*), and the ^{13}C-NMR spectra of CH pure and AZ pure (*Fig. 5*). The nuclear magnetic spectrum of CH, which ^{1}H-NMR (300 MHz, DMSO) appearance of multiple signals at the site 6.6-7.8 ppm date back to protons benzene rings, also showed referring at the site 5.3 ppm back to protons (NH_2) and appearance signals at the site 7.5-7.9 ppm back to protons (CH = CH). ^{1}H-NMR spectra of AZ appearance of multiple signals at the site 7.6 -8.5 ppm date back to protons benzene rings, also showed referring at the site 6.5 ppm back to protons (NH_2) and

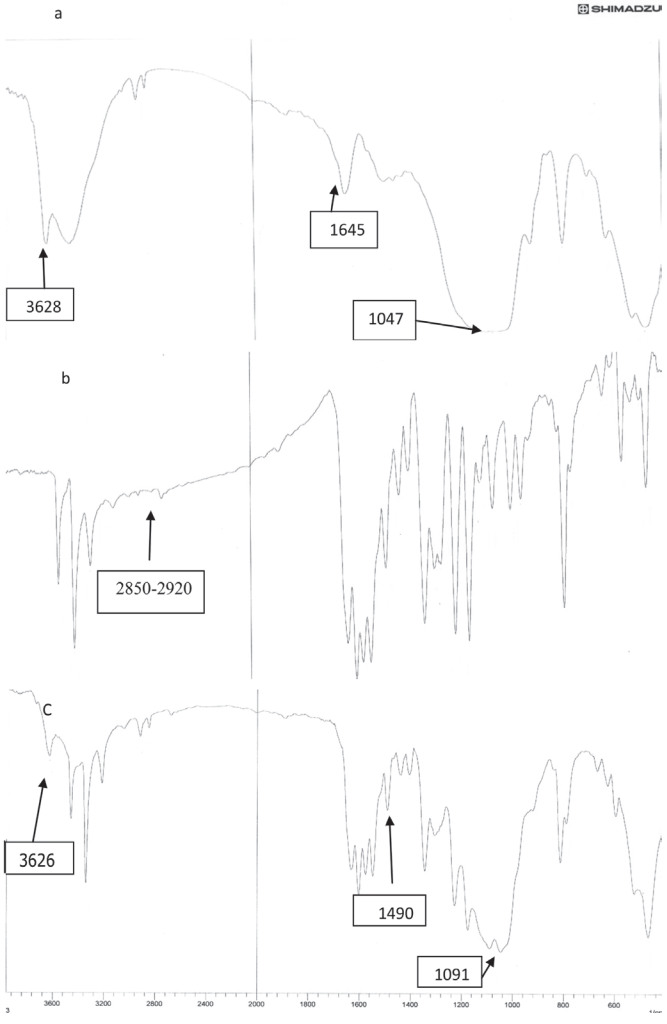

Fig. 2. FTIR Spectra of (a) Na-BNT; (b) CH; (c) CH-BNT
2. ábra FTIR spektrumok (a) Na-BNT; (b) CH; (c) CH-BNT

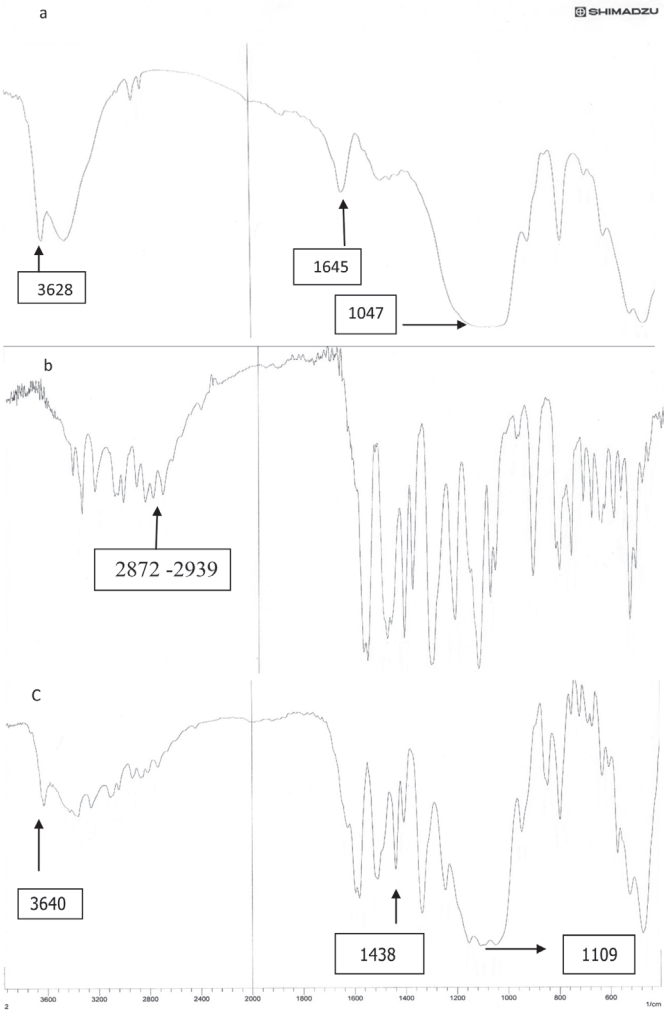

Fig. 3. FTIR Spectra of (a) Na-BNT; (b) AZ; (c) AZ-BNT
3. ábra FTIR spektrumok (a) Na-BNT; (b) AZ; (c) AZ-BNT

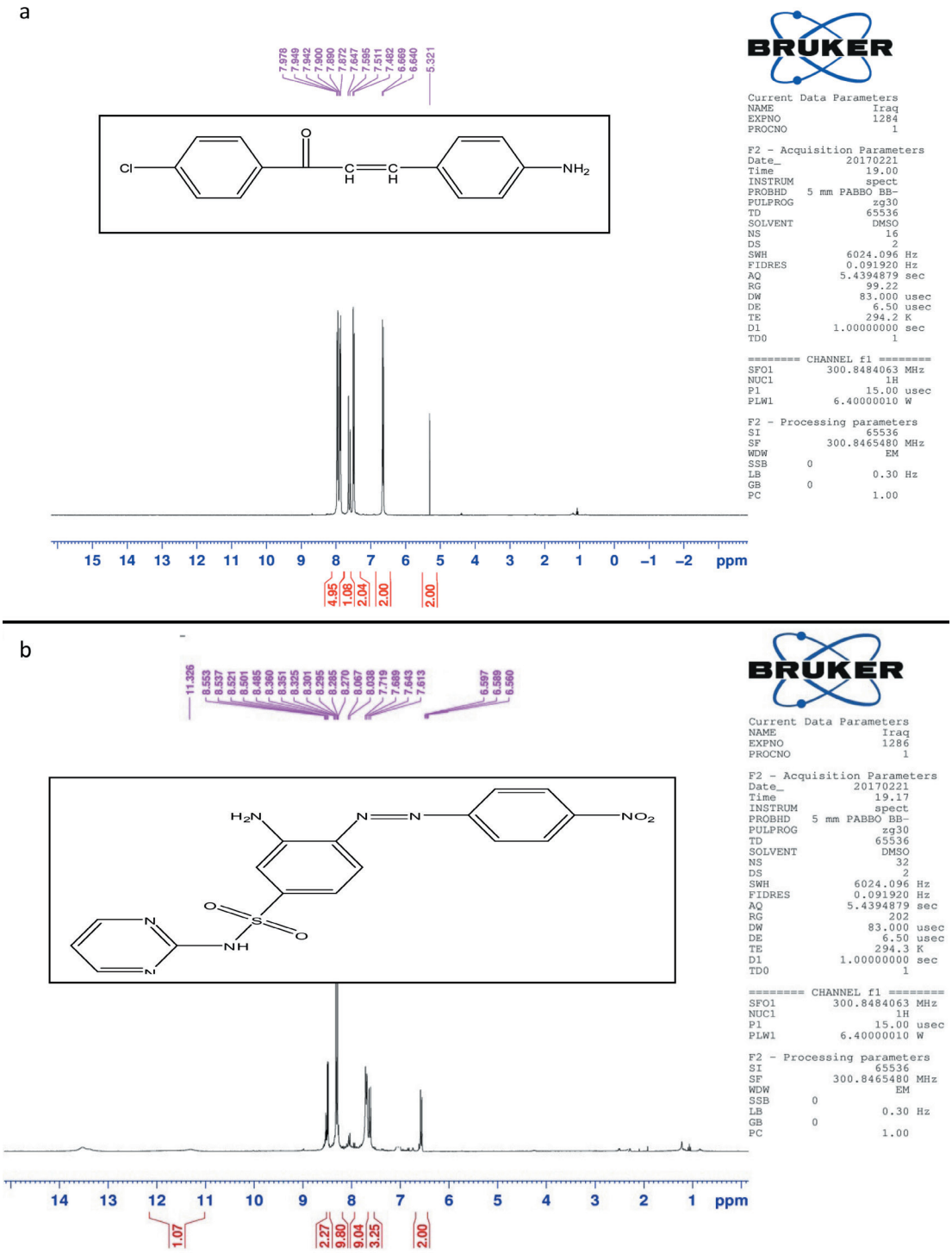

Fig. 4. H-NMR Spectra of (a) CH; (b) AZ
4. ábra H-NMR spektrumok (a) CH; (b) AZ

appearance signals at the site 11.32 ppm back to protons (NH) in sulfadiazine. The nuclear magnetic spectrum of CH, which ^{13}C-NMR (300 MHz, DMSO) appearance of multiple signals at the site 113.2-130.6 ppm date back to carbons benzene rings, also showed referring at the site 186.2 ppm back to carbon (C=O) and appearance signals at the site 145.2-123.6 ppm back to carbon (CH=CH). ^{13}C-NMR spectra of AZ appearance of multiple signals at the site 115.9 -165.134 ppm date back to carbon benzene rings.

3.4 Thermogravmetric analysis (TGA)

Fig. 6 shows the weight loss curves for increasing temperatures of Na-BNT, CH-BNT, AZ-BNT.

Thermogravimetric analysis (TGA) gives information on the structure of the intercalating molecules by the weight loss steps. Thermal degradation of BNT shows before 200 °C because of the volatilization of water adsorbed on the external surfaces of the BNT and water inside the interlayer space.

The thermal degradation of the modified BNT can be explained occurs at below 200 °C due to the vaporization of water.

The weight loss curves (TGA) of the BNT, CH-BNT and AZ-BNT were illustrated in *Fig. 6.* BNT contains water due to hydrated sodium (Na^+) cations intercalated inside the clay layers. The presence of alkyl ammonium groups within the BNT interlayer spacing lowers the surface energy of the inorganic structure and will transform organophobic to organophilic materials.

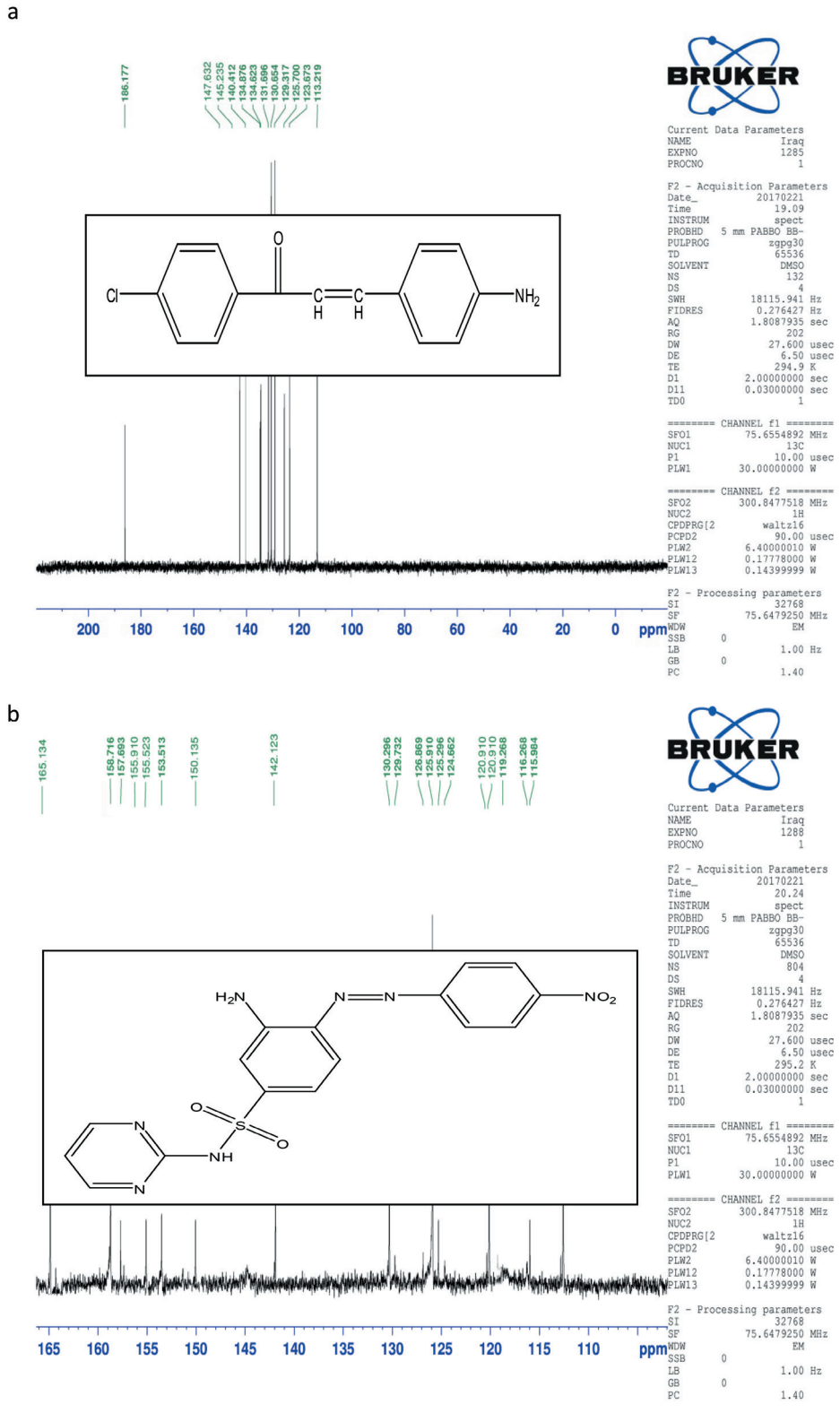

Fig. 5. H-NMR Spectra of (a) CH; (b) AZ
5. ábra H-NMR spektrumok (a) CH; (b) AZ

The major difference between the thermogram of the unmodified clay and that of the organoclay is that the organic constituents in the organoclay decompose in the range from 180 to 500 °C, as the organic constituent in the organoclay decomposes in this range.

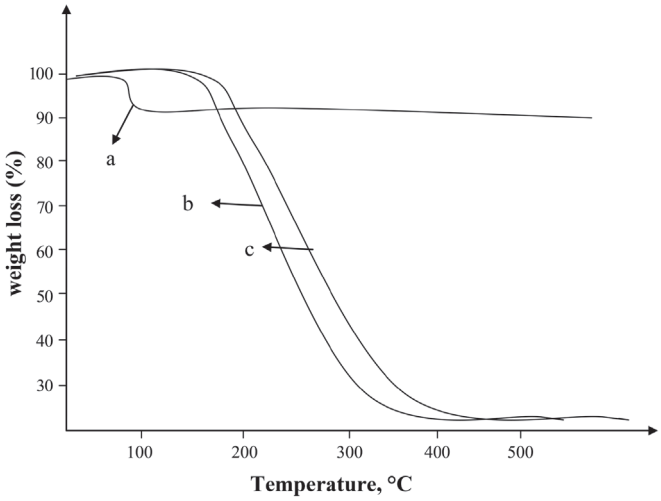

Fig. 6. TGA of (a) Na-BNT; (b) CH-BNT; (c) AZ-BNT
6. ábra TGA görbék (a) Na-BNT; (b) CH-BNT; (c) AZ-BNT

4. Conclusions

Two new ammonium cations CH and AZ were used to modify bentonite clay in an attempt to create susceptible clay to polymers. The organoclays were characterized using FTIR, XRD, ^{1}HNMR, ^{13}CNMR and TGA. Based on result of this study, the following conclusion can be drawn:

- These ammonium cations can be successfully incorporated in the bentonite clay.
- The basal spacing of the bentonite clay increases as a result of incorporating CH and AZ.
- The new organoclay can be susceptible to polymers.
- Thermal stability was enhanced by incorporation of clay into CH and AZ.

References

[1] Yun-Hwei S. (2001): Preparations of organobentonite using nonionic surfactants. Chemosphere, Vol. 44, No. 5, pp. 989-995. https://doi.org/10.1016/S0045-6535(00)00564-6

[2] Motawie, A. M. – Madany, M. M. – El-Dakrory, A. Z. – Osman, H. M. – Ismail, E. A. – Badr, M. M. – El-Komy, D. A. – Abulyazied, D. E. (2014): Physico-chemical characteristics of nano-organo bentonite prepared using different organo-modifiers. *Egyptian Journal of Petroleum*, Vol. 23, No. 3, pp. 331-338. https://doi.org/10.1016/j.ejpe.2014.08.009

[3] Jaynes, W. F. – Boyd S. A. (1991): Clay mineral type and organic compound sorption by hexadecyltrimethyl ammonium exchanged clays. *Soil Science Society of America Journal*, Vol. 55, No. 1, pp. 43-48.

[4] Zhang, J. – Wilkie, C. A. (2003): Preparation and flammability properties of polyethylene-clay nanocomposites. *Polymer Degradation and Stability,* Vol. 80, No. 1, pp. 163-169. https://doi.org/10.1016/S0141-3910(02)00398-1

[5] Maiti, M. – Bhowmick, A. K. (2005): Structure and properties of some novel fluorolastomer/clay nanocomposites with special reference to their interaction. *Journal of Polymer Science*, Part B, Polymer Physics, Vol. 44, No. 1, pp. 162-176. https://doi.org/10.1002/polb.20680

[6] Dutta, A. – Singh, N. (2015): Surfactant-modified bentonite clays: preparation, characterization, and atrazine removal. *Environmental Science and Pollution Research*, Vol. 22, No. 5, pp. 3876–3885. https://doi.org/10.1007/s11356-014-3656-3

[7] Motawie, M. A. – Ahmed, N. M. – El Mesallamy, S. M. – Sadek, E. M. – Kandile, N. G. (2014): Unsaturated Polyesters / Layered Silicate Nanocomposites: Synthesis and Characterization. *IOSR Journal of Applied Chemistry (IOSR-JAC)*, Vol. 7, No. 10, pp. 34-43.

[9] Khazaal, M. S. – Tomma, J. H. (2011): Synthesis and Characterization of Novel Schiff Bases Containing Isoxazoline or Pyrazoline. *Ibn Al-Haitham Journal for Pure & Applied Sciences*, Vol. 24, No. 2, pp. 1-14.

[10] Salman, F. W. – Radhi, S. W. – Jodh, A. M. (2015): Preparation and study antibacterial activity of a new polymer. *Journal of Babylon University, Pure and Applied Sciences*, Vol. 23, No. 2, pp. 759-770.

[11] Al-Mulla, E.A. J. – Yunus, W. M. Z. – Ibrahim, N. A. (2010): Enzymatic synthesis of fatty amides from palm olein. *Journal of Oleo Science*, Vol. 59, pp. 59–64.

[12] Yunus, W. M. Z. – Ibrahim, N. A. – Mohm, Z. A. (2011): Epoxidized palm oil plasticized polylactic acid/fatty nitrogen compound modified clay nanocomposites: preparation and characterization. *Korean Journal of Chemical Engineering*, Vol. 28, No. 2, pp. 620–626. https://doi.org/10.1007/s11814-010-0373-6

[13] Yunus, W. M. Z. – Ibrahim, N. A. – Zaki, A. (2010): Difatty acyl urea from corn oil: synthesis and characterization. *Journal of Oleo Science*, Vol. 59, pp. 157–160.

[14] Phua, Y. J. – Chow, W. S. – Mohd Ishak, Z. A. (2013): Organomodification of Montmorillonite and Its Effects on the Properties of Poly(butylene succinate) Nanocomposites, *Polymer Engineering and Science*, Vol. 53, No. 9, pp. 1947–1957. https://doi.org/10.1002/pen.23460

[15] Mansor, B. A. – Wisam, H. H. – Nor Azowa B. I. – Emad, A. J. A. (2009): Modification of Montmorillonite by new surfactants. *Journal of Engineering and Applied Science*, Vol. 4, No. 3, pp. 184-188.

[16] Khalaf, A. I. – Hegazy, M. A. – El-Nashar, D. E. (2015): Synthesis and Characterization of Cationic Gemini Surfactant Modified Na–Bentonite and Its Applications for Rubber Nanocomposites. *Polymer composites,* Vol. 38, No. 2, pp. 396–403. https://doi.org/10.1002/pc.23598

[17] Guo, L. – Wu, S. – Zeng, F. – Zhao, J. (2006): Synthesis and Fluorescence property of terbium complex with novel Schiff-base macromolecular legend**,** *European Polymer Journal*, Vol. 42, pp. 1670-1675. https://doi.org/10.1016/j.eurpolymj.2006.01.025

[18] Ramachandranl, E. – Baskaran, K. – Natarajan, S. (2007): XRD, Thermal, FTIR and SEM studies on gel grown glycine crystals. *Crystal Research and Technology*, Vol. 42, No. 1, pp. 73-77. https://doi.org/10.1002/crat.200610774

Ref.:
Abd-Almutalib Al-Mosawy, Manar Ghyath – **Al-Mulla,** Emad A. Jaffa – **Mohamad**, Majed Jari: *Bentonite-based organoclays using chalcone and azo dye as organophilic reagents*
Építőanyag – Journal of Silicate Based and Composite Materials, Vol. 69, No. 2 (2017), 49–54. p.
https://doi.org/10.14382/epitoanyag-jsbcm.2017.9

Bentonit alapú szerves agyagok szintézise kalkon és azovegyület szerves reagensekkel
A cikk szerves reagensekkel szintetizált szerves agyagok előállítását és jellemzőit mutatja be. Az előállított vegyületek struktúráját és a bentonit alapanyaghoz kapcsolódásának mértékét Fourier transzformációs infravörös spektroszkópiával (FTIR) és röntgendiffrakcióval (XRD) vizsgálták. Az FTIR és XRD vizsgálatok igazolták, hogy a szerves komponensek sikeresen megkötődtek a bentonit agyagban. Termoanalitikai (TGA) vizsgálatokkal vizsgálták a vegyületek stabilitását. A TGA vizsgálatok rámutattak, hogy a szerves agyagok stabilitása jobb a tiszta bentoniténál. A szintetizált szerves agyagok alkalmazása sikeres lehet eldobható, lebomló nanokompozit csomagolóanyagok előállítása során.
Kulcsszavak: nátrium bentonit, modifikálás, felületaktív anyagok, szerves kationok

The effect of saturation degree of cement paste on fair-faced concrete surfaces

Kitti KÁROLYFI
Graduated as an Architect at István Széchenyi University in 2016. PhD student at the Department of Structural and Geotechnical Engineering (SZE). Main research area: concrete technology, fair-faced concrete.

Kitti KÁROLYFI ▪ István Széchenyi University, Department of Structural and Geotechnical Engineering ▪ k.kitti93@gmail.com

Érkezett: 2017. 03. 30. ▪ Received: 30. 03. 2017. ▪ https://doi.org/10.14382/epitoanyag-jsbcm.2017.10

Abstract

The aim of this study is to examine the quality of fair-faced concrete surfaces with respect to differently saturated mixtures. Technical literature recommends an oversaturated concrete composition with 20-40 l/m³ in the case of fair-faced concrete [1]. This paper evaluates the implementation of 4 mixtures made with different saturation degree (22, 55, 88, 121 l/m³) of the cement paste, fixed quality formwork and release agent. A unique formwork was used for implementation of the specimens, which enabled to examine the critical points of the fair-faced concrete technology (oblique surfaces, sharp-angled corner, exclusion) and the effect of the different absorbent form liners (plywood and steel). The main aspects of the evaluation of the surfaces were porosity, discoloration and the texture based on Hungarian standard [2] and German guideline [3]. Compressive strength of mixtures was examined on standard cubes at 7 and 28 days of age. Based on the results the optimal saturation degree was high beyond the recommended value in the tested range with respect to the surface quality of the specimens. However, the compressive strength was reduced by increasing the saturation degree, which is an observable point in the design of fair-faced concrete members.

Keywords: fair-faced concrete, concrete technology, saturation degree, surface-quality

1. Introduction

In the last decades the concrete as a building material got a reinterpretation. The XXI century's concrete architecture is characterized by multifarious forms and high surface-quality. This quality is influenced by numerous factors, for example the material and geometry of the applied formwork, the concrete composition, the applied release agent, the environmental conditions and the construction work. Therefore, the reason of the occurring defects of the surface appearance can be hardly discovered and the surface is not reparable afterwards. The goal of this research is the examination of the fair-faced concrete surfaces referring to the different saturation degree of cement paste of the concrete composition. According to the literature in the case of fair-faced concrete the application of an oversaturated mixture with a value of 20-40 l/m³ is recommended [1]. Accordingly this research includes a wider examination of the oversaturated mixtures with a value from a nearly saturated mixture (22 l/m³) to a significantly oversaturated mixture (121 l/m³), increasing it in 3 steps.

2. Applied materials

2.1 Concrete technology

4 concrete mixtures were prepared in the laboratory of Holcim Zrt. in Győr, according to *Table 1*. In the course of the research CEM I 52,5 N white cement was used in order to facilitate the discovering of the surface defects. The applied material was produced in one cycle therefore there was a constant quality provided during the research. *Schlumpf* et al [4] recommended the application of cement content with a minimum value of 300 kg/m³ in the case of fair-faced concrete. For this reason the first mixture was designed with a cement content of 320 kg/m³ and a water content of 160 kg/m³, which was a nearly saturated mix (V_{sa} = + 22 l/m³). The main variable parameters were the amount of cement, water and the aggregate, and therefore the saturation degree of the cement paste, assuring a constant water to cement ratio.

In all mixtures the same type of aggregate (sand and gravel from Danube River) was used. In all cases a fixed proportion of particle size distribution was applied as 48% sand (0-4 mm),

Mixtures	m_c Cement (kg/m³)	V_w Water (l/m³)	m_a Aggregate (kg/m³)	m_{pl} Plasticizer (kg/m³)	V_{sa} Value of Saturation (l/m³)	w/c Water to cement ratio	Consistency class (flow table test) [5]
1	320	160	1919	2,8	+ 22	0.50	F4
2	360	180	1832	1,5	+ 55	0.50	F4
3	400	200	1745	1,0	+ 88	0.50	F4
4	440	220	1658	0	+ 121	0.50	F4

Table 1. The parameters of the examined concrete mixtures
1. táblázat A 4 vizsgált betonösszetétel jellemző paraméterei

20% small gravel (4-8 mm), and 32 % medium gravel (8-16 mm), respectively. Maximum size of aggregate was D_{max}=16 mm.

2.2 Formwork

Two main aspects were considered in the design process of the formwork. In one hand the performance of the formwork should enable the examination of the critical points of fair-faced concrete technology. According to *Fig. 1* it has a thin, wall-like geometry, whose one side is beveled in order to examine the differences of the porosity of the differently positioned surfaces. It allows to discover to what extent can the differently oversatured mixtures fulfill the sharp-angled (54°) corner. There was an exclusion created on the one vertical side of the formwork in order to examine the development of the blisters in this sensitive area too.

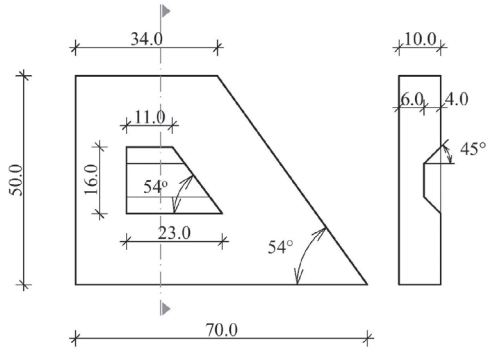

Fig. 1. Performance of the applied formwork (cm)
1. ábra Az alkalmazott zsaluzat terve (cm)

On the other hand the examination of the effect of the differently saturated concrete mixtures and differently absorbent form liners on concrete surfaces was an important aspect too. Hence steel plate and plywood was used as form liners according to *Fig. 2.* SIKA Release agent 2a was used as form release agent, this is a solvent-free, mineral-oil based release agent for metal, wood and plastic.

Fig. 2. The applied form liners
2. ábra Az alkalmazott zsaluhéjak

2.3 Construction work

The consistency class was obtained by performing the most diluted (4.) mixture, using flow table test. The constant consistency class (F4) in the case of the other mixtures was assured by applying plasticizer. The mixtures were filled in the formwork in three layers and were compacted on a vibrating table. The test pieces were kept in the formwork for 3 days as curing.

3. Aspects of the evaluation

The evaluation of the test pieces was accomplished based on MSZ 24803-6-3:2010 [2] and the German Code of Practice for Fair-Faced Concrete [3] edited by German Concrete and Construction Engineering Association (DBV) and the Federal German Association of the Cement Industry (BDZ). The obtained results were compared to each other. The main aspects of the examination were the porosity, the discoloration and the texture (honeycombing). In addition, the 7- and the 28-days compressive strength of the mixtures was examined on standard cube specimens.

4. Experimental results

4.1 Examination of the porosity

Despite of the careful design and construction work the formation of pores is unavoidable. The porosity of the concrete surface must not exceed the limit value of the given concrete class defined by the standards. According to the Hungarian standard and the German guideline the pores with a diameter of 1-15 mm and 2-15 mm were taken into account [2,3]. The examination was accomplished on each surface of the 4 specimens. As the area of the pores smaller than 2 mm is minimal, the difference between the porosity values of the two standards was negligible. In pursuance of the evaluation there were 3 surface groups defined depending to their position to the pouring-in direction (*Fig. 3*):

- P1-5 (vertical) surfaces: Parallel with the pouring-in direction
- V1 (horizontal) surface: Perpendicular to the pouring-in direction
- F1-4 (beveled) surfaces: Angular with the pouring-in direction.

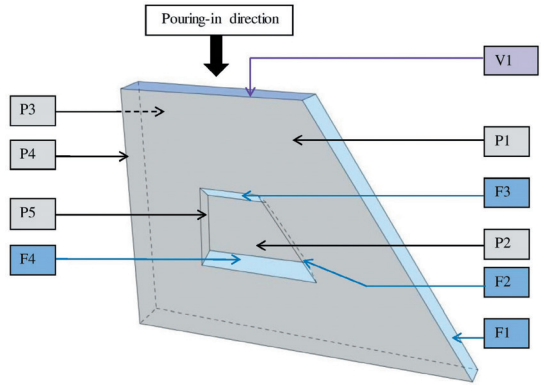

Fig. 3. Grouping of the surfaces
3. ábra Felületek csoportosítása

Fig. 4 illustrates the results of the porosity examination of the specimens by surface groups. The most significant change was shown in the surrounding area of the exclusion on the surfaces P2 and P5 (*Fig. 5*), and on the beveled surfaces F1 (*Fig. 6*). Increasing the saturation degree to the value of 88 l/m^3 – which is nearly fourfold of the recommended value – the porosity

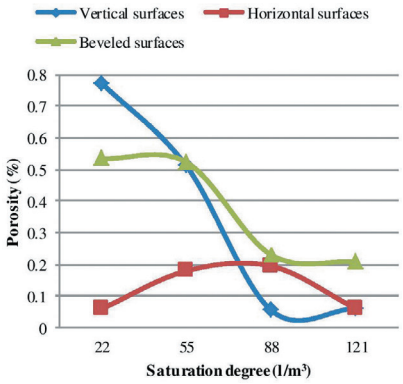

Fig. 4. The average porosity of surface groups by cement slurry saturation
4. ábra Felületcsoportok átlagos pórustartalmának változása a péptelítettség növekedésével

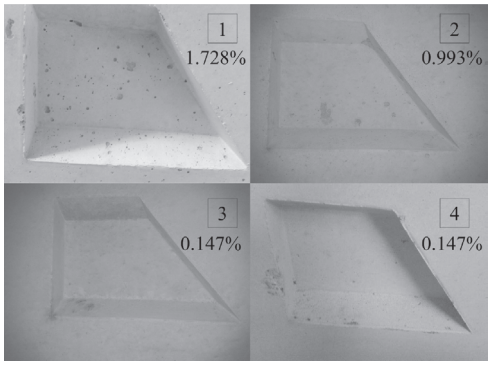

Fig. 5. Porosity of the surface P2 of the 4 specimens
5. ábra A 4 próbatest P2 felületének porozitás változása

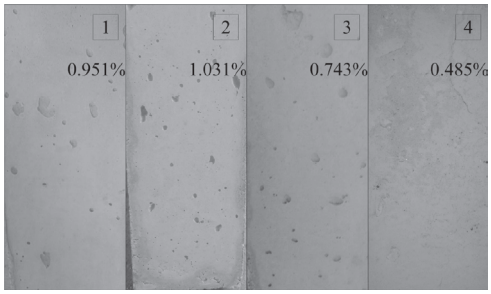

Fig. 6. The change of the porosity of the surface F1 by specimens
6. ábra F1-es felület pórustartalmának változása próbatestenként

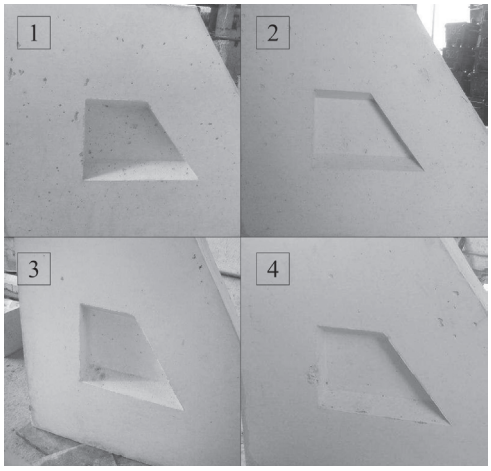

Fig. 7. The porosity of surfaces made by steel form liner
7. ábra Fém zsaluhéjjal készült felületek pórustartalma

of the vertical surfaces decreased with 90% and the beveled surfaces' with 66% on average. The porosity of surfaces made by unabsorbent (steel) form liners was more than 90% higher, than the maximal porosity of surfaces made by absorbent (plywood) form liner. In regard to the porosity, the last specimen, made with significantly oversaturated mixture (121 l/m^3) can be classified into the highest fair-faced concrete class according to both the Hungarian and German guidelines. This establishment can be confirmed by visual inspection too, see *Fig. 7*. The porosity of surfaces made by absorbent form liner did not even reach the limit of the highest concrete class (MSZ: 0,6%, DBV: 0,3%) in the case of every specimens. Considering the average porosity of the surface groups the optimal degree of saturation was between 88 and 121 l/m^3 in the tested range.

4.2 Discoloration

Regarding the discoloration it is expedient to examine the surfaces made by absorbent and unabsorbent form liners separately. On the surfaces made by plywood (P3) some dark discolorations were shown on the first three specimens, which can be explained with the local difference of absorbency of the form liner [6] (see *Fig. 8*). The degree of the dark coloration decreased and became even smoother by increasing the level of oversaturation. The surfaces made by steel form liner were self-colored, but the other surface defects were more conspicuous. As a result of visual inspection the fourth specimen – where the value of oversaturation was 121 l/m^3 – showed absolutely homogeneous surface quality. Additionally, this specimen can be classified into the highest class (FT3) of texture based on the German guideline.

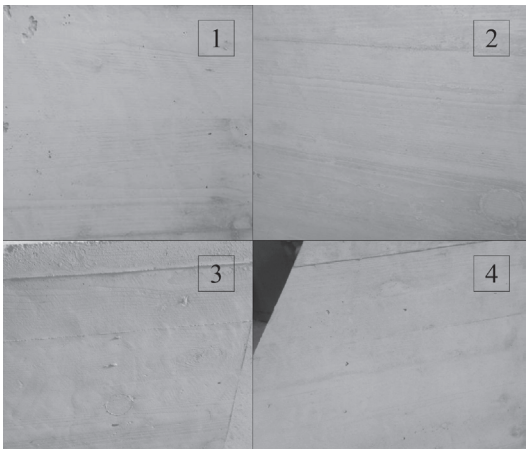

Fig. 8. The discoloration of surface P3, made by absorbent form liner
8. ábra P3-mas, nedvszívó zsaluhéjjal készült felület elszíneződései próbatestenként

4.3 Texture

In the course of the experiment the right and sharp-angled corner of the specimens showed honeycombing. The joints of the form liners were leak on purpose to examine the sensitivity of the different mixtures to this phenomenon under the same circumstances. In the case of honeycombing any unequivocal trend cannot be established in the tested range. The degree of honeycombing was a bit higher in the case of the fourth specimen, otherwise the test pieces were nearly equivalent, see *Fig. 9*.

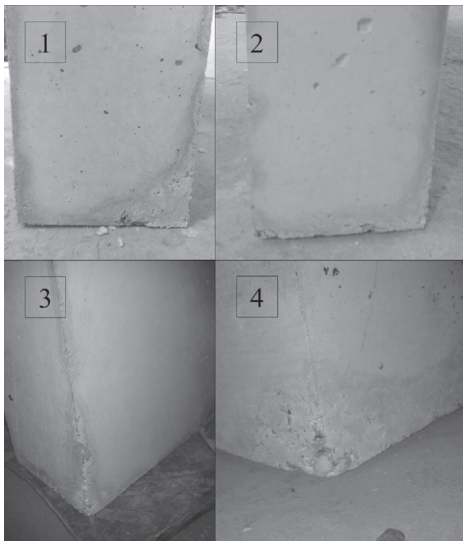

Fig. 9. Honeycombing in the corner of the 4 specimens
9. ábra Fészkesedés a próbatestek sarkában

4.4 Compressive strength

In the point of the compressive strength the hardened cement paste gets a greater significance with increasing saturation degree of the concrete composition [7]. Since the strength of the aggregates used is generally higher, than that of the cement paste, obviously the higher saturation degree of cement paste used, the lower the compressive strength of concrete. The values of the compressive strength with respect to saturation degree are presented in *Fig. 10*. At the age of 7 days, concrete mixtures showed a decrease of 7% in compressive strength, and a decrease of 9.8 % is corresponding to the age of 28 days. The relationship between compressive strength and saturation degree was found to be nearly linear in the tested range.

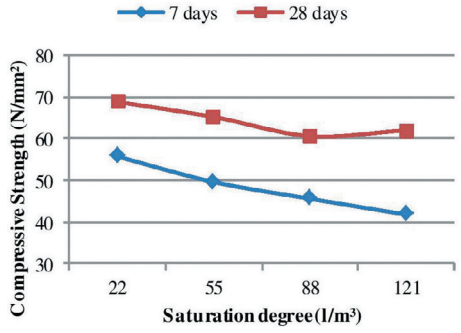

Fig. 10. The values of 7- and 28-days compressive strength with respect to the saturation degree [8]
10. ábra A 7 és 28 napos nyomószilárdsági értékek a péptelítettség függvényében [8]

5. Conclusions

The classification of the test pieces based on the German guideline is shown in *Table 2*. Based on the presented examination concerning the effect of different levels of saturation on fair-faced concrete surfaces, the following conclusions can be drawn:

- The overall surface-quality of the mixtures became even higher with increasing saturation degree in the tested range.
- Based on the previous result the optimal level of saturation was between 88 and 121 l/m^3, which noticeably exceeds the recommended value (20-40 l/m^3).
- The surface-quality in the critical points (the sharp-angled corner, the environment of exclusion) increased significantly with the higher saturation degree.
- There was a difference between surfaces in different positions; the porosity of vertical surfaces was averagely higher, than the beveled surfaces', and the lowest was the horizontal surfaces'.
- The porosity of the surfaces made by absorbent form liner was appreciably lower, than in the case of unabsorbent form liner.
- The surfaces made by absorbent form liner showed more discolorations.
- In the case of oversaturated mixtures the sealing of joints is especially important.
- The increase of saturation degree improved the quality of the surfaces made by unabsorbent form liner to a great extent.
- The examination of compressive strength of the specimens confirms that higher saturation degree reduces the value of compressive strength [7].

Mixtures	Aspects of evaluation						
	Porosity		Discolor-ation		Texture		Classification [3]
	U	A	U	A	U	A	
1.	-	P4	FT3	FT1	T3	T2	-
2.	P1	P3	FT3	FT1	T3	T2	SB2
3.	P2	P4	FT3	FT2	T3	T2	SB3
4.	P3	P4	FT3	FT3	T3	T2	SB4

Table 2. Classification of the specimens by the German Code of Practice for Fair-Faced Concrete (A: absorbent, U: unabsorbent form liner) [3]
2. táblázat Próbatestek osztályba sorolása a „Merkblatt Sichtbeton" vizsgálati szempontjai alapján (A: nedvszívó, U: nem nedvszívó zsaluhéj) [3]

References

[1] Kapu László: Látszóbeton – Látványbeton, TERC Kft., Budapest, 2014.
[2] MSZ 24803-6-3:2010. Épületszerkezetek megjelenési módjának előírásai. 6-3. rész: Monolit beton- és vasbeton szerkezetek. A helyi alakhűség és a felületi állapot követelményei (Specifications for appearance of building structural elements. Part 6-3: Specifications for appearance of concrete and reinforced concrete structures. Requirements for local surface conditions and shape conformity)
[3] DBV/BDZ-Merkblatt Sichtbeton, Deutscher Beton- und Bautechnik-Verein e.V. Berlin, und Bundesverband der Deutschen Zementindustrie, Köln, 2004.
[4] Dipl.-Ing. HTL Jürg Schlumpf – Dipl.-Ing. Bastian Bicher – Dipl.-Ing. Oliver Schwoon: Sika Beton Handbuch, Sike Services AG, Zürich, 2013.
[5] EN 12350-5:2009. Testing fresh concrete – part 5: Flow table test
[6] Doris Elisabeth Strehlein: Fleckige Dunkelverfärbungen an Sichtbetonoberflächen – Charakterisierung – Entsehung – Vermeidung, PhD Dissertation, Technische Universität München, Lehrstuhl für Baustoffkunde und Wersktoffprüfung, München, 2012.
[7] Dr. Balázs György: Barangolásaim a betonkutatás területén, Akadémiai Kiadó, Budapest, 2001.
[8] EN 12390-3:2009. Testing hardened concrete. Compressive strength of test specimens

Ref.:
Károlyfi, Kitti: *The effect of saturation degree of cement paste on fair-faced concrete surfaces*
Építőanyag – Journal of Silicate Based and Composite Materials, Vol. 69, No. 2 (2017), 55–58. p.
https://doi.org/10.14382/epitoanyag-jsbcm.2017.10

Long term mechanical properties of self-compacting concrete made with slag cement and supplementary cementitious materials

Abdulkader EL MIR ▪ BME Department of Construction Materials and Technologies ▪ abdelkader.elmir@hotmail.com

Salem Georges NEHME ▪ BME Department of Construction Materials and Technologies ▪ sgnehme@yahoo.com

Érkezett: 2017. 04. 03. ▪ Received: 03. 04. 2017. ▪ https://doi.org/10.14382/epitoanyag-jsbcm.2017.11

Abstract:
Self-compacting concrete (SCC) is becoming more popular in terms of application and innovation in the building industry. Durable concrete structures can be established when SCC is used with the proper mix design and selection of materials. The amount and type of filler or supplementary cementitious materilas (SCMs) are among the most important parameters affecting the fresh and hardened properties of SCC. Mainly, SCMs improve the hydration of cement due to their physical characteristics and chemical compositions, thus a more sustainable and eco-friendly SCC product could be achieved by the substitution of cement clinker by SCMs. The aim of this study was to evaluate the effect of total powder content, cement content and SCMs type on the fresh and hardened properties of SCC. The compressive strength, splitting tensile strength, modulus of elasticity and total porosity properties were the experimental tests carried out in this investigation. The finding of this study showed that the compressive strength of SCC with metakaolin (MK) gives higher values, as compared to mixtures with silica fume (SF), at the age of 400 days. MK and SF showed a negligible effect on the splitting tensile strength and modulus of elasticity, as compared to the reference mixtures. Total porosity test results were lower with the increase of total powder content and by the addition of SCMs.
Keywords: Self-compacting concrete, Mechanical properties, Sustainability, Metakaolin, Silica fume

Abdulkader EL MIR
MSc Civil Engineer, PhD student at BME, Department of Construction Materials and Technologies. Fields of interest: porosity of concrete, self compacting concretes, high performance concretes.

Salem Georges NEHME
MSc Civil Engineer, PhD, Associate Professor at BME, Department of Construction Materials and Technologies. Fields of interest: concrete technology, mass concrete, self-compacting concrete, fibre reinforced concrete, quality control of building materials, non-destructive testing, reinforced concrete structures, recycling of building materials.

1. Introduction

Concrete is a composite, time dependent material that is characterized by a complex pore structure. The latter affects the properties of concrete which can be controlled by the application of the proper combination of ingredients in the mix design. Pore size, shape and distribution highly affect the mechanical response of concrete such as the compressive strength, modulus of elasticity and other properties [1-3]. Self-compacting concrete (SCC) is a highly workable, non-segregating concrete which is able to fill the formwork under its own weight and expand into the reinforcement without any mechanical intervention [4]. In general, SCC which falls into the high performance concrete category differs from normally vibrated concrete (NVC) with relatively higher paste content in order to achieve the desired rheological properties in the fresh stage [5]. Multiple fillers or supplementary cementitious materials (SCMs) with relatively different physical properties such as the particle size distribution and the specific surface area can be used to obtain the targeted paste in the design. Metakaolin (MK), silica fume (SF) and other SCMs are introduced into the concrete to enhance its performance and microstructure due to their physical and chemical effect on the hardened cement paste. Thereby, a more confined and less porous concrete network could be obtained [6-10]. Several studies had evaluated SCC characteristics in terms of the fresh and hardened properties. Today, the building industry main objective is towards applying more sustainable and eco-friendly materials. Hence the aim of this study was to evaluate the long term mechanical properties of SCC mixtures incorporating slag cement and SCMs.

The literature shared a lot of information regarding the compressive strength of concrete incorporating slag cement [11-13]. *Shariq* et al. [13] observed that concrete made with 40% replacement of the cement clinker by slag attained higher compressive strength as compared to the 20% and 60% replacement level of slag in concrete.

Most published articles acknowledged that for a selected compressive strength value, SCC could reach a tensile strength value which is slightly smaller than of NVC [14-18]. For instance, *Parra* et al. [14] registered lower values of splitting tensile strength of SCC made with limestone powder (LP) filler than that of NVC, however, *Felekoglu* et al. [17] showed that higher splitting tensile strength values were obtained in SCC rather than NVC.

Regarding the modulus of elasticity, SCC mixtures are considered to be more deformable as compared to NVC [17]. There are small differences in stiffness between SCC and NVC due to the high powder content in SCC, however, *Su* et al. [18] revealed that increasing the fine to total aggregate ratio did not have a major effect on SCC modulus of elasticity.

In almost all results available in the literature, SCC was mostly prepared with high amount of cement (higher than

400 kg/m³) and other additives, filler or SCMs such as fly ash, slag and others. Therefore, the authors aimed to evaluate the performance of SCC with a selective range of the total powder and cement content.

2. Experimental program

2.1 Materials

Slag cement (C) CEM III/A 32.5 R, LP, MK, SF, natural Danube river sand (0-4 mm) and gravel (4-8 mm, 8-16 mm) were the used materials in this study. LP served as the filling material for SCC mixtures to ensure the desired rheological properties. MK and SF were the SCMs implemented to enrich the mechanical properties. A high range water reducing admixture (HRWRA) "Sika Viscocrete 5 Neu" was applied to serve the workability of SCC mixtures. Particle size distribution fractions of aggregates were: sand (0-4 mm, 45%), small gravel (4-8 mm, 20%) and medium gravel (8-16 mm, 35%). The physical properties and chemical compositions of the C, LP and SCMs are summarized in *Table 1*. Regarding the powder materials, the particle size distribution curves are shown in *Fig. 1*.

Chemical composition	C (%)	SF (%)	LP (%)	MK (%)
SiO_2	25.53	95.09	5.63	52.79
Al_2O_3	6.3	0.24	1.4	42.07
Fe_2O_3	2.29	0.06	0.9	1.25
CaO	55.59	0.91	50.32	0.37
MgO	4.05	0.32	0.65	0.38
SO_3	2.34	0.07	0.08	< 0.01
K_2O	0.78	0.51	0.29	1.22
Na_2O	0.33	0.2	0.07	0.02
TiO_2	0.28	< 0.01	0.08	0.2
Mn_2O_3	0.3	0.03	0.01	0.04
P_2O_5	0.03	0.07	0.02	0.06
Physical properties				
Specific gravity	3.1	2.35	2.69	2.6
Blaine (cm²/g)	3450	20450	3470	15244
loss on ignition (%)	2.15	2.49	40.55	1.59

Table 1 Chemical and physical characteristics of binders and filler materials
1. táblázat Cement és kiegészítő anyagok kémiai és fizikai jellemzői

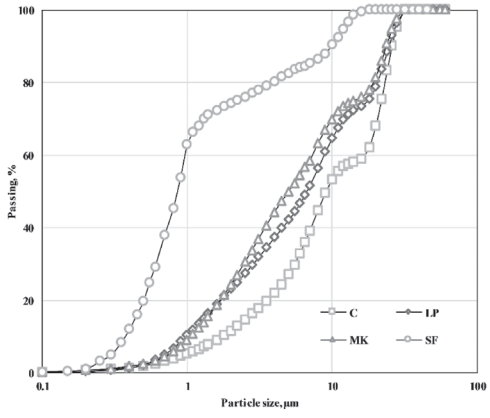

Fig. 1. Particle size distribution of powder materials
1. ábra Cement és kiegészítő anyagok szemcseméret eloszlása

2.2 Mixtures proportion

A total of twenty-seven SCC mixtures were planned in 3 main series: reference series (R), MK series (M) and SF series (S). Each of these series held 3 separate cement and total powder content (320, 360, 400), (620, 580, 520) respectively. The total powder content is defined as the sum of cement, SCMs and LP used in this investigation. A constant amount of 40 kg/m³ of MK or SF was added to the relevant M and S series independently. Also a constant amount of water was added for all SCC mixtures (180 kg/m³). For more details, *Table 2* shows the mixtures composition of all series. The mixing procedure started by mixing the aggregates, LP, cement and water together for one minute. MK or SF were added afterwards to the mixer with the required amount of HRWRA.

This selection of parameters contributed to the understanding of powder and binder effect on the mechanical response of SCC mixtures. Due to scope of the experiment, parameters related to the compressive strength and other mechanical properties were taken from a previous study [19].

Mix ID	Cement	MK	SF	Total powder	Aggregates	HRWRA
R1	320	0	0	620	1520	3.04
R2	360	0	0	620	1524	3.06
R3	400	0	0	620	1529	3.56
R4	320	0	0	580	1560	1.92
R5	360	0	0	580	1565	2.02
R6	400	0	0	580	1569	2.72
R7	320	0	0	520	1618	1.74
R8	360	0	0	520	1624	1.55
R9	400	0	0	520	1629	1.76
M1	320	40	0	620	1518	3.36
M2	360	40	0	620	1524	3.96
M3	400	40	0	620	1524	4.4
M4	320	40	0	580	1557	2.72
M5	360	40	0	580	1562	2.92
M6	400	40	0	580	1564	4
M7	320	40	0	520	1616	2.27
M8	360	40	0	520	1620	2.34
M9	400	40	0	520	1625	2.84
S1	320	0	40	620	1506	5.44
S2	360	0	40	620	1514	4.86
S3	400	0	40	620	1520	5.2
S4	320	0	40	580	1551	2.88
S5	360	0	40	580	1556	3.17
S6	400	0	40	580	1560	3.76
S7	320	0	40	520	1611	2.31
S8	360	0	40	520	1616	2.34
S9	400	0	40	520	1620	2.72

Table 2. Mixtures composition for SCC mixtures series (R, M and S)
2. táblázat Vizsgált betonok összetétele (R, M és S)

2.3 Fresh state evaluation

In order to examine the adequacy of deformability and viscosity of the prepared SCC mixtures, slump flow and V-funnel tests were carried out according to European

Standards [20-21]. Also, refereeing to EFNARC guidelines for SCC [22], the aim of the evaluation was to obtain a slump flow criterion which belong to SF3 category. The latter could be achieved by the proper addition of HRWRA and selection of the maximum aggregate size of 16 mm.

2. 4 Hardened state evaluation

To characterize SCC mixtures in the hardened state, four types of tests were carried out: compressive strength, splitting tensile strength, modulus of elasticity and total porosity tests. As for the compressive strength test, 150 mm cubic specimens were tested at the age of 28 and 400 days in accordance with European standards [22]. However, the splitting tensile strength and modulus of elasticity were evaluated at the age of 400 days only [24-25]. The specimen dimensions were 150 mm cubes (splitting tensile strength) and 150 × 300 mm cylinders (modulus of elasticity).

Total porosity in hardened concrete was calculated. It was determined based on the ratio of bulk (containing open and closed pores) and particle (containing no pores) densities of concrete specimens. Bulk density was measured referring to ASTM C642 standards [26]. Shredded specimens were crushed and grounded into fine powder reaching an average diameter size of 0.02 mm in order to evaluate true densities using the pycnometer [27]. Hence, the total porosity was obtained from the following equation:

$$P_T = 1 - \frac{\rho_b}{\rho_p}$$

ρ_b *and* ρ_p are the bulk and particle densities (g/cm³) respectively.

3. Results and analysis

3.1 Rheological properties

The amount of HRWRA varied between SCC series. In case of S1 mixture, the highest dosage of HRWRA (5.44 kg/m³) was required. It appeared that with higher total powder content, more HRWRA amount is needed to ensure the workability of concrete. As it can be seen in *Fig. 3*, SCC mixtures with highest total powder content (620 kg/m³) have a mean amount of HRWRA of 4.1 kg/m³. This value decreases with the decrease of total powder content reaching 2.90 and 2.20 kg/m³ in case of 580 and 520 kg/m³ respectively. This behavior could be explained by the effect of powder on enhancing the plastic viscosity of the mixture, thus, requiring additional HRWRA to obtained the desired workability [28].

The same pattern can be noticed with the cement content variation. According to Fig. 4, SCC mixtures with a corresponding value of 400 kg/m³ of cement, showed a mean dosage value of 3.44 kg/m³ of HRWRA. However, SCC mixtures with lower cement content (320 or 360 kg/m³) had lower mean values of HRWRA (2.85 and 2.91 kg/m³) respectively. Furthermore, the effects of MK and SF on SCC mixtures were also noticeable as compared to their reference mixtures. S and M series required additional amount of HRWRA (up to 52% and 35%) in accordance with R series. Due to the higher specific surface area of SF particles compared with MK and C, the corresponding dosage of HRWRA was higher. Hassan et al. confirmed such behaviour by acknowledging that the addition of MK required less amount of HRWRA than SF at the same level of cement substitution [29].

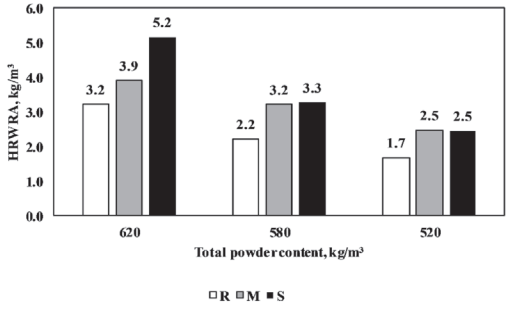

Fig. 3. Mean values of HRWRA dosages in terms of similar total powder content for SCC mixtures
3. ábra Folyósítószer adagolása azonos finomrész tartalmú SCC keverékekben

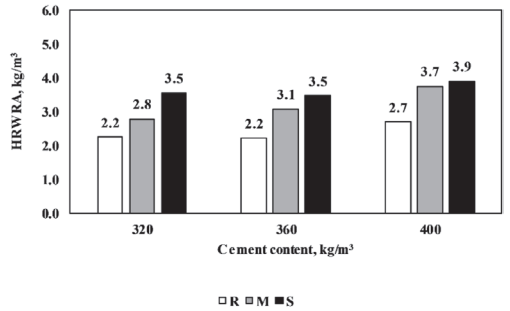

Fig. 4. Mean values of HRWRA dosages in terms of similar cement content for SCC mixtures
4. ábra Folyósítószer adagolása azonos cementtartalmú SCC keverékekben

3. 2 Compressive strength

Absolute mean compressive strength values of SCC mixtures are summarized in *Table 3*. As it can be observed, SCC mixtures with MK or SF (M and S series) have higher compressive strength values than of those mixtures without SCMs (R series).

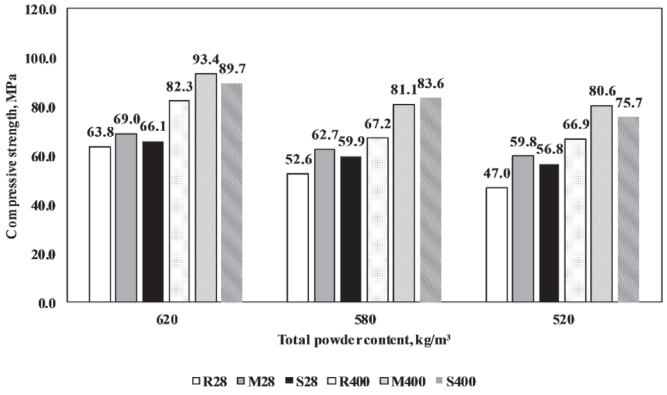

Fig. 5. Mean values of compressive strength in terms of similar total powder content for SCC mixtures at 28 and 400 days
5. ábra Megszilárdult beton nyomószilárdságának átlagos értéke 28 és 400 napos korban azonos finomrész tartalmú SCC keverékekre vonatkozóan

According to *Fig. 5*, The effect of total powder content and SCMs on the magnitude of the compressive strength is obvious. A decreasing tendency in the compressive strength is noticed with the decrease of the total powder content. SCC mixtures which possess the total powder content values of 580 and 520 kg/m³ showed a mean decrease of the compressive strength of 13% and 21% at 28 days with respect to the highest total

powder content (620 kg/m³). Same pattern is noticed at 400 days of age with a mean decrease of 14% and 18% respectively. Therefore, the application of more LP filler considerably enhanced the strength of concrete once it was used along with SCMs (pozzolanic activity) [8]. To visualize the magnitude of SCMs, SCC mixtures were divided into three series. Maximum compressive strength values (77 MPa at 28 days) was recorded for MK mixture (M3) which was considered to have the overall best performance. This behaviour would be explained by the high amount of total powder (620 kg/m³) and binder content (400 C + 40 MK kg/m³) as compared to other mixtures. In addition, S3 mixture which combines the same amount of powder and binder showed the second highest values of mean compressive strength as compared to M3 mixture.

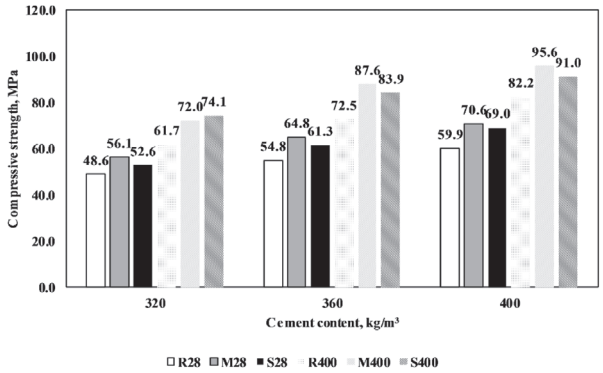

Fig. 6. Mean values of compressive strength in terms of similar cement content for SCC mixtures at 28 and 400 days
6. ábra Megszilárdult beton nyomószilárdságának átlagos értéke 28 és 400 napos korban azonos cementtartalmú SCC keverékekre vonatkozóan

Considering *Fig. 6*, the mean compressive strength values exhibited an increasing tendency with the increase of the cement content. In case of SCC mixtures that held a cement content of 400 kg/m³, a mean increase of 26 % was noticed with respect to SCC which held 320 kg/m³ of cement. The same pattern was observed by 15% in case of SCC mixtures with 360 kg/m³ of cement content. M and S series resulted in highest mean compressive strength values of 64 and 61 MPa in comparision with R series of 54 MPa. The additional pozzolanic reaction (by converting $Ca(OH)_2$ to extra calcium silicate hydrate in the accessible pore microstructure of the hardened cement paste) explains the MK and SF effect as compared to their reference mixtures. This is in agreement with the established fact in the literature [30,31].

3.3 Splitting tensile strength

Splitting tensile strength of concrete is considered to indicate a primary mechanical characteristic that highly influences the size and extent of tension failure behaviour, such as flexural in beams and splitting which results from rebar friction interaction with the concrete [32]. Referring to *Table 3*, maximum splitting tensile strength was recorded to R3 mixture with 5.47 MPa. Looking at mixtures that correspond to 620 kg/m³ of total powder content, it could be seen that these mixtures showed the highest mean splitting tensile strength value (4.9 MPa) in comparison with lower total powder content mixtures (580 and 520 kg/m³) which have showed lower mean splitting tensile strength values (4.36 and 4.35 MPa) (*Fig. 7*).

Mixtures ID	Compressive strength (MPa)		Splitting Tensile strength (MPa)	Modulus of elasticity (GPa)	Total porosity (V %)
	*fcm,cube	fcm,cube	**fspm,cube	***Ecm,cyl	Pt
Days	28	400	400	400	400
R1	57.90	71.68	4.68	30.94	12.78
R2	63.04	83.43	5.06	32.50	11.11
R3	70.39	91.83	5.47	37.85	9.06
R4	47.21	59.61	3.61	31.84	13.03
R5	52.76	65.66	4.21	33.44	12.07
R6	57.71	76.24	4.87	36.14	11.20
R7	40.72	53.74	3.31	25.81	14.84
R8	48.49	68.28	4.13	33.67	13.04
R9	51.66	78.67	4.51	33.55	10.85
M1	61.33	80.53	3.99	34.05	10.98
M2	68.80	94.88	4.66	37.92	11.54
M3	76.99	104.84	5.87	41.11	6.34
M4	56.11	70.53	3.78	31.96	12.50
M5	61.96	82.60	4.32	33.89	11.89
M6	69.90	90.22	5.12	33.27	8.98
M7	50.85	64.82	3.97	27.66	13.12
M8	63.61	85.44	4.44	29.64	10.23
M9	64.91	91.61	5.28	36.76	8.63
S1	59.00	77.44	4.16	31.79	7.59
S2	65.01	89.74	5.11	32.69	5.65
S3	74.43	101.87	5.20	37.70	5.15
S4	49.79	73.68	3.98	30.02	9.26
S5	59.41	85.55	4.25	33.36	8.86
S6	70.46	91.61	5.17	36.58	6.25
S7	48.91	71.16	4.04	29.91	12.48
S8	59.50	76.41	4.53	31.09	10.12
S9	61.98	79.53	4.94	35.39	8.16

$*f_{cm,cube}$: mean compressive strength of tested cubic specimens;
$f_{cm,cube}$: mean splitting tensile strength of tested cubic specimens;
$***E_{cm,cyl}$: mean modulus of elasticity of tested cylindrical specimens.

Table 3. Mechanical characteristics of the tested SCC mixtures
3. táblázat A vizsgált SCC keverékek mechanikai jellemzői

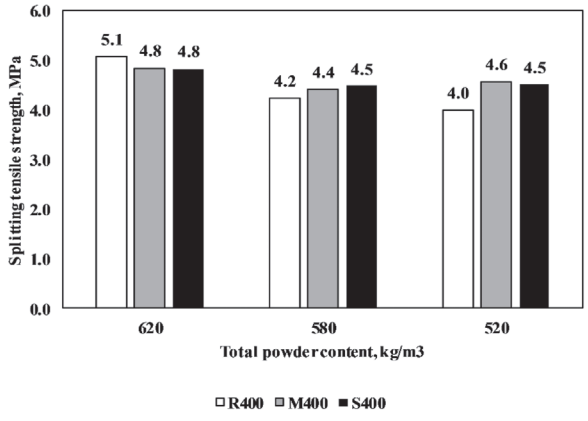

Fig. 7. Mean values of the splitting tensile strength in terms of similar total powder content for SCC mixtures at 400 days
7. ábra Megszilárdult beton hasító-húzószilárdságának átlagos értéke 400 napos korban azonos finomrész tartalmú SCC keverékekre vonatkozóan

Same pattern is observed in *Fig. 8*. With the increase of cement content, highest splitting tensile strength values are recorded in case of 400 kg/m³ of cement. Therefore, it was obvious that the property of the splitting tensile strength for SCC mixtures is not too dependent on the disparities of the cement and total powder content parameters as it was in the compressive strength. This can be explained by the difference in mixtures combinations of materials, hence the variation in splitting tensile strength results may not give a clear relation with the variations in compressive strengths.

Generally, M and S series mixtures enhanced the splitting tensile strength by 4 % with respect to R series. MK seemed to be slightly more effective in enhancing the splitting tensile strength of the mixture as compared to the SF mixtures.

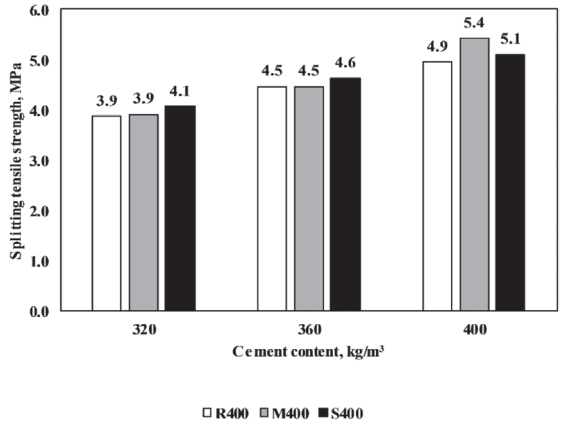

Fig. 8. Mean values of splitting tensile strength in terms of similar cement content for SCC mixtures at 400 days
8. ábra Megszilárdult beton hasító-húzószilárdságának átlagos értéke 400 napos korban azonos cementtartalmú SCC keverékekre vonatkozóan

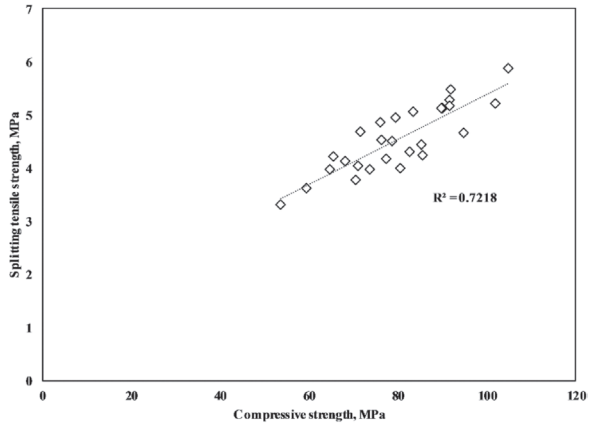

Fig. 9. Compressive and splitting tensile strength for SCC mixtures
9. ábra Vizsgált SCC keverékek nyomó- és hasító-húzószilárdsága

The compressive and splitting tensile strength for SCC mixtures are correlated together and plotted in *Fig. 9*. A linear correlation with a good R^2 value was found for R and S series. Thereby, it can be concluded that the splitting tensile strength of SCC directly relate to the compressive strength values.

3.4 Modulus of elasticity

Several concerns and interpretation have been reported regarding the behaviour of SCC towards the modulus of elasticity [33,34]. Thereby, this paper also covered the evaluation of the modulus of elasticity. Maximum values of the modulus of elasticity were recorded for M3 mixture with 41 GPa (*Table 3*). Referring to *Fig. 10*, when mixtures with highest powder content (620 kg/m³) were compared to the lower ones (580 and 520 kg/m³), the modulus of elasticity values that correspond to the highest showed the highest mean value 35.17 GPa as compared to the others (580 and 520 kg/m³) which possess lower mean values of the modulus of elasticity (33.39 and 31.5 GPa).

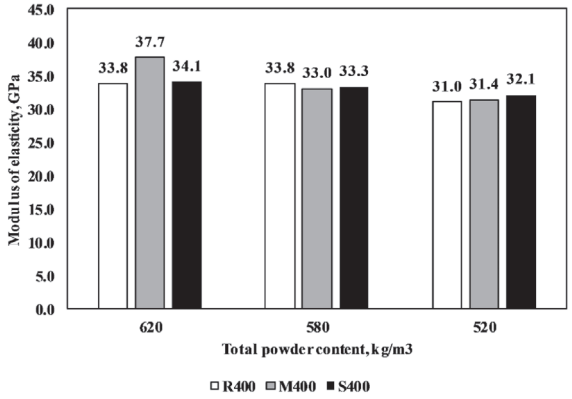

Fig. 10. Mean values of modulus of elasticity in terms of similar total powder content for SCC mixtures at 400 days
10. ábra Megszilárdult beton rugalmassági modulusának átlagos értéke 400 napos korban azonos finomrész tartalmú SCC keverékekre vonatkozóan

Also, with the increase of the cement content, a positive effect on the modulus of elasticity results was achieved. As shown in *Fig. 11*, SCC mixtures with 400 kg/m³ of cement content had higher mean value of modulus of elasticity as compared to 360 and 320 kg/m³ respectively. The effect of MK and SF on enhancing the modulus of elasticity was shown to perform an negligible effect since the mean values of modulus of elasticity of M and S series are (34.03) and (33.17) GPa with respect to reference series R (32.86 GPa).

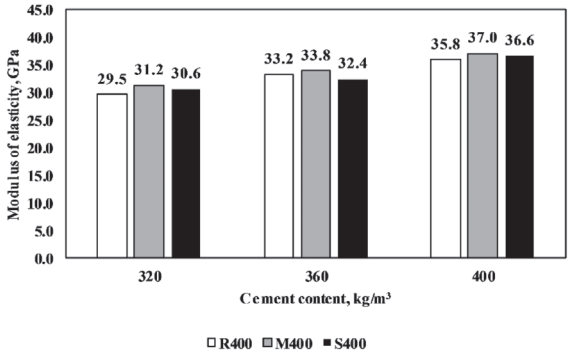

Fig. 11. Mean values of modulus of elasticity in terms of similar cement content of SCC mixtures at 400 days
11. ábra Megszilárdult beton rugalmassági modulusának átlagos értéke 400 napos korban azonos cementtartalmú SCC keverékekre vonatkozóan

Fig. 12 shows the relationship between the compressive strength and the modulus of elasticity of SCC series mixtures at the age of 400 days. The modulus of elasticity increases along with the compressive strength. Results showed acceptable correlation coefficient value (R^2 = 0.607).

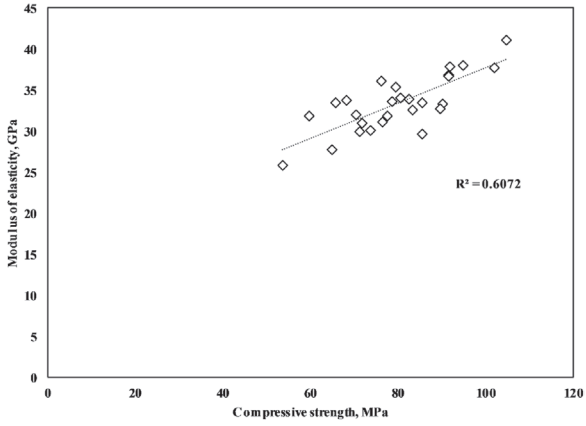

Fig. 12. Compressive strength and modulus of elasticity for SCC mixtures
12. ábra Vizsgált SCC keverékek nyomószilárdsága és rugalmassági modulusa

3.5 Total porosity

Absolute results of the mean values of the total porosity are presented in *Table 3*. R series held the highest total porosity mean value of 12%, whereas lower values were shown for M and S series (10.47% and 8.17 %) respectively. Reference mixture R4 holds the maximum total porosity value of 13.19% which corresponds to the lowest cement content (320 kg/m³). At the highest binder content (400 C + 40 SF kg/m³), mixture S3 showed the lowest value of the total porosity (4.76%).

Fig. 13 illustrates the mean values of total porosity of R, M and S series with respect to the total powder content.

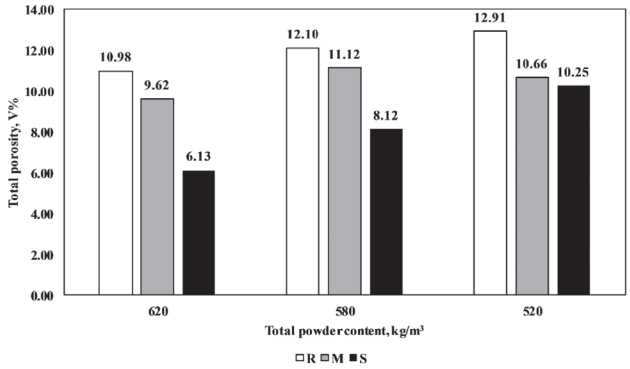

Fig. 13. Mean values of total porosity in terms of similar total powder content for SCC mixtures at 400 days
13. ábra Megszilárdult beton teljes porozitásának átlagos értéke 400 napos korban azonos finomrész tartalmú SCC keverékekre vonatkozóan

Generally, an increasing pattern is noticed for the total porosity along with the decrease of the total powder content. In case of the highest value of the total powder content (620 kg/m³), the mean value of the total porosity is 8.91 %. When the total powder content decreases, the mean values of the total porosity increase (reaching 10.45% and 11.27 % for 580 and 520 kg/m³ respectively). Likewise, referring to *Fig. 14*, the same pattern was noticed when the cement content decreases. Regarding the effect of SCMs' on the total powder or cement content, MK and SF improved the total porosity in a mean value about 14% and 46 % as compared to the reference series R. It was also proved by mercury intrusion porosimetry analysis that SCC with high powder content, the filling effect provided by the powder materials helped making the concrete porosity lower than NVC [35].

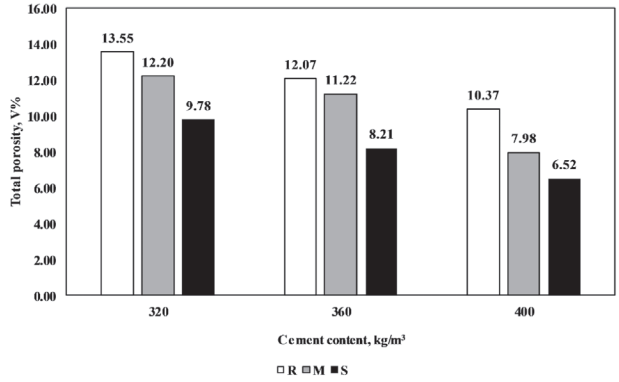

Fig. 14. Mean values of total porosity in terms of similar cement content for SCC mixtures at 400 days
14. ábra Megszilárdult beton teljes porozitásának átlagos értéke 400 napos korban azonos cementtartalmú SCC keverékekre vonatkozóan

Fig. 15 shows the linear correlation between the compressive strength and total porosity of SCC series mixtures at 400 days. A descending trend is observed when the total porosity and compressive strength values increase.

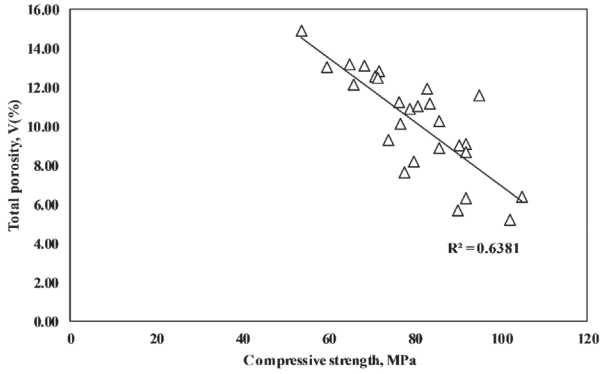

Fig.15. Compressive strength and total porosity for SCC mixtures
15. ábra Vizsgált SCC keverékek nyomószilárdsága és teljes porozitása

4. Conclusions

As the SCC obliges a high amount of binders or additional filling materials for its production, the implementation of slag cement along with SCMs, is a good alternative leading to the reduction of clinker consumption. Based on the above study, the following conclusions can be drawn regarding the properties of the fresh and hardened SCC utilizing MK or SF as SCMs:

- HRWRA demand has increased along with the rise of the total powder content reaching up to 52% for S series as compared to the R series.
- The maximum compressive strength values were reported for the highest total powder content.
- The addition of MK as a SCM (M series) resulted in the highest values in terms of strength at the same level of addition (40 kg/m³) as compared to SF (S series).
- As for the splitting tensile strength and modulus of elasticity tests, the experimental results showed that there is no correlation between them and the compressive strength.
- MK and SF had a negligible effect on enhancing the splitting tensile strength and the modulus of elasticity.

- Total porosity results highly depend on the total powder and cement content.
- Total porosity was improved by the addition of SF and MK.

5. Acknowledgment

Authors would like to acknowledge the support of Sika Corp. and Lafarge for providing the necessary materials.

References

[1] Kondraivendhan. B. – Sabet Divsholi, B. – Teng, S. (2013): Estimation of strength, permeability and hydraulic diffusivity of pozzolana blended concrete through pore size distribution. *Journal of Advanced Concrete Technology*. Vol. 11, pp. 230-237, https://doi.org/10.3151/jact.11.230

[2] Patil, S. G. – Bhattacharjee, B. – ASCE, M. (2008): Size and volume relationship of pore for construction materials. *Journal of Materials in Civil Engineering*. Vol. 20, pp. 410-418. https://doi.org/10.1061/(ASCE)0899-1561(2008)20:6(410)

[3] Barluenga, G. – Palomar, I. – Puentes, J. (2015): Hardened properties and microstructure of SCC with mineral additions. *Construction and Building Materials*. Vol. 94, pp. 728-736. https://doi.org/10.1016/j.conbuildmat.2015.07.072

[4] Okamura, H. – Ouchi, M.: Self-compacting concrete. Development, present use and future. Kochi University of Technology, Japan, pp. 1-14.

[5] Okamura, H. – Ouchi, M. (2003): Self-Compacting Concrete. *Journal of Advanced Concrete Technology*. Vol. 1, pp. 5-15.

[6] Kavitha, O. R. – Shanthi, V. M. – Prince Arulraj, G. – Sivakumar, P. (2015): Fresh, micro- and macrolevel studies of metakaolin blended self-compacting concrete. *Applied Clay Science*. Vol.114, pp. 370-374. https://doi.org/10.1016/j.clay.2015.06.024

[7] Borosnyói, A. (2016): Long term durability performance and mechanical properties of high performance concretes with combined use of supplementary cementing materials. *Construction and Building Materials*. Vol. 112, pp. 307-324. https://doi.org/10.1016/j.conbuildmat.2016.02.224

[8] Nehme, S. G. (2015): Kiegészítőanyagok hatása a szokványos és az öntömörödő betonokra (Influence of supplementary cementing materials on conventional and self-compacting concretes). *Journal of Silicate Based and Composite Materials*. Vol. 67, pp. 28-33. (In Hungarian) https://doi.org/10.14382/epitoanyag-jsbcm.2015.6

[9] Rashad, A. M. (2013): Metakaolin as cementitious material: History, scours, production and composition – A comprehensive overview. *Construction and Building Materials*. Vol. 41, pp. 303-318. https://doi.org/10.1016/j.conbuildmat.2012.12.001

[10] Siddique, R. (2011): Utilization of silica fume in concrete: Review of hardened properties. *Resources, Conservation and Recycling*. Vol. 55, pp. 923-932. 2011. https://doi.org/10.1016/j.resconrec.2011.06.012

[11] Li, Y. – Tian, P. (1997): Effect of slag and silica fume on mechanical properties of high strength concrete. *Cement and Concrete Research*. Vol. 27, pp. 833-837, 1997. https://doi.org/10.1016/S0008-8846(97)00076-8

[12] Olorunsogo, F. T. – Wainwright, P. J. (1998): Effect of GGBFS particle-sized distribution on mortar compressive strength. *Journal of Materials in Civil Engineering*. Vol. 10, pp. 180-187.

[13] Shariq, M. – Prasad, J. – Masood, A. (2010): Effect of GGBFS on time dependent compressive strength of concrete. *Construction and Building Materials*. Vol. 24, pp. 1469-1478. https://doi.org/10.1016/j.conbuildmat.2010.01.007

[14] Parra, C. – Valcuenbe, M. – Gomez, F. (2011): Splitting tensile strength and modulus of elasticity of self-compacting concrete. *Construction and Building Materials*. Vol. 25, pp. 201-207. https://doi.org/10.1016/j.conbuildmat.2010.06.037

[15] Dehn, F. – Holschemacher, K. – Weiße, D. (2000): Self-Compacting Concrete (SCC) Time Development of the Material Properties and the Bond Behaviour. *LACER*. Vol. 5, pp. 115-124.

[16] Bosiljkov, V. B. (2003): SCC mixes with poorly graded aggregate and high volume of limestone filler. *Cement and Concrete Research*. Vol. 33, pp. 1279-1286. 2003. https://doi.org/10.1016/S0008-8846(03)00013-9

[17] Felekog˘ lu, B. – Türkel, S. – Baradan, B. (2007): Effect of water/cement ratio on the fresh and hardened properties of self-compacting concrete. *Building and Environment*. Vol. 42, pp. 1795-1802. https://doi.org/10.1016/j.buildenv.2006.01.012

[18] Su, N. – Hsu, K. – Chai, H. (2001): A simple mix design method for self-compacting concrete. *Cement and Concrete Research*. Vol. 31, pp. 1799-1807.

[19] El Mir, A. – Nehme, S. G. (2016): A comparative study on ultrasonic pulse velocity for normally vibrated and self-compacting concretes. *Concrete Structures*. Vol. 17, 8-12.

[20] BSI Standards Publication (2010): Testing fresh concrete Part 8: Self-compacting concrete — Slump-flow test. British Standard Institution. BS EN 12350-8:2010.

[21] BSI Standards Publication (2010): Testing fresh concrete Part 9: Self-compacting concrete — V-funnel test. British Standard Institution. BS EN 12350-9:2010.

[22] The European Guidelines for Self-Compacting Concrete. Specification, Production and Use. 2005.

[23] BSI Standards Publication (2013): Testing hardened concrete. Part 3: Compressive strength of test specimens. British Standard Institution. 2013. BS EN12390-3:2009.

[24] BSI Standards Publication (2013): Testing hardened concrete. 2013 Part 6: Tensile splitting strength of test specimens. British Standard Institution. BS EN12390-6:2009

[25] Hungarian Standards Publication (2013): Testing hardened concrete. Part 13: Determination of secant modulus of elasticity in compression. Magyar Szabványügyi Testület. MSZ EN 12390-13

[26] American Society of Testing Materials: 1997Standard Test Method for Density, Absorption, and Voids in Hardened Concrete. ASTM C 642.

[27] BSI Standards Publication (2014): Geotechnical investigation and testing - Laboratory testing of soil. Part 3: Determination of particle size density. ISO/DIS 17892-3

[28] Girish, S. – Ranganath, R. V. – Vengala, J. (2010): Influence of powder and paste on flow properties of SCC. *Construction and Building Materials*. Vol. 24, pp. 2481-2488. 2010. https://doi.org/10.1016/j.conbuildmat.2010.06.008

[29] Hassan, A. – Lachemi, M. – Hossain, K. (2012): Effect of metakaolin and silica fume on the durability of self-consolidating concrete. *Cement & Concrete Composites*. Vol. 34, pp. 801-807. https://doi.org/10.1016/j.cemconcomp.2012.02.013

[30] Güneyisi, E. – Gesoglu, M. – Karaoglu, S. – Mermerdas, K. (2012): Strength, permeability and shrinkage cracking of silica fume and metakaolin concretes. *Construction and Building Materials*. Vol. 34, pp. 120-130. https://doi.org/10.1016/j.conbuildmat.2012.02.017

[31] Adekunle, S. – Ahmad, S. – Maslehuddin, M. – Al-Gahtani, H. (2015): Properties of SCC prepared using natural pozzolana and industrial wastes as mineral fillers. *Cement & Concrete Composites*. Vol. 62, pp. 125-133. 2015. https://doi.org/10.1016/j.cemconcomp.2015.06.001

[32] McCormac, J. C. – Brown, R. H. (2014): Design of Reinforced Concrete. Ninth Edition. Welter, J., Hong, S., Goldstein, S., John Wiley & Sons, Inc., United States of America.

[33] Holschemacher, K. – Klug, Y. (2002): Database for the Evaluation of Hardened Properties of SCC. *LACER*. Vol.7, pp. 123-134.

[34] Leemann, A. – Hoffmann, C. (2005): Properties of self-compacting and conventional concrete – differences and similarities. *Magazine of Concrete Research*. Vol. 57, pp. 315-319.

[35] Liu, S. et al (2010): Effect of limestone powder on microstructure of concrete. *Journal of Wuhan University of Technology-Mater. Sci. Ed.* Vol.25, pp. 328-331. https://doi.org/10.1007/s11595-010-2328-5

Ref.:
El Mir, Abdulkader – **Nehme,** Salem Georges: *Long term mechanical properties of self-compacting concrete made with slag cement and supplementary cementitious materials*
Építőanyag – Journal of Silicate Based and Composite Materials, Vol. 69, No. 2 (2017), 59–65. p.
https://doi.org/10.14382/epitoanyag-jsbcm.2017.11

Managing the process of machining on machines on the basis of dynamic modelling for a technological system

Viacheslav MAKSAROV ▪ Department of Mechanical Engineering, Saint-Petersburg Mining University ▪ maks78.54@mail.ru
Aleksey KHALIMONENKO ▪ Department of Mechanical Engineering, Saint-Petersburg Mining University ▪ khalim76@spmi.ru
Jüri OLT ▪ Department of Production Engineering, Institute of Technology, Estonian University of Life Sciences ▪ jyri.olt@emu.ee
Érkezett: 2017. 04. 22. ▪ Received: 22. 04. 2017. ▪ https://doi.org/10.14382/epitoanyag-jsbcm.2017.12

Abstract
The article considers the issues related to improving the efficiency of multipoint machining by the use of rotary cutters which are equipped with replaceable ceramic inserts on CNC machines by developing a method of multipoint machining process control. A dynamic model is proposed for the multipoint cutting process on the basis of continuum theory, and a mathematical model which is cognisant of the specific nature of the multipoint metal cutting problem, and ensuring efficiency in the description of various chip-making process modes.
Keywords: multipoint machining, dynamic model, cutting process, generic mathematical model, milling.

Viacheslav MAKSAROV
Professor at Saint-Petersburg Mining University. Head of department of mechanical engineering from 2012 and dean of electromechanical faculty from 2015. Specializes in the field of dynamics of machining technological systems.

Aleksey KHALIMONENKO
Associate professor at Saint-Petersburg Mining University. Specializes in the field of automation and control of production processes, processing quality when using cutting ceramics and methods of increasing processing quality.

Jüri OLT
Professor at Estonian University of Life Sciences. Head of department of production engineering from 2005. His main researching area are fundamentals of production engineering, materials cutting and design of technological machinery.

1. Introduction

At present, process control in mechanical engineering is one of the most promising directions of development in this field. Improving the efficiency of multipoint cutting by means of rotary tools which are equipped with replaceable ceramic bits determines the need for the widespread use of high-performance equipment which permit automated machining processes. The control of machining processes in automated production is only possible on the basis of new approaches to the study of the phenomena which accompanies the metal cutting process.

The loss of stability in the multipoint cutting process results in self-oscillation, increasing the intensity of cutting tool wear and reducing the service of machine operating mechanisms; it also leads to deterioration of machining quality and accuracy [1, 2]. Therefore, reducing the intensity of any oscillation in industrial process systems which are operated on an automatic cycle mode is at present a pressing issue [3, 5, 7].

Creating preliminary local physical impact (LPI) on the external surface of the layer which is being sheared off is, according to certain laws, one of the most efficient methods of allowing metal deformation conditions to be changed during cutting [8]. Periodical changes of cutting conditions as compared to the basic material are a peculiarity of the process of machining the work pieces subjected to such action. Such a method allows to carry out control of the multipoint cutting process, in its turn affording the opportunity to improve the multipoint machining technology in a wide range of materials and cutting conditions [4, 8].

The following problems should be solved successively in order to implement the proposed method:

- isolating the causes of emergence of plastic deformation instability and the conditions of transition to an unstable state in the process of multipoint cutting leading to self-oscillations excitation in the closed process scheme of machining by cutting [2, 10];
- choosing and substantiating the rheological model of multipoint cutting process allowing to carry out dynamic modelling of machining process system [8, 13];
- developing a dynamic model of industrial process system with regard for rheological peculiarities of multipoint cutting process and oscillations in the closed system loops on the basis of dynamic models proposed earlier [6, 9, 12];
- developing a theoretical basis for efficient control of multipoint machining industrial process systems deformation process and vibration immunity [3, 10];
- carrying out a set of experimental studies with the purpose of confirming the validity of the theoretical ideas obtained in the process of previous work [7];
- developing guidelines for improvement of the efficiency of multipoint cutting industrial process on the basis of chip formation process control [11].

2. Materials and methods

Before the experimental studies, available research papers have been analysed. The analysis allowed to select hypotheses about the sources of self-oscillations onset in the machining industrial process system. The principal hypotheses are as follows:

- the existence of a coordinate connection in an elastic system in the presence of nonconservative cutting force;
- closeness of the machine dynamic system in the presence of cutting dynamic response;

- delay of cutting forces as compared to the respective disturbances arising upon local deformation of metals in the process of cutting.

The hypothesis of cutting forces delay connected to plastic deformation delay is used most frequently in dynamical analysis. It is adopted that the delay of both kinds of forces as compared to the respective disturbances inevitable upon breaking strain of viscoelastic metals is the phenomenological factor making system instability possible.

A study was undertaken in order to find out whether it is possible to suppress the self-oscillations arising in the process of cutting by local physical impact (LPI). The study allowed to extract formulas to assess the degree of local physical impact influence on the dominant system beyond the stability area boundary as the LPI is created and applied to the surface being machined by various methods.

The proposed study flow chart allowed to assess the influence of local physical impact on the cutting kinematics. It is possible to find out the regularities with whose help it is possible to assess possible LPI depth, allowing to suppress the self-oscillations arising in the system by implementing the proposed scheme of mutual arrangement of the local physical impact area and the area of transversally sheared-off layer of chips during multipoint machining (*Fig. 1*).

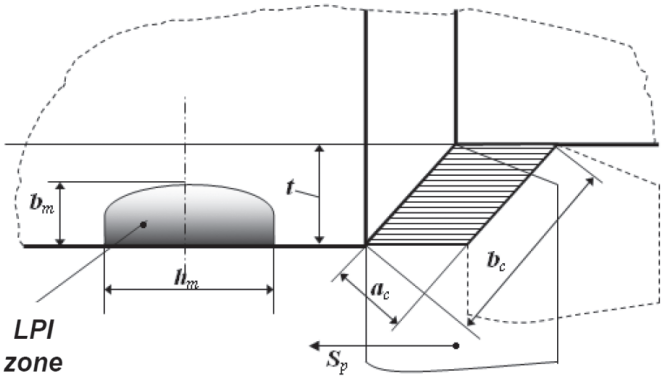

Fig. 1. Diagram of mutual arrangement of the local physical impact area and the transversally sheared layer of chips: S_p – feed direction, a_c and b_c – width and thickness of the layer being sheared off, t – cutting depth, b_m and h_m – LPI depth and width.

1. ábra A lokális megmunkálási terület és a keresztirányban leválasztott forgács kölcsönös viszonya: S_p – előtolás iránya, a_c és b_c – a leválasztott réteg szélessége és vastagsága, t – fogásmélység, b_m és h_m – LPI mélysége és szélessége.

Analysis of the research papers study result allowed to present the process of plastic metals cutting by the following diagrams (*Fig. 2*).

The obtained data allowed to carry out mathematical modelling of chip formation in the process of cutting [12]. Physical properties of the metal being deformed can be visualized as a mechanical analogy (a discrete rheological model) presented as a certain totality of mechanical elements: elasticity, viscosity and plasticity, allowing to come over to the implementation of a generalized rheological model in the form of a series combination of the elastoviscoplastic relaxing *Ishlinsky* medium and the *Voigt* medium with deformation delay (*Fig. 3*).

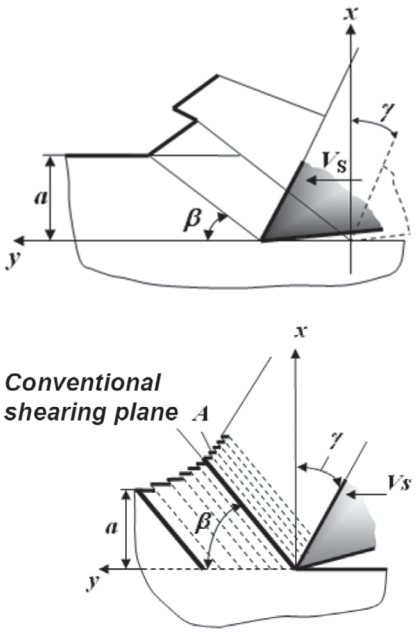

Fig. 2. Conventional model of chip making process: a) – formation of saw-shaped chip elements; b) – formation of laminose fine texture where S_p is feed direction, β is shear angle, γ is face angle, a is thickness of the layer being sheared off.

2. ábra Forgácsképződés hagyományos modellje: a) – forgácselem leválasztása; b) – finom textúra kialakulása, ahol S_p az előtolás iránya, β anyírási szög, γ a felületi szög, a a leválasztott réteg vastagsága.

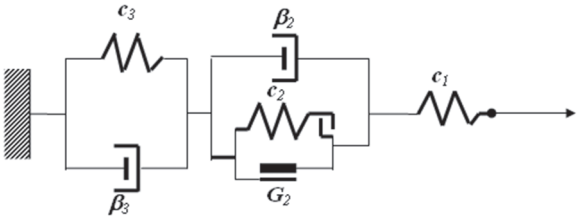

Fig. 3. Rheological model of chip formation in the process of cutting: G_2, c_1 are quasi-elastic and dissipative coefficients.

3. ábra Forgácsképződés reológiai modellje forgácsolás során: G_2, c_1 a kvázi-rugalmas és disszipatív együtthatók.

Such a combination of elements reflects dynamic interaction between the process of metal plastification in the layer being sheared off (*Ishlinsky* medium) and the process of removed chips deformation and friction (*Voigt* medium), and therefore, describes the cutting process in sufficient detail [8, 11].

Having presented the rheological model of chip formation in the operator form and having carried out the appropriate transformation, we obtain formulas (1, 2) characterizing the process of a body reversion to its undeformed state expressed through the principal characteristics of relaxation.

$$\tau_{rel}^{(1)} = \frac{1}{\gamma_3 + \omega} = \frac{c_3}{2 \cdot \beta_3} + \frac{c_2}{2 \cdot \beta_2} + \left| \frac{c_3}{2 \cdot \beta_3} - \frac{c_2}{2 \cdot \beta_2} \right| \quad (1)$$

$$\tau_{rel}^{(2)} = \frac{1}{\gamma_3 - \omega} = \frac{c_3}{2 \cdot \beta_3} + \frac{c_2}{2 \cdot \beta_2} - \left| \frac{c_3}{2 \cdot \beta_3} - \frac{c_2}{2 \cdot \beta_2} \right| \quad (2)$$

where γ_3 and ω are, respectively, damping factor and frequency, c_2, c_3 are quasi-elastic and β_2, β_3, are dissipative coefficients.

The dependencies determined above allowed us to come over to dynamic modelling of the machining industrial process system during multipoint cutting by rotary cutters equipped

with ceramic bits. A simplified dynamic model was developed for that purpose. That model was based on the industrial process system element parameters measured on the milling machine used for the experiments: reduced mass m, resistance force to speed proportionality coefficient b and stiffness coefficient c.

For a torsional system, respectively: reduced inertia moment J, proportionality coefficient b_ϕ and torsional stiffness coefficient c_ϕ.

Natural loop oscillations and logarithmic decrement frequencies were determined in the same way. The apparatus used for that purpose included an inertia oscillation sensor with an intermediate amplifier, a NI SC-2043-SG analog-digital converter board and a computer on which a LabVIEW 13.0 data processing system was installed. A virtual instrument for receiving and post processing of damped oscillation was created in it. Load to displacement dependency diagrams were plotted on the basis of the measurements. Those diagrams were used to determine system element stiffness coefficient.

As a result, the simulation model boiled down to a simplified system of a quadruple dynamic module of the small-size machining industrial process system (*Fig. 4*) with dissipative characteristics taking into account the structural damping and rheological processes of the global model under consideration to which two subsystems with four generalized coordinates correspond:

a) is the work piece subsystem B with coordinates u , w;

b) is the tool subsystem T with coordinates x , y;

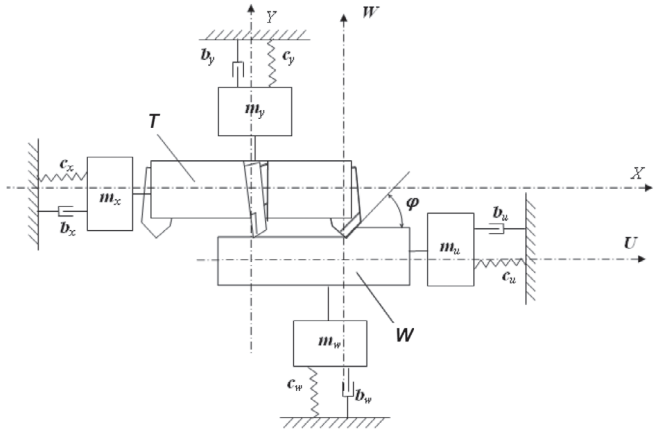

Fig. 4. Dynamic model of a quadruple industrial process system: W – work piece; T – Tool; X, Y – tool axes; U, W – work piece axes; m_x, m_y, m_u, m_w – reduced inertia parameters; b_x, b_y, b_u, b_{wk} – energy dissipation coefficients; c_x, c_y, c_u, c_w – stiffness coefficients.

4. ábra Négy szabadságfokú megmunkálási rendszer dinamikus modellje: W – munkadarab; T – szerszám; X, Y – szerszámtengelyek; U, W – munkadarab tengelyei; m_x, m_y, m_u, m_w – redukált inercia paraméterek; b_x, b_y, b_u, b_{wk} – energia disszipációs együtthatók; c_x, c_y, c_u, c_w – merevségi együtthatók.

The subsystems communicate through the chip making process presented by a rheological model in the normal n and tangent τ directions (*Fig. 5*). The chip making process can be conventionally divided into two stages: deformation before the shearing plane ($\sigma < \sigma_{pl}$) and shearing of an element of small thickness along the shearing plane ($\sigma \geq \sigma_{pl}$). In the process of building differential equation systems of the quadruple model of machining industrial process system, the transition condition can be presented as an inequality system:

$$\text{with } \sigma < \sigma_{pl},\ c_{1\tau}\cdot(x-u)^2 + c_{1n}\cdot(y-w)^2 \geq \sigma_{pl}\cdot S_{sh} \quad (3)$$

$$\text{with } \sigma \geq \sigma_{pl},\ c_{1\tau}\cdot(x-u)^2 + c_{1n}\cdot(y-w)^2 < \sigma_{pl}\cdot S_{sh} \quad (4)$$

where x, y, u, w are the mechanical system coordinates; $c_{1\tau}$, c_{1n} are stiffness coefficients characterizing the elastic behavior of chip formation rheological model in the lines τ and n, N/m; σ_{pl} is the yield (plasticity) limit, N/m²; S_{sh} is the area of the layer being sheared off ($a \times b$) in mm²; β is the shearing angle.

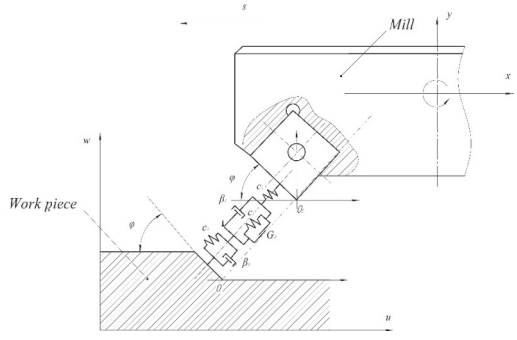

Fig. 5. Rheological model of chip formation in the process of cutting: where: c, G, β - quasi-elastic and dissipative coefficients (n – normal, τ - tangent), φ – entering angle.

5. ábra Forgácsleválasztás reológiai modellje: ahol c, G, β - kvázi-rugalmas és disszipatív együtthatók (n – normál, τ - érintő), φ – homlokszög.

In a number of cases, chips friction against the front tool surface caused by eternal friction and secondary plastic deformation of the chips layer is accompanied by adhesion phenomena on the micro areas of the chips to tool elastic contact. That being the cased, it was established that this physical phenomenon between the tool and the chip can be presented as two phase transitions: sliding and seizure [6, 11].

Transition from one phase to the other is shaped sequentially by the system itself. The conditions for phase transitions implementation are determined by kinematic and force characteristics of subsystems interactions and expressed as a switchover function $Sg(w)$:

$$Sg(w) = \begin{cases} w > [V] \\ w \leq [V] \end{cases} \quad (5)$$

where $\boldsymbol{w = V_S + \dot{x} - \dot{u}}$; V_s is cutting speed, $\dot{\boldsymbol{x}}$ and $\dot{\boldsymbol{u}}$ are the work piece and the tool subsystem speeds.

That being said, the behavior of the selected dynamical quadruple model of machining industrial process system in accordance with the adopted rheological model of chip forming is presented in general terms as a system of differential equations:

$$\begin{aligned}
&T_{x2}^2\ddot{x} + (T_{x1}+T_{x3})\dot{x} - T_{x3}\dot{u} + 2x - u = Q;\\
&T_{y2}^2\ddot{y} + (T_{y1}+T_{y3})\dot{y} - T_{y3}\dot{w} + 2y - w = P;\\
&T_{u2}^2\ddot{u} + (T_{u1}+T_{u3})\dot{u} - T_{u3}\dot{x} + 2u - x = -Q;\\
&T_{w2}^2\ddot{w} + (T_{w1}+T_{w3})\dot{w} - T_{w3}\dot{y} + 2w - y = -P;\\
&(T_P + T_{P1})\dot{P} + P = -(k_x - k_{PX})(x-u) -\\
&-\left[T_{ky1} - k_{PY}(T_P + T_{P2})\right](\dot{y}-\dot{w}) +\\
&+ k_{PY}(y-w) - \left[k_x T_{P1} - k_{PX}(T_P + T_{P2})\right](\dot{x}-\dot{u})\\
&T_Q\dot{Q} + Q = P - T_{kx}(\dot{x}-\dot{u}) - T_{ky2}(\dot{y}-\dot{w}).
\end{aligned} \quad (6)$$

where T_{x2}, T_{y2}, T_{u2}, T_{w2} are loop time constants x, y, u, w; T_{x1}, T_{y1}, T_{u1}, T_{w1}, T_{x3}, T_{y3}, T_{u3}, T_{w3} are loop damping time constants x, y, u, w; k_x is system loop x transmission coefficient; T_P, T_Q are time constants; k_{Px}, k_{Py}, T_{P1}, T_{P2} are coefficients and time constants in view of rheological peculiarities of the chip making process. The system of differential equation (6) was solved by the piecewise approximation method. For that purpose, this system was presented in the vector-matrix form:

$$T \cdot \dot{q} + N(q) \cdot q = 0 \quad (7)$$

where q - *(n×1)* is the vector-function of generalized system coordinates; T is lumped size matrix *(n×n)*; $N(q)$ is size matrix *(n×n)*. In the model under consideration $n = 10$; whereupon the number of loops n corresponds to the model size.

3. Results and discussion

On the ground of the rheological models developed above, the problem of controlling the process of multipoint cutting with ceramic bit rotary cutters by the face milling method. The relationship between the volume of the local impact zone with altered structure and properties W'_{LPI} and the total volume W'_{ch} of the metal layer sheared by one bit in the LPI area:

$$\frac{W'_{LPI}}{W'_{ch}} = \frac{b_m h_m}{2\pi\left[D(\cos\psi_H - \cos\psi_K) + S_Z\left(\frac{\psi_H - \psi_K}{2} + \frac{\sin\psi_K - \sin 2\psi_H}{4}\right)\right]} \quad (8)$$

where ψ_H is the *LPI* zone bit entry angle, ψ_K is the *LPI* zone bit exit angle, D is the rotary cuter diameter, S_Z is the bit feed, h_m is the local impact zone width, b_m is the *LPI* zone depth, t is milling depth determining the reliability and efficiency of periodically changing stress-strain state conditions in the cutting zone needed for controlling the multipoint cutting process.

Fig. 6 presents the general appearance of a cylinder block face that must be machined in compliance with the technical requirements for mating face accuracy (0.03 mm for 100x100 mm size) and surface roughness R_a = 1.6 μm (*Fig. 7*).

The implemented set of comparative calculation and experimental studies of work pieces milling with a wide variation of machining parameters allowed us to propose a scheme of local physical impact application to the work piece surface being machined modelling the cylinder block face (*Fig. 8*).

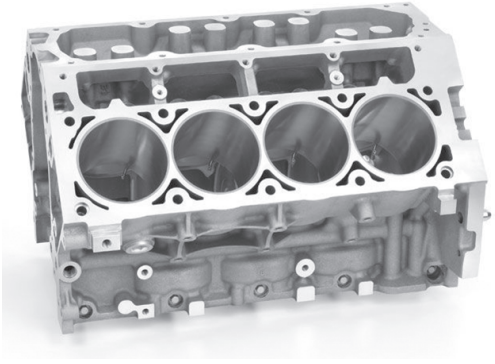

Fig. 6. General appearance of the cylinder block face.
6. ábra A hengerblokk felület általános képe.

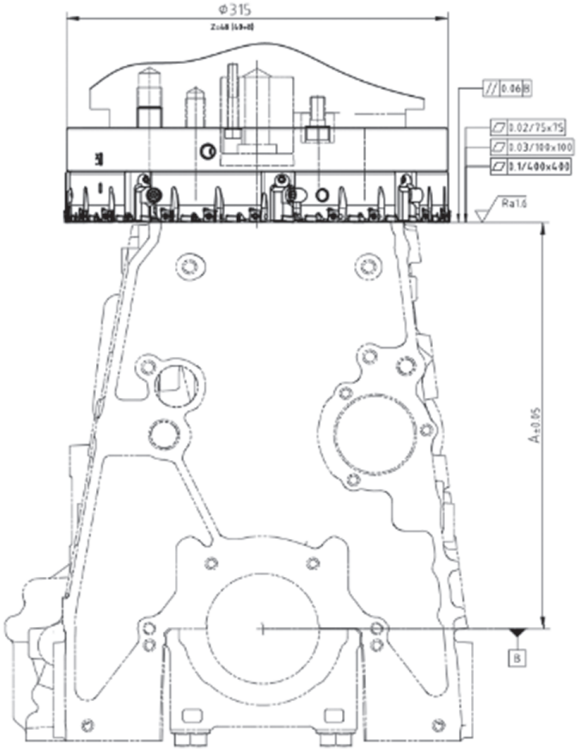

Fig. 7. Technical requirements for the cylinder block face.
7. ábra Technikai követelmények a hengerblokkra vonatkozóan.

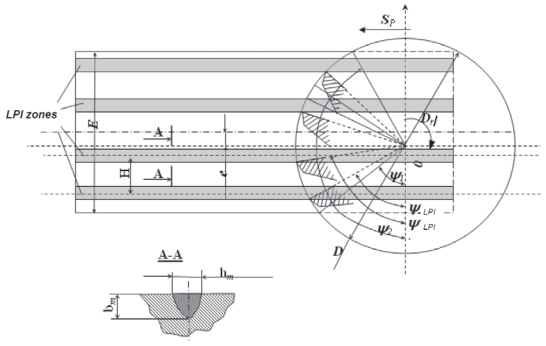

Fig. 8. LPI zones layout diagram during face milling: E – work piece width; e – rotary cutter axis to work piece axis offset; S_p – feed direction; D – rotary cutter diameter; D_r – rotary cutter rotation direction; ψ_1,ψ_2 – bit work piece entry and exit angles; ψ_{LPI1}, ψ_{LPI2} – LPI bit entry and exit angles; H – distance between LPI zones; h_m and b_m – LPI zone width and depth.
8. ábra LPI zónák elhelyezkedése fúrás során: E – munkadarab szélessége; e – fúrótengely eltolása a munkadarab tengelyhez képest; S_p – előtolás iránya; D – fúró átmérő; D_r – fúró forgásiránya; ψ_1,ψ_2 – fúrószerszám belépési és kilépési szöge; ψ_{LPI1}, ψ_{LPI2} – LPI belépési és kilépési szög; H – távolság az LPI zónák között; h_m és b_m – LPIzóna szélessége és mélysége.

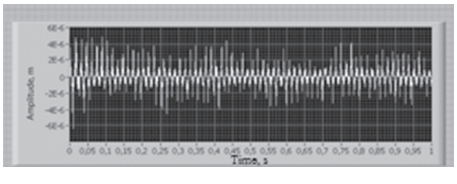

Fig. 9. Calculated (a) and experimental (b) vibration displacement during face milling of Gh190B grade cast iron.
9. ábra Számított (a) és kísérleti (b) rezgéskép Gh190B minőségű öntöttvas felületi fúrása során.

A comparison of calculation (*Fig. 9.a*) and experimental (*Fig. 9.b*) data has shown that the difference between theoretical and practical results does not exceed 15%, which is evidence of

qualitative concordance of the nature of oscillations and affords grounds for claiming that the rheological models developed by us are operable.

Experimental studies of face milling of the mating face of a Gh190B grade cast iron cylinder block over a discontinuous surface using local metastability allows to obtain maximum deviation within 0.015 mm in rapid machining modes (Fig. 10).

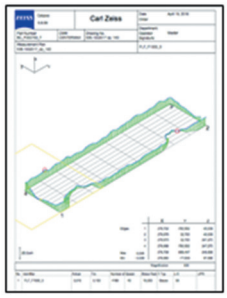

Fig. 10. A fragment of cylinder block mating surface shape accuracy deviations measurement result.
10. ábra Mérési eredmény hengerblokk felületi megmunkálási alakpontosságának eltérésére.

4. Conclusions

A dynamical model of multipoint cutting process has been proposed and substantiated. The model is based on a continuum theory where the metal primary plastic deformation zone and the chip coming off the tool face are presented as continuum elements each subjected to a dynamic load imitating a multipoint tool.

The model is largely universal, it is in line with the present-day concepts of the cutting process mechanics. It reflects the elastic response, the plastic flow process and the delay effects in the machined metal in reference to each other.

A mathematical model has been proposed that takes account of the specific nature of the multipoint metal cutting problem and ensures efficient description of various chip formation process modes. The rheological processes taking place during multipoint cutting were studied by computer simulation with the help of LabVIEW 13.0 graphical programming environment. The set of research works implemented by us forms the basis for applying computer simulation methods to solving the crucial tasks of cutting process dynamics and machining modes optimization.

A generalized mathematical model has been implemented, reflecting the multipoint cutting process in view of elasoplastic properties in the dynamics of tool-to-work piece contact interaction and the rheological peculiarities of chip forming process in the active plastic deformation zone. A rheological model has been proposed in the form of a series combination of the elastoviscoplastic relaxing Ishlinsky medium (reflecting the process of primary deformation of the sheared-off layer metal) and the Voigt medium with two elastic-dissipative elements (reflecting the sheared chips deformation and friction process).

We have solved the task of space dynamic modelling of variable conditions based on the developed rheological models reflecting molecular processes interaction in the chip formation zone and the elastic-dissipative characteristics of the machining industrial process system.

Guidelines have been developed for determining elastic-dissipative coefficients of the multipoint cutting rheological models, based on a set of analog-digital hardware controlled by LabVIEW 13.0 system.

A set of comparative and experimental studies of work pieces milling with a wide variety of machining parameters has been performed.

A machining stability area has been refined, allowing to increase cutting speed without product quality deterioration. A comparison of calculation and experimental data has shown that the deviation between calculation and experimental data did not exceed 15%, which is evidence of qualitative concrordance of the nature of oscillations and affords grounds for claiming that the rheological models developed by us are operable.

References

[1] Atkins, A. G. (2003): Modelling metal cutting using modern ductile fracture mechanics: Quantitative explanations for some longstanding problems. *International Journal of Mechanical Sciences*, Vol. 45, No. 2, pp. 373-396, https://doi.org/10.1016/S0020-7403(03)00040-7

[2] Bäker M. (2003): The influence of plastic properties on chip formation. *Computational Materials Science*, Vol. 28, pp. 556–562, https://doi.org/10.1016/j.commatsci.2003.08.013

[3] Brown C. A. (1987): Strain analysis in machining using metallographic methods. *Metallography*, Vol. 20, pp. 465-483, https://doi.org/10.1016/0026-0800(87)90020-6

[4] Ee, K. C. – Balaji, A. K. – Li, P. X. – Jawahir, I. S. (2002): Force decomposition model for tool-wear in turning with grooved tool, *Wear*, Vol. 249, No. 10-11, pp. 985–994. https://doi.org/10.1016/S0043-1648(01)00837-7

[5] Gao, Y. – Sun, R. L. – Chen, Y. N. – Leopold, J. (2016): Mechanical and thermal modeling of modulation-assisted machining. *International Journal of Advanced Manufacturing Technology*, Vol. 86, No. 9-12, pp. 2945-2959, https://doi.org/10.1007/s00170-016-8421-y

[6] Gonzalez, D. – Simonovski, I. – Withers, P. J. – Quinta Da Fonseca, J. (2014): Modelling the effect of elastic and plastic anisotropies on stresses at grain boundaries. *International Journal of Plasticity*, Vol. 61, pp. 49-63, https://doi.org/10.1016/j.ijplas.2014.03.012

[7] Madissoo **M.** – Rossner A. – Maksarov V. – Olt J. (2015): Testing of the external turning tool holder equipped with alternate bars in its construction. *Medziagotyra*, Vol. 21, No. 3, pp. 391-395, https://doi.org/10.5755/j01.ms.21.3.7351

[8] Maksarov V. – Madissoo M. – Olt J. (2013): Increasing the Effectiveness of the Cutting Process in the Course of Milling. *Journal of Mechanics & Industry Research*, Vol. 1, No. 4, pp. 75 -81, https://doi.org/10.12966/jmir.11.02.2013

[9] Martinkovič, M. – Pokorný, P. (2015): Estimation of local plastic deformation in cutting zone during turning. *Key Engineering Materials*, Vol. 662, pp. 173-176, https://doi.org/10.4028/www.scientific.net/KEM.662.173

[10] Olt J. – Madissoo M. – Maksarov V. (2012): Dynamic stabilization of technological systems for processing edge cutting through local metastability. *Proceedings – 2011 IEEE International Symposium on Assembly and Manufacturing, ISAM 2011*; Tampere; Finland; 25 May 2011 through 27 May 2011; Category number CFP11ATP-ART; Code 86199, pp. 6 – 12, https://doi.org/10.1109/ISAM.2011.5942348

[11] Olt J. – Maksarov V. (2015): Cutting process simulation on the basis of rheological properties of metals. *Annals of DAAAM and Proceedings of the DAAAM symposium*. Vienna, Austria, pp. 229-237. https://doi.org/10.2507/26th.daaam.proceedings.032

[12] Olt J. – Liyvapuu, A. – Madissoo M. – Maksarov V. (2016): Dynamic simulation of chip formation in the process of cutting. *Journal of Materials & Product technology*, Vol. 53, No. 1, pp. 1-14, https://doi.org/10.1504/JMPT.2016.076363

[13] Rao G. V. G. – Mahajan P. – Bhatnagar N. (2007): Micro-mechanical modeling of machining of FRP composites – Cutting force analysis. *Composes Science and Technology*, Vol. 67, No. 3–4. pp. 579–593, https://doi.org/10.1016/j.compscitech.2016.08.010

Ref.:
Maksarov, Viacheslav – **Khalimonenko,** Aleksey – **Olt,** Jüri: *Managing the process of machining on machines on the basis of dynamic modelling for a technological system*
Építőanyag – Journal of Silicate Based and Composite Materials, Vol. 69, No. 2 (2017), 66–71. p.
https://doi.org/10.14382/epitoanyag-jsbcm.2017.11

Forgácsolási művelet vezérlése szerszámgépeken dinamikus modell felhasználásával technológiai rendszerben

A cikk bemutatja cserélhető kerámia megmunkáló szerszámokkal történő CNC esztergálás hatékonyságának javítási lehetőségeit többpontos megmunkálás során. A szerzők bemutatnak egy dinamikus modellt, amelynek az alapja a kontinuum elmélet, és egy matematikai modellt, amely követi a többpontos fémmegmunkálási folyamat természetét. A szerzők a modellek hatékonyságát több forgácsképződési módhoz is illusztrálják.

Kulcsszavak: többpontos forgácsolás, dinamikus modell, forgácsolási eljárás, generikus matematikai modell, fúrás.

GUIDELINE FOR AUTHORS

The manuscript must contain the followings: title; author's name, workplace, e-mail address; abstract, keywords; main text; acknowledgement (optional)**; references; figures, photos with notes; tables with notes; short biography** (information on the scientific works of the authors).

The full manuscript should not be more than 6 pages including figures, photos and tables. Settings of the word document are: 3 cm margin up and down, 2,5 cm margin left and right. Paper size: A4. Letter size 10 pt, type: Times New Roman. Lines: simple, justified.

TITLE, AUTHOR

The title of the article should be short and objective.

Under the title the name of the author(s), workplace, e-mail address.

If the text originally was a presentation or poster at a conference, it should be marked.

ABSTRACT, KEYWORDS

The abstract is a short summary of the manuscript, about a half page size. The author should give keywords to the text, which are the most important elements of the article.

MAIN TEXT

Contains: materials and experimental procedure (or something similar), results and discussion (or something similar), conclusions.

REFERENCES

References are marked with numbers, e.g. [6], and a bibliography is made by the reference's order. References should be provided together with the DOI if available.

Examples:

Journals:

[6] Mohamed, K. R. – El-Rashidy, Z. M. – Salama, A. A.: In vitro properties of nano-hydroxyapatite/chitosan biocomposites. *Ceramics International.* 37(8), December 2011, pp. 3265–3271, http://dx.doi.org/10.1016/j.ceramint.2011.05.121

Books:

[6] Mehta, P. K. – Monteiro, P. J. M.: Concrete. Microstructure, properties, and materials. *McGraw-Hill*, 2006, 659 p.

FIGURES, TABLES

All drawings, diagrams and photos are figures. The **text should contain references to all figures and tables**. This shows the place of the figure in the text. Please send all the figures in attached files, and not as a part of the text. **All figures and tables should have a title**.

Authors are asked to submit color figures by submission. Black and white figures are suggested to be avoided, however, acceptable.

The figures should be: tiff, jpg or eps files, 300 dpi at least, photos are 600 dpi at least.

BIOGRAPHY

Max. 500 character size professional biography of the author(s).

CHECKING

The editing board checks the articles and informs the authors about suggested modifications. Since the author is responsible for the content of the article, the author is not liable to accept them.

CONTACT

Please send the manuscript in electronic format to the following e-mail address: femgomze@uni-miskolc.hu and epitoanyag@szte.org.hu or by post: Scientific Society of the Silicate Industry, Budapest, Bécsi út 122–124., H-1034, HUNGARY

We kindly ask the authors to give their e-mail address and phone number on behalf of the quick conciliation.

Építőanyag – *Journal of Silicate Based and Composite Materials*, Quarterly peer-reviewed periodical of the Hungarian Scientific Society of the Silicate Industry, SZTE.
http://epitoanyag.org.hu

ERMCO

EUROPEAN READY MIXED CONCRETE ORGANIZATION
ASSOCIATION EUROPEENNE DU BETON PRET A L'EMPLOI
EUROPÄISCHER TRANSPORTBETONVERBAND

About ERMCO

Ready-mixed concrete is the bedrock of the wider construction industry, one of the foundations of the European economy today and for the foreseeable future. Since 1967 the European Ready Mixed Concrete Organization (ERMCO) has represented the common interests of the ready-mixed concrete industry in Europe. This is a firmly local industry, with over 6200 plants owned by a majority of small and medium enterprises, and a big employer, with more than 63.000 workers. Conscious of its importance and responsibility to local communities, ERMCO was an early champion of implementing policies based on the economic, social and environmental aspects of sustainability. ERMCO acts as a conduit through which its members' views on policies, standardisation, safety standards, environmental, economic and technical issues are communicated to European policy makers; and it makes an active contribution itself in formulating those European policies. Last but not least, using its network of Europe and non-European affiliates, ERMCO promotes innovation and best practice across the continent and abroad.

WWW.ERMCO.EU

EUROPEAN NANOSCIENCE AND NANOTECHNOLOGY ASSOCIATION – ENNA

Who We Are

European Nanoscience and Nanotechnology Association (ENNA) is a scientific and professional organization that represents chemists, biologists, physicists and material scientists in Europe, Asia and America. European Nanoscience and Nanotechnology Association (ENNA) is a nonprofit organization and its mission is to promote interdisciplinary sciences. ENNA will ensure public services on all research and education matters within the scope of nanoscience and nanotechnology. It provides a common platform for the exchange of ideas among scientists, technologists, teachers, and students. ENNA is aiming at becoming the largest association of nanoscientists in Europe. The mission of the ENNA is to advance the creation, communication and application of nanoscience knowledge to benefit society and improve people's lives.

Mission

ENNA seeks to advance science, engineering, and innovations throughout the World for the benefit of all people. To fulfill this mission, the ENNA board has set these goals:

- enhance communications among scientists and the public;
- promote and defend the integrity of science;
- strengthen the support for science & technology enterprise;
- promote the responsible use of science in public policy;
- strengthen and diversify the science & technology workforce;
- foster education in science and technology for everyone;
- Increase public engagement with science & technology;
- Advance international cooperation in science.

WWW.EUROPENANOSCIENCE.ORG